The State Scientific Center of Russia
The Budker Institute of Nuclear Physics, SB RAS

S.E. Baru, A.E. Blinov, V.E. Blinov, A.E. Bondar,
A.D. Bukin, V.R. Groshev, Yu.I. Eidelman, V.A. Kiselev,
S.G. Klimenko, G.M. Kolachev, S.I. Mishnev, A.P. Onuchin,
V.S. Panin, V.V. Petrov, I.Ya. Protopopov, A.G. Shamov,
V.A. Sidorov, Yu.I. Skovpen, A.N. Skrinsky, V.A. Tayursky,
V.I. Telnov, Yu.A. Tikhonov, G.M. Tumaikin, A.E. Undrus,
A.I. Vorobiov, V.N. Zhilich

EXPERIMENTS WITH THE MD-1 DETECTOR AT THE e^+e^- COLLIDER VEPP-4 IN THE ENERGY REGION OF Υ-MESONS

Budker INP 95-36

Novosibirsk
1995

The State Scientific Center of Russia
The Budker Institute of Nuclear Physics, SB RAS

S.E. Baru, A.E. Blinov, V.E. Blinov, A.E. Bondar,
A.D. Bukin, V.R. Groshev, Yu.I. Eidelman, V.A. Kiselev,
S.G. Klimenko, G.M. Kolachev, S.I. Mishnev, A.P. Onuchin,
V.S. Panin, V.V. Petrov, I.Ya. Protopopov, A.G. Shamov,
V.A. Sidorov, Yu.I. Skovpen, A.N. Skrinsky, V.A. Tayursky,
V.I. Telnov, Yu.A. Tikhonov, G.M. Tumaikin, A.E. Undrus,
A.I. Vorobiov, V.N. Zhilich

EXPERIMENTS WITH THE MD-1 DETECTOR AT THE e^+e^- COLLIDER VEPP-4 IN THE ENERGY REGION OF Υ-MESONS

Budker INP 95-36

Novosibirsk
1995

Contents:

Abstract:

This paper reviews physical results obtained at the e^+e^- collider VEPP-4 with the MD-1 detector. The results of experiments on the Υ meson physics and study of the hadron production in continuum in the energy region 7.2÷10.3 GeV as well as the results of study of the two photon reactions are presented. Among results obtained in the upsilon physics: the precise measurement of the $\Upsilon(1S)$, $\Upsilon(2S)$, $\Upsilon(3S)$ masses and the precise determination of the $\Upsilon(1S)$ and $\Upsilon(2S)$ electronic widths. In the experiments on study of the hadron production in continuum the precise measurement of the R was carried out. The peculiarity of the detector is the magnetic field transverse to the orbit plane which provided the possibility to study two photon reactions with tagging one or both scattered electrons even at zero emission angle. Among results on the $\gamma\gamma$ reactions is the measurement of the two photon total hadronic cross section performed in the double-tag mode. In the QED experiments a new QED effect – the impact parameter cut-off in single bremsstrahlung was discovered.

Submitted to Physics Reports

1.Introduction

With the discovery of the $\Upsilon(1S)$ and $\Upsilon(2S)$ mesons at FNAL (USA) in 1977 [1] studies of the Υ meson family occupied an important place in programs of high energy physics laboratories. Though Υ-mesons were discovered in experiments with a proton beam, the dominant contribution to their study came from e^+e^- -colliders: DORIS-II in Germany, CESR in the USA and VEPP-4 in Russia.

About a dozen of detectors worked at these colliders: PLUTO, LENA, DESY-Heidelberg, DASP-II, ARGUS, Crystal Ball at DORIS-II; CLEO, CUSB, CUSB-II, CLEO-II at CESR; MD-1 at VEPP-4. In the large number of experiments performed the bound states $\Upsilon(1S)$, $\Upsilon(2S)$, $\Upsilon(3S)$, and $\Upsilon(4S)$ were investigated. The most fruitful experiments appeared to be those at the $\Upsilon(4S)$ state decaying to $B^0\bar{B}^0$ or B^+B^- meson pairs. Reviews on Υ- and B- mesons studies can be found elsewhere [2, 3].

Rich physics in the Υ meson energy region, and particularly an opportunity to observe CP violation in decays of neutral B mesons, generated plans to build high luminosity e^+e^- -machines (B-factories) in several countries and two of these machines, in SLAC (USA) and in KEK (Japan), are now under construction.

Since the beginning of eighties experiments with the MD-1 detector at the e^+e^- collider VEPP-4 began in Novosibirsk. The project of the MD-1 detector was developed in the middle of seventies and the detector was optimized for $\gamma\gamma$ physics. Since in $\gamma\gamma$ reactions the scattered electrons as well as reaction products are emitted predominantly in the beam direction, the detector was constructed with the magnetic field transverse to the orbit plane, and at both sides of the MD-1 additional deflecting magnets were installed in front of quadrupoles. Compared to other detectors these features gave us a possibility to study tagged $\gamma\gamma$ reactions with quasi real photons and to have a high detection efficiency of the scattered electrons combined with the best accuracy of their energy measurement.

However, a large distance between the lenses appeared to be an essential drawback of the detector for experiments on Υ physics, since it did not allow to have a small beta-function necessary to obtain a high luminosity at the VEPP-4. The luminosity ($\sim 3 \cdot 10^{30}\, cm^{-2} sec^{-1}$ at $\Upsilon(1S)$) was about one order lower than that of DORIS-II or CESR. Such luminosity could not provide a possibility to collect sufficient statistics at the $\Upsilon(4S)$ which has small production cross section, so that the MD-1 concentrated on the precise studies of lower bound states as well as on the e^+e^- annihilation in nearby continuum. Concurrently a series of experiments on the $\gamma\gamma$ physics was performed.

2. MD-1 detector and VEPP-4 collider

2.1. VEPP-4 collider

Schematic drawing of the VEPP-4 [4] (VEPP is acronym of the Russian name for the colliding electron positron beams) is shown in Fig.2.1. The circumference of the storage ring is 366 m. The ring is composed of the two semi-rings filled with FODO-type cells and two straight sections matched by magnetic optics. One of the 40 meter straight sections serves for the injection system and contains cavities of the RF system. The collision point of beams with small β-function (A) is organized for the MD-1 detector in the other straight section. At the first stage of operation additional collision point C was used where experiments with the OLYA detector on

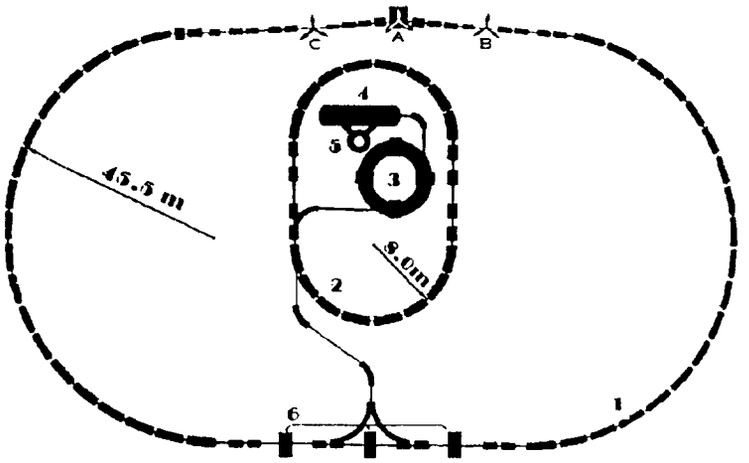

Fig. 2.1: The VEPP-4 collider. 1 – VEPP-4 ring, 2 – intermediate storage ring VEPP-3, 3 – synchrotron B-4, 4 – linear accelerator, 5 – pulse microwave frequency generator of the gyrocon type, 6 – accelerating cavities of the VEPP-4. A – interaction area in MD-1, B and C – additional collision points of beams.

the measurement of ψ and ψ'-meson masses were carried out [5]. The length of the experimental straight section A was increased up to 55 meters after removal of the last cells of the semi-rings. The 18° rotation deficit was provided by the MD-1 detector with the magnetic field transverse to the orbit plane. The VEPP-4 collider has the system of electrostatic beam separation installed in the injection and experimental straight sections which gives the possibility of separation of the electron and positron beam orbits independently of each other.

Table 2.1: Main parameters of the VEPP-4 collider.

Maximum beam energy (E)	5.8 GeV
Luminosity $(cm^{-2} \cdot sec^{-1})$	$3 \cdot 10^{30}$ at E=4.75 GeV $1 \cdot 10^{30}$ at E=3 GeV
Mode of operation	One bunch
Beam currents	2 x 10 mA
Vertical β-function at the collision point	12 cm
Length of bunch σ_x	5 cm
Transverse beam sizes σ_r, σ_z	0.07 cm, 0.002 cm
Life time (currents 2 x 10 mA)	6 hours
Rate of positron accumulation	0.5 mA/min

The injection system includes the linac supplied by the gyrocon RF-source developed according to idea of G.I.Budker, the synchrotron with an energy of 350 MeV, and the intermediate storage ring VEPP-3 with the ejection energy of 1.8 GeV. Positrons with the energy of 7 MeV are produced by conversion of 50 MeV electrons at the exit of the linac. The linac and the synchrotron operate with 1 Hz frequency.

Main parameters of the storage ring VEPP-4 are listed in Table 2.1.

The standard experimental run took 2–3 hours. The time required for injection to the VEPP-4, acceleration from the injection energy of 1.8 GeV to the energy of the experiment, and the readjustment of the focusing system for the operation with the maximum luminosity was no longer than 6 minutes.

2.2. MD-1 detector

The MD-1 (Magnetic Detector) (Fig.2.2) is an universal detector designed for investigation of the two-photon processes and the e^+e^- annihilation [6].

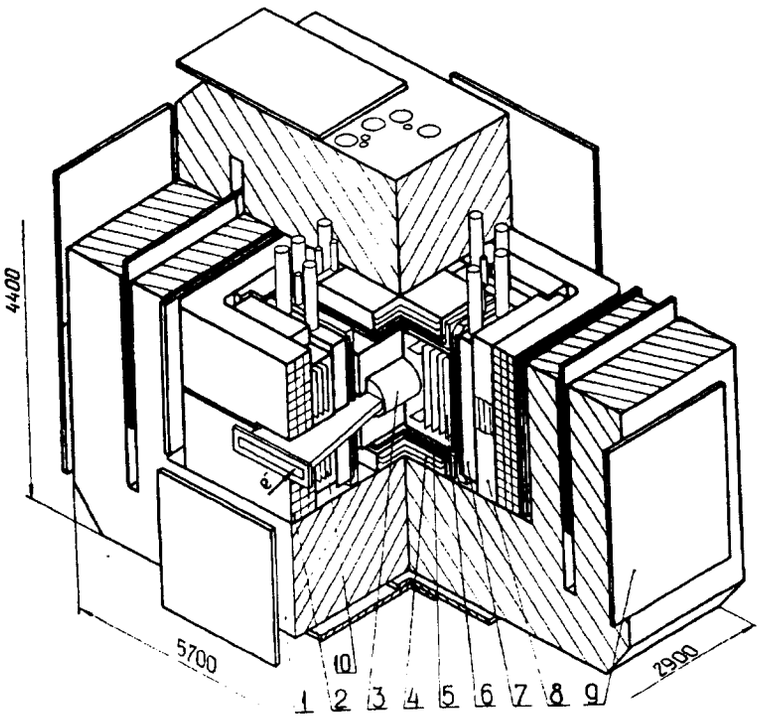

Fig. 2.2: Layout of the MD-1 detector. 1 – magnet yoke, 2 – copper coil, 3 – beam pipe, 4,8,10 – shower-range chambers, 5 – scintillation counters, 6 – coordinate chambers, 7 – gas Cherenkov counters, 9 – muon chambers.

The magnetic field transverse to the orbit plane allows to detect particles produced at small angles to the beam axis. The tagging system of the MD-1 detects electrons coming even at zero angle. These features are especially important for study of two-photon processes.

The MD-1 detector includes the following systems: the magnet, the beam-pipe, the coordinate chambers, the shower-range chambers, the muon chambers, the scintillation counters, the gas Cherenkov counters, the tagging system of scattered electrons, and the luminosity monitor.

The main magnet is the solenoid with the outer sizes of $2.9 \times 5.7 \times 4.4$ m^3, the inner sizes of 2.3×2.3 m^2 and the gap of 1.8 m. The weight of the copper coil is 40 tons and its thickness is 32 cm. The 400 tons steel yoke provides the magnetic flux return. The magnetic field in the

detector is equal to 12 kG at the beam energy of 5 GeV. The large aperture additional bending magnets are placed at both sides of the main magnet (see Fig.2.3). These magnets allow to

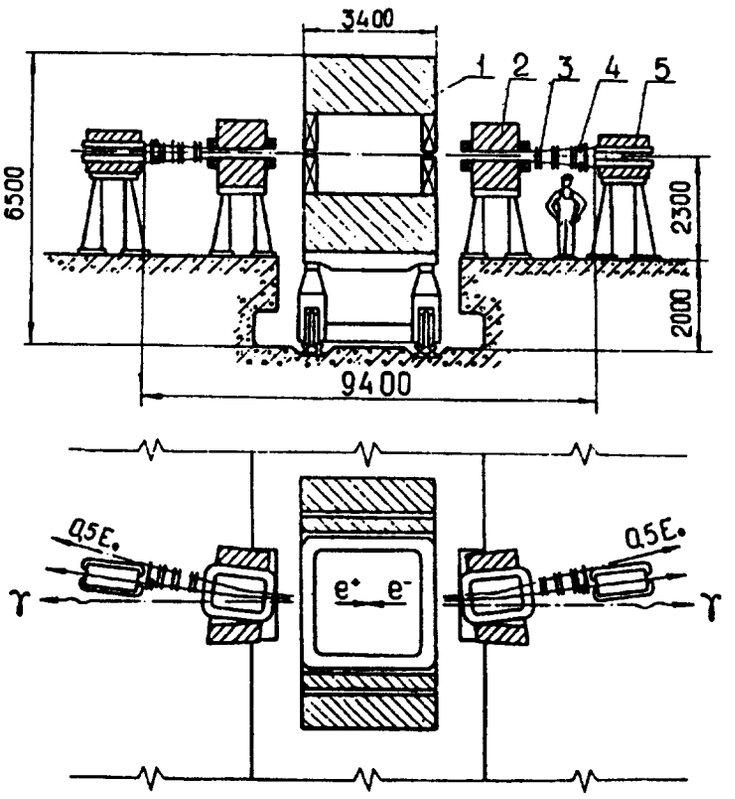

Fig. 2.3: The interaction region: 1 – detector MD-1, 2 – additional bending magnet, 3,4 – system of tagging of scattered electrons and luminosity monitor, 5 – lens.

detect scattering of electrons with a smaller energy loss and improves the accuracy of their energy measurement.

The design of the beam pipe is optimized for reduction of the background from synchrotron radiation. The interaction region is surrounded with the cylindrical part of the beam pipe of 40 cm diameter and 1 m length. The thickness of beam pipe walls is 3 mm of Al. It has special windows with 0.17 mm thickness of Fe for passing of scattered electrons. The ends of the vacuum chamber are equipped with the special probes with outlets for synchrotron radiation. The special collimators protect the detector from synchrotron radiation reflected from the probes.

The charged particles are detected and their momenta are measured by the system of 38 coordinate chambers covering the solid angle of $0.8 \times 4\pi$. The maximum size of the chamber is $0.86 \times 0.9\text{m}^2$. Anode planes are made of tungsten wires of 28 μm diameter stretched with the step of 2 mm in the chambers for momentum measurements and 4 mm in other chambers. Electronics of the coordinate chambers consists of 64 channels modules. The total number of electronic channels is 12000. The output signal of 0.4 V is transmitted by 30 m long twisted pairs to logic electronics in the control room. This electronics includes the univibrators of 500

ns delay, the coincidence circuits, and the memory triggers. The chambers are placed inside two containers filled with the Ar + 20%CO_2 + 0.15%CF_3Br gas mixture. The width of the inlet windows is 0.5 mm of Al. The momentum is measured in the solid angle of $0.4 \times 4\pi$ sr with the resolution of $\sigma_p/p = 10\% \times p(GeV/c)$. For multiparticle events, when the vertex of event can be used for reconstruction, the momentum resolution is $\sigma_p/p = (4-12)\% \times p(GeV/c)$ in the solid angle of $0.6 \times 4\pi$ sr.

The coordinate chambers are surrounded by 24 scintillation counters placed at the surface of the cube of 1.2 m long edge. The counters are made of the NE-110 scintillator of $0.6 \times 0.6 \times 0.01 m^3$ size and employ 56DVP photomultipliers. The system covers the solid angle of $0.9 \times 4\pi$ sr. The pulse height resolution is 20 % for the minimum ionization particles. The time of flight resolution for cosmic particles is 0.6 ns.

The eight gas Cherenkov threshold counters are installed behind the scintillation counters. They cover the solid angle of $0.6 \times 4\pi$. The counters are filled with the ethylene at the pressure of 25 atm. The refraction index is 1.02, $\gamma_{thr} = 5$. The thickness of the counter vessel is 2 cm of Al. This system provides electron-muon separation up to momentum of 0.5 GeV/c and electron-pion separation up to 0.7 GeV/c. Pions and kaons are separated in momentum region from 0.7 to 2.5 GeV/c. In each counter the light is collected via quartz windows and mirror light guides on four 58DVP photomultipliers. The detection efficiency for relativistic particles is 95 % (Fig.2.4). The pre-threshold efficiency depends on the particle velocity and is less than 12 %, if one PM is required. After requirement of two PM's, the pre-threshold efficiency is less than 0.5 % with the detection efficiency for relativistic particles of 70 %.

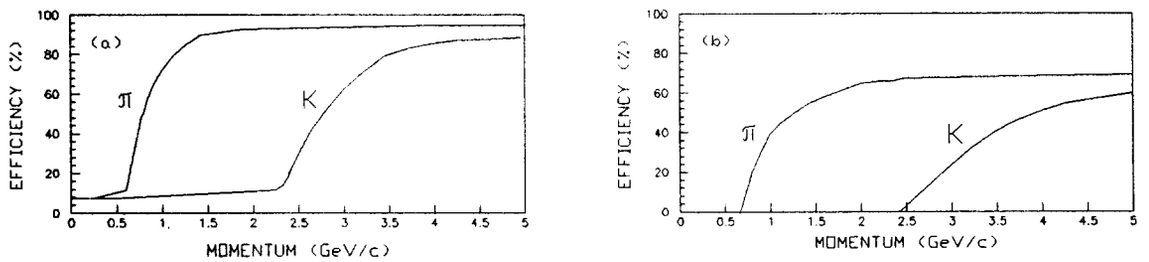

Fig. 2.4: Calculated dependence of the trigger probability of at least one (a) and at least two (b) PM of a Cherenkov counter versus the particle momenta for orthogonal incidence of pions and kaons

The shower-range system consists of 14 separate units each containing 10 layers of proportional chambers alternating with the 13 mm thick stainless steel plates. Gas mixture is Ar + 20%CO_2. Each layer has 16 electronics channels for coordinate measurements. One linear output signal is taken from each chamber for pulse height analysis. The covered solid angle is $0.8 \times 4\pi$ sr. The maximum size of the unit is $1.75 \times 0.81 m^2$. The energy resolution is $\sigma_E^2/E^2 = (12.6)^2 + (20.5)^2/E(GeV)$ while the angular resolution is $1-2^\circ$. The measurement of ionization losses and ranges allows to separate electrons, muons, and hadrons.

The muon system consists of 50 units with active area of 2.3 m^2 and 10 units with active area of 0.9 m^2. Each unit contains two proportional chambers which measure two orthogonal coordinates with the accuracy of 25 mm (rms). The muon chambers are placed behind the coil ($t \approx 420 g/cm^2$), inside the yoke ($t \approx 750\ g/cm^2$), and behind the yoke ($t \approx 1000\ g/cm^2$). The muon system covers the solid angle of $0.6 \times 4\pi$ sr.

The system for detecting of scattered electrons or the tagging system (TS) (Fig.2.3) contains two blocks with 7 proportional chambers and 3 scintillation counters at each side of the interaction region. The blocks are placed 3.5 m downstream from the interaction point at the distance 50 mm from the beam. Three chambers in each block measure the radial (Y) coordinate, three — the vertical (Z) one, and one serves for measurement of the oblique (T) coordinate. The chambers have a C -like shape and envelope the beam pipe from three sides. The sensitive radial size of the chambers is 500 mm, the vertical - 200 mm. For the Z- and T-coordinate measurements the usual proportional chambers were used. For the Y-coordinate measurements the induction chambers with cathode delay line read-out were chosen [7]. The anode wires of all chambers have 28 μm diameter and are made of the gold plated tungsten, its spacing is 4 mm. The 50 μm diameter cathode wires are made of bronze, its spacing is 1 mm. The gas mixture is Ar + 25%C_4H_{10} + 0.25%CF_3Br + 3%$C_3H_8O_2$. Behind the TS there is the system of four scintillation counters for luminosity measurement by elastic scattering at the small angles and sandwich ($5X_0$) used both for luminosity measurement and triggering. The system provides the resolution $\sigma_Z \sim 1$ mm and $\sigma_Y \sim 0.25$ mm.

The TS detects electrons emitted at zero angle with the energy loss $(E - E')/E = 0.1 - 0.5$. Electrons with beam energy E are detected for angles between 12 and 100 mrad. The momentum resolution of the TS is determined by multiple scattering in the entrance window of 0.035 X_0 thickness, chamber space resolution, the radial and longitudinal beam sizes. At the beam energy of 5 GeV the momentum resolution is 1.75% [8]. Fig.2.5 shows the TS invariant mass resolution of the double-tagged events versus the invariant mass. Fig.2.6 shows its efficiency for detection of one and both scattered electrons versus the invariant mass.

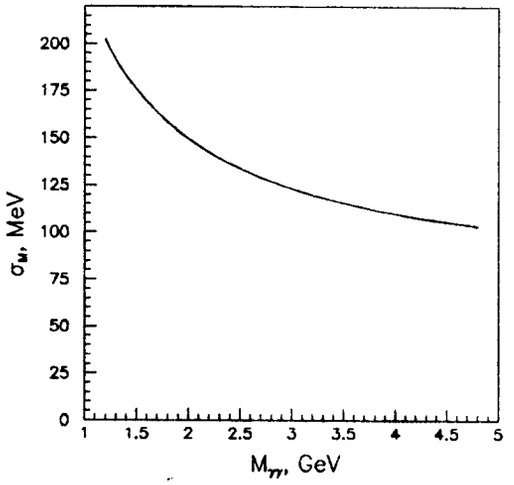

Fig. 2.5: Calculated dependence of $\sigma(M_{\gamma\gamma})$ on $M_{\gamma\gamma}$ for double-tagged events.

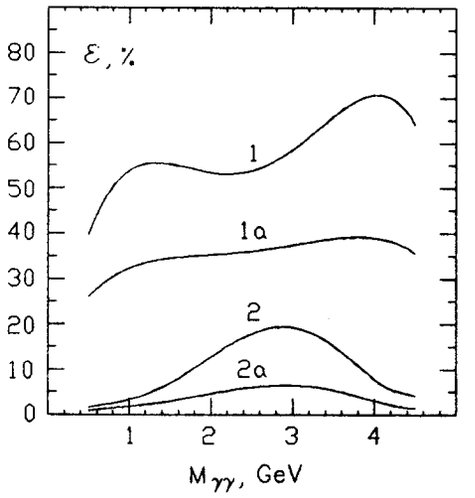

Fig. 2.6: Calculated efficiency for detection of scattered electrons vs invariant mass. Curves 1 and 1a: efficiency for the single-tagged events without and with $\vartheta_Z > 0.5$ mrad cut on emission angle of scattered electron. Curves 2 and 2a: efficiency for the double-tagged events without and with ϑ_Z cuts.

During experiments with the MD-1 the luminosity integral about 30 pb^{-1} was collected in the energy region 2E=7.2–10.4 GeV including about 23 pb^{-1} with detection of scattered electrons.

2.3. Trigger

As compared to detectors with the axial magnetic field, the background conditions in the MD-1 is considerably worse since all low-energy particles emitted mainly at small angle to the beam axis and swept by magnetic field go into the detector. At the luminosity of 10^{30} $cm^{-2}sec^{-1}$ this background was about 50 kHz ($\sim$ 6% of beam collision rate).

The trigger of MD-1 [9] included three levels; this permitted to suppress the background effectively without loss of the efficiency for the processes of interest.

For the first level trigger at least one scintillation counter and one unit of shower-range chambers (that is $\geq$ one layer in each projection) with switched off area $\pm$ 11 cm near the orbit plane was required. This trigger generated strobing pulses in 0.4 μs, during which "yes-no" information from wires was stored in memory modules and operation of ADCs and TDCs started.

For the second level trigger special sets of information from different parts of the detector were used and 32 "yes-no" arguments were formed. Then logical sum (having no more than 24 terms) of products of several arguments (preselected in advance) was obtained and in the case of positive decision all information was written to the memory of the M-6000 (HP-2116) computer. Operation time of the secondary trigger was 5 μs.

After event read out into M-6000, some additional on-line analysis based on the geometrical features of the effect and background events was performed which additionally suppressed the beam background and cosmic rays events (we call it as the third level trigger). The criteria for the first, second, and third level triggers could be flexibly changed with the help of the on-line program on M-6000. In the first approximation the trigger of MD-1 selected events with at least one scintillation counter and 2 units of shower-range chambers.

At the luminosity of $3 \cdot 10^{30}$ $cm^{-2}sec^{-1}$ the typical rate after the first level trigger was 1.5 kHz, after the second level trigger – 8 Hz, after the third level trigger – 3 Hz.

In the experiments on study of QED processes $\gamma e \to ee^+e^-$ and $e^+e^- \to e^+e^-e^+e^-$ nearby threshold a special trigger conditions were used (see subsection 3.2).

2.4. Background conditions

Our measurements have shown the following nature of the beam-gas background in the detector.

Firstly, there are particles leaving the equilibrium orbit and performing many turns before their ruin. The spatial density distribution of these particles (halo) is fairly broad and has sharp edges. The cut-off of the halo occurs at the point where the effective storage ring aperture is the smallest. If this point is near the detector, it causes an increase in the background counting rate. The cut-off of the halo was performed in radial direction in the VEPP-4 injection section.

Secondly, the beam electrons lose their energy by the bremsstrahlung on the residual gas in the straight section in front of the detector and hit the detector after deflection by the magnetic field.

To decrease the background trigger rate due to the bremsstrahlung of electrons in the straight section we used behind the detector special scintillation sandwiches detecting the bremsstrahlung photons. The vacuum chamber has thin windows in these directions. The angular distribution

of these photons is fairly sharp, therefore the sizes of the sandwiches are small (10×10 cm^2). These sandwiches were included in the trigger as veto counters that resulted in the reduction of the trigger counting rate by a factor of $2 \div 3$.

Thus in the case of separated beams the counting rate of the first level trigger via the charged particles channel (at least one particle was needed in the unit of three coordinate chambers and firing of at least one scintillation counter) was about 0.2 kHz/mA and via the neutral channel (two of ten chambers in the shower-range module were required) it was about 0.5 kHz/mA.

In the case of the beams collision the background rate was determined by the process $e^+e^- \to e^+e^-\gamma$. All electrons and positrons lost large fraction of their energy ($E_{e\pm} \leq 0.8$ GeV) were deflected by the transverse magnetic field into the detector. This leads to 30 kHz background rate in the detector at $L = 3 \cdot 10^{30}\, cm^{-2}sec^{-1}$. Most of these events have one particle with very small transverse momentum which hits the detector in the orbit plane. To suppress this background we switched off from the trigger the area of shower-range chambers adjacent to the orbit plane (± 11 cm). As a result the total rate of the first level trigger was reduced up to 1.5 kHz.

The second and third level triggers allowed to reduce the rate of the tape recorded events up to 3 Hz at the luminosity of $3 \cdot 10^{30}$cm^{-2}sec^{-1} and 10 mA beam currents.

A special study was devoted to solve the background problem caused by synchrotron radiation in the MD-1 detector [10]. The special vacuum chamber allowing synchrotron radiation to pass the detector without touching the beam pipe walls was created. Radiation receivers were placed at a rather long distance from the detector center, so that only backward scattered photons hit the detector. This allowed to reduce the photon flux on the central part of the vacuum chamber considerably especially in the hard part of the spectrum The movable collimators allowed to choose an optimal size of the vertical aperture. The radiation receivers are made of copper and were water cooled.

Such construction of the vacuum chamber has reduced the photon flux at the central part of the detector by a factor of 10^6. An additional attenuation was achieved by placing a thin foil on the cylindrical part of the vacuum chamber and in front of the TS. The cylindrical part was covered by the 3 mm thick Al and 0.1 mm Ta foils ($0.08\ X_0$) while the tagging system window was covered by the 0.17 mm thick Fe and 0.3 mm Sn foils ($0.03\ X_0$).

The background due to synchrotron radiation was essential only for the coordinate chambers and for the tagging system. The remaining elements of the detector were selfprotected by a thick layer of material.

The measurement at the beam energy of 4.7 GeV showed that the number of fired wires during one beam passage at the current of 1 mA was 0.1 for the coordinate chamber nearest to the beam and 0.03 for the most distant one. For the chamber of the tagging system the corresponding value was 0.01. The experimental data agree with calculations within a factor of two. These background conditions allowed to operate at the Υ-meson energy with the currents up to 10×10 mA^2.

2.5. Data acquisition and processing

2.5.1. Data acquisition

The mode of the detector operation, data readout and recording to magnetic tape was controlled by the single program on the M-6000 computer. This program gave possibility to set

up selection criteria for the first and second level triggers, to start and to stop runs, to monitor background conditions, to display events and so on. The mean time of event readout via CAMAC crates was equal to 8 ms, total time of event processing was about 60 ms.

Events with average length equal to 500 byte could be written on magnetic tape with rate up to 5 Hz. During the experiment losses of luminosity due to the dead time of the data acquisition system did not exceed several percent.

2.5.2. The detector simulation

The MD-1 simulation was based on the UNIMOD1 code [11] developed in our Laboratory, which is a general-purpose detector simulation code for the complicated detector geometry including a detailed simulation of electromagnetic and hadronic particle interactions. Nuclear interactions were simulated by the NUCRIN code [16] slightly improved for low energy particles. The program UNIMOD1 and a new version UNIMOD2 [12] were written at the same time as GEANT [13] at CERN which is now the most widely used code. Results of simulation are similar for both codes [14]. The main difference lies in organization of data input. In the UNIMOD codes the detector description is written on separate numerical files on disk. This is more convenient for simulation of large detectors. Besides the MD-1, the UNIMOD1 was used for the simulation of the ND (Neutral Detector) experiments [15] as well as for methodical calculations.

2.5.3. Data processing

The most hard point of our data processing work was that we could not afford to keep the sufficient amount of data on magnetic disks. Our experimental and simulated data were written onto magnetic tapes with 800 bpi density. There were about 3000 tapes used for all experiments with the MD-1 detector.

In order to make the operations with this number of tapes convenient and reliable we developed a specialized data management system allowing to request the data with the help of catalogue names and run numbers [17].

This system combined with the special event selection and histogramming package [18] provided good conditions for cooperating of efforts of all physicists involved in data processing.

The detector simulation and data processing were carried out with ES-1061 computers (of IBM-360 type).

2.6. Luminosity measurement

The elastic e^+e^- scattering at small angles ($\sim 1°$) was used in MD-1 at VEPP-4 for operative luminosity measurements in most experiments [19]. Special studies showed that this monitor (SA monitor) provides good accuracy, results of these studies are presented below. For the large cross section experiments ($e^+e^- \to e^+e^-e^+e^-$ nearby threshold [20] and $\gamma e \to ee^+e^-$ [21]) the single and double bremsstrahlung (DB) were employed.

The SA monitor provided good relative accuracy (better than 1.5 %) of the luminosity measurement. But calculation of the visible cross section for the Bhabha scattering could not be performed with high accuracy in our case because of the complicated geometry of the SA monitor. The absolute calibration of the SA monitor was done during two runs by three independent methods: using double bremsstrahlung in a special experiment [19], the large angle e^+e^--scattering (LA) at $\Theta > 45°$ and the process $e^+e^- \to \mu^+\mu^-$ (MM) [22]. In Table 2.2 the results of this

calibration are presented. It contains also the results of the relative calibration using elastic e^+e^--scattering at medium angles (MA, $12° < \Theta < 45°$).

Table 2.2: The results of the SA monitor calibration. 2E=9.46 GeV

Method	Run	$\sigma_{SA} \times 10^{29}\text{cm}^2$	$\sigma_{SA}^{(1)}/\sigma_{SA}^{(2)} - 1, [\%]$
DB	1	$3.58 \pm 0.05 \pm 0.11$	
LA	1	$3.75 \pm 0.07 \pm 0.04$	
		± 0.06	6.8 ± 3.3
	2	$3.51 \pm 0.08 \pm 0.04$	
MM	1	3.88 ± 0.13	
		± 0.06	8.9 ± 3.6
	2	3.56 ± 0.05	
MA	-	-	6.0 ± 1.8

The cross section σ_{SA} of the SA monitor is different for the first and second runs. This difference is associated with the modification in the SA monitor during the shutdown between the runs. Using the results of the relative calibration by MA, weighted value of $\overline{\sigma}_{SA}$ for the second run was obtained (at $2E = 9.4$ GeV): $\overline{\sigma}_{SA} = (3.52 \pm 0.05) \cdot 10^{-29}\text{cm}^2$.

The comparison between the calibration by the central part of the detector (LA,MM) and by the DB gives $\chi^2 = 1.8$ for 1 degree of freedom. Applying the scale factor of $\sqrt{1.8}$ we obtained an 1.9% accuracy for the absolute calibration of the SA monitor.

The final value of the visible cross section $\overline{\sigma}_{SA}$ is:

$$\overline{\sigma}_{SA} = (3.52 \pm 0.07) \cdot \left(\frac{9.46}{2E(\text{GeV})}\right)^2 \cdot 10^{-29}\text{cm}^2.$$

3. QED experiments

3.1. Process $e^+e^- \to e^+e^-\gamma$

The process of single bremsstrahlung (SB) $e^+e^- \to e^+e^-\gamma$ was the first process observed with colliding beams [23]. The SB cross section was measured with an accuracy of 30% at the VEP-1 storage ring [24]. Before this experiment [25] (excluding the studies of large-angle photon production), there were no other publications devoted to the experimental investigation of SB. The SB cross section was calculated in Refs. [26, 27].

In 1953 Landau and Pomeranchuk noticed that the bremsstrahlung of relativistic electrons on nuclei is formed at a large length (the coherent length) [28]:

$$l_c \sim \gamma(E - \omega)/m_e\omega \quad (\hbar = c = 1),$$

where $\gamma = E/m_e$, ω is the photon energy, m_e is the electron mass, and E is the electron energy. If an electron undergoes any external influence at this length then radiation fails. For example, multiple scattering appears to be such an influence [28]. This phenomenon was observed in [29]. The influence of an external magnetic field on the bremsstrahlung of electrons on the nucleus was considered in Ref. [30] where this effect was shown to be small for the practically used fields. In

experiments with colliding e^+e^- beams as it was shown by Nikishov [31] and Baier and Katkov [32] the influence of the magnetic field should be much stronger than in the radiation on the nucleus.

The first results obtained by us in 1980 showed that the SB cross section is less than that given by the standard QED calculation. We have suggested that the effect is due to the large impact parameter cut-off since the characteristic impact parameters in the process are considerably larger as compared to the transverse sizes of the colliding beams. The results of this experiment stimulated the theoretical research (see Refs. [33]-[35]). In 1981 we carried out the second cycle of experiments for the more detailed investigation of this effect.

In the standard QED the SB cross section has the form [26, 27]:

$$d\sigma/d\omega = 4\alpha r_0^2 \omega^{-1}[(E-\omega)/E](v - \frac{2}{3})[ln(m_e/q_{min}) - \frac{1}{2}], \tag{3.1}$$

where $v = (E-\omega)/E + E/(E-\omega)$, $q_{min} = m_e\omega/4\gamma^2(E-\omega)$, α is the fine structure constant, and r_0 is the classical electron radius.

The main contribution to the photon emission with energy ω is given by virtual photons with energy $\omega_v = m_e\omega/4\gamma(E-\omega)$, which are formed at the length [32]:

$$l_v \sim 4\gamma^3(E-\omega)/m_e\omega.$$

In our experiment at E=1840 MeV for the minimal photon energy $\omega \sim 0.5$ MeV, $l_v \sim 1$ km!

For the applicability of the formula (3.1) in experiments the following macroscopic effects impose restrictions:

(1) The length L of the straight section of the storage ring must be larger than l_v [33, 36]:

$$L > l_v.$$

(2) The transverse beam sizes $\sigma_\perp$ must be larger than the characteristic impact parameter ρ :

$$\sigma_\perp > \rho \sim 1/q_{min} = 4\gamma^2(E-\omega)/m_e\omega.$$

The finiteness of the transverse sizes of the beam results in a decrease of the virtual photon forming length to the value:

$$l_\perp \sim \sigma_\perp^2\omega/\gamma^2.$$

In our experiment $l_\perp = 0.5$ mm.

(3) The magnetic field must be less than H_c (Refs.[32], [35]-[38]):

$$H < H_c \sim (H_0/4\gamma^3)\omega/(E-\omega),\ H_0 = 4.41 \cdot 10^{13}\ \text{G}.$$

At E=1840 MeV and ω=0.5 MeV, $H_c \sim 0.064$ G.

In Table 3.1 the criteria of applicability of the standard QED cross section are listed for our conditions. One can see that in our experiment formula (3.1) could be valid only for the hard component of the spectrum at $\omega > 1000$ MeV. The most essential effect is that associated with the finite transverse sizes of the beams. It is predominant for the other operating storage rings as well.

Table 3.1: Values of parameters necessary for applicability standard QED bremsstrahlung cross section. Energy of experiment E=1840 MeV

Effect	Valid (3.1)	Typical value	At ω=0.5 MeV	At ω=1000 MeV
Straight section length (L)	$L > l_v$	L=1÷10 m	l_v ~1000 m	l_v ~1 m
Transverse beam size ($\sigma_\perp$)	$\sigma_\perp > \rho$	$\sigma_\perp \sim 3 \cdot 10^{-3}$ cm	$\rho \sim 5$ cm	$\rho \sim 10^{-3}$ cm
Magnetic field (H)	$H < H_c$	H=0÷5 kG	H_c ~0.06 G	H_c ~280 G

After the first cycle of our experiment a formula which takes into account the beam transverse sizes has been derived [34, 35]. For the gaussian distribution of the beam density the cross section takes the form:

$$d\sigma/d\omega = 4\alpha r_0^2 \omega^{-1}[(E-\omega)/\omega](v - \frac{2}{3}) \times \{ln[\sigma_x\sigma_z/\lambda_C(\sigma_x+\sigma_z)] + ln2 \qquad (3.2)$$

$$+\frac{1}{2}C + (v - \frac{5}{9})/(v - \frac{2}{3})\},$$

where C=0.577, σ_z and σ_x are the vertical and radial beam sizes respectively, and λ_C is the Compton wavelength of the electron. The formula holds when $q_{min}\sigma_z\sigma_x/\gamma(\sigma_x+\sigma_z) \ll 1$.

The other possible macroscopic effects in the process $e^+e^- \to e^+e^-\gamma$ were analyzed in Refs. [33, 35].

The experiment was carried out at the energy of 2 x 1840 MeV in the interaction region intended for the detector MD-1, with the magnetic field perpendicular to the orbit plane of a storage ring. During the first series of measurements three magnets were installed instead of the MD-1. The presence of these magnets made it possible to have any field within the range ±6 kG at the interaction region. The second series of measurements was carried out with the magnet of the MD-1 detector.

The scheme of the last measurement in 1981 is shown in Fig.3.1. The arrangement of the inter-

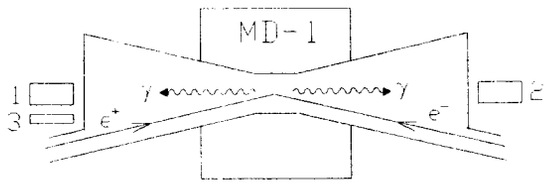

Fig. 3.1: Schematic view of the experimental layout: 1,2 - NaI(Tl) counters for SB and DB detection; 3 - NaI(Tl) counter for control of background.

action region in the transverse magnetic field provides a low background from the bremsstrahlung on the residual gas, since the radiation from only a small part of the orbit gets to the counter.

The photon spectrum in the range of 0.4 – 1840 MeV was measured. To detect the photons a NaI(Tl) crystal with a size of 47 × 12 × 12 cm^3 was used (counter 1 in Fig.3.1).

Normalization was performed by the double bremsstrahlung (DB) process $e^+e^- \to e^+e^-\gamma\gamma$. This process [39] occurs at distances $\sim \lambda_C$ and macroscopic effects do not affect it. To detect the DB, counter 1 was switched on in coincidence with counter 2.

In 1980 three measurement series were performed at three values of the magnetic field at the interaction point: $0, +3$ kG and -3 kG. In 1981 several series of measurements were performed, in which the vertical and azimuthal sizes of the beams and the electron current were varied as well as the measurement with the beams separated in the vertical direction by $3\sigma_z$. The magnetic field in the 1981 experiment was not changed and was equal to 5 kG.

The background due to the bremsstrahlung on the residual gas was measured when beams were separated in the vertical direction by $15\sigma_z$. The background magnitude was controlled by the counter 3.

The other source of background is due to the Compton scattering of the synchrotron radiation produced in magnetic field by a colliding beam. This phenomenon was not earlier studied experimentally. In the paper [35] it was noted that there is no sharp boundary between real intermediate photons and virtual photons in the bremsstrahlung process in a magnetic field. In our computation of this background we assumed all the photons to be real. Some estimates, according to Ref. [35], show that this can lead to errors in the measured spectrum which do not exceed 3% in the whole range of the spectrum.

Fig.3.2 presents the results of the measurements of the spectrum carried out in 1980 and 1981. In both cases the calculated background from the scattering of the synchrotron radiation by a

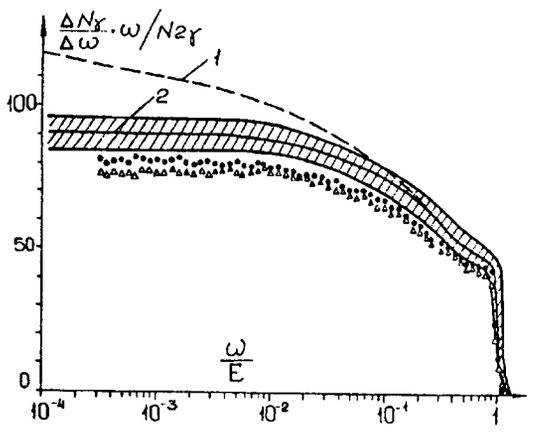

Fig. 3.2: A spectrum of SB photons: dark circles – the experiment in 1980, $\sigma_z = 23 \pm 3$ μm; open triangles – the experiment in 1981, $\sigma_z = 24 \pm 3$ μm; 1 – the standard QED calculation; 2 – the calculation taking into account the effect of the large impact parameter cut-off [34, 35].

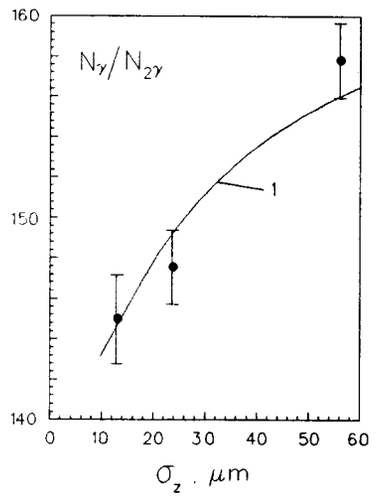

Fig. 3.3: The dependence of the ratio $N_\gamma/N_{2\gamma}$ on the vertical beam sizes. N_γ is the number of SB photons in the range 0.5–3.0 MeV, $N_{2\gamma}$ is the number of DB photons. 1 – calculation taking into account the effect of the large impact parameter cut-off [34, 35].

colliding beam has been subtracted. Curve 1 is the standard QED calculation. Curve 2 is the calculation when the large impact parameter cut-off was taken into account. The width of the

shaded area corresponds to two mean-square errors. The error of 6% is due mainly to systematic errors. The results of the 1980 and 1981 experiments agree with each other and are in agreement with the theoretical calculation.

Fig.3.3 demonstrates the dependence of the ratio $N_\gamma/N_{2\gamma}$ on vertical beam sizes, where N_γ is the number of SB events in the range 0.5 – 3.0 MeV, $N_{2\gamma}$ is the number of DB events. Curve 1 is the calculation by the formula (3.2). The experiment is in agreement with the calculation: $p(\chi^2) = 0.45$.

Since in the process $e^+e^- \to e^+e^-\gamma$ the large impact parameters are essential, the probability of the occurrence of SB is noticeable, even in the case when the beams are separated by distances larger than their sizes. The corresponding calculations for the gaussian distribution of the particles density in the beams were performed in Ref.[34]. In the experiment the ratio $R = N_\gamma/N_{2\gamma}$ has been measured at the beam separation $\Delta z = 3\sigma_z$ and at $\Delta z = 0$. The experimental result $R(\Delta z = 3\sigma_z)/R(\Delta z = 0) = 1.20 \pm 0.05$ is in agreement with the calculated ratio of 1.24.

In conclusion we point out that the effects associated with the cut-off of the large impact parameters are expected for the single photon bremsstrahlung and e^+e^- pair production at existing and planned high energy ee, ep and eγ colliders [40]. At the HERA collider the luminosity measurement by the process $ep \to ep\gamma$ is being carried out with account of this effect [41].

3.2. Process $\gamma e \to ee^+e^-$

Production of e^+e^- -pairs by high-energy photons in the field of an electron [42] belongs to the reactions studied by Bethe and Heitler as early as the beginning of 30's [43]. The transverse magnetic field of MD-1 gave a possibility of experimental study of this process with the detector [21]. In our case the Bethe-Heitler process

$$\gamma e \to ee^+e^- \tag{3.3}$$

is caused by synchrotron radiation (SR) photons produced in the detector, which collide with the second beam electrons in the interaction region (see Fig.3.4).

Unlike previous experiments on atomic electrons [44, 45] in this case photons interact with free electrons.

However another problem arises in such an experiment: a considerable part of SR photons is formed inside the "target" - a colliding electron bunch. In this case the photon can cause the Bethe-Heitler process (or the Compton scattering process [46]) when its formation has not been finished. As far as we know, the problem of cross section calculation in this situation has not yet been solved. Naturally, the difference from the case of real photons depends on the relationship between the photon formation length l_c [47] and the effective distance to the colliding bunch electron. In our experiment we had $l_c \leq 0.4$ cm, and the effective distance which the photon flights before collision with an electron was [10]

$$l_0 \approx \sqrt{2R\sigma_r}, \tag{3.4}$$

where R is the orbit radius, σ_r is the rms radial beam size. For our experiment $l_0 \approx 14$. Hence, for the 10 % accuracy of this experiment one should not see a contribution of interactions with distance $\sim l_c$.

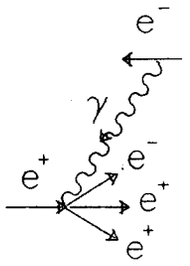

Fig. 3.4: Schematic view of the process $\gamma e \rightarrow ee^+e^-$.

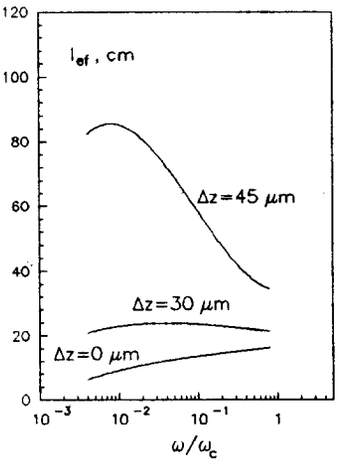

Fig. 3.5: Energy dependence of the effective length l_{ef} for E=5.14 GeV, magnetic field H=12.5 kG, σ_z=12.5 μm, σ_r=0.07 cm.

It is convenient to introduce an "effective" cross section connected with the luminosity of electron-positron beams by the usual relationship $\dot{N} = \sigma_{ef} \cdot L$:

$$\sigma_{ef} = \int_{\omega_{min}}^{\omega_{max}} \frac{dN}{d\omega dt} \frac{l_{ef}(\omega)}{c} \sigma(E,\omega) d\omega. \tag{3.5}$$

Here $dN/d\omega dt$ is the SR spectrum, ω_{min} and ω_{max} are the limits on the SR energy determined by detection conditions, $l_{ef}(\omega)$ is the effective length of the beam orbit from which SR photons contribute to the counting rate, $\sigma(E,\omega)$ is the cross section of the process under consideration, E, ω are the beam and SR photon energy, and c is the velocity of light.

The result of the calculation of $l_{ef}(\omega)$ for several values of the vertical distance between beams Δz and typical experimental conditions is shown in Fig.3.5. The calculation was carried out using formula for l_{ef} obtained for gaussian beams [21]. One can see that the vertical displacement of the beams increases l_{ef}, causing an increase of the "effective" cross section (but not the counting rate).

For the Monte Carlo generator of events we used the differential cross section calculated for main diagrams and unpolarized particles. We checked that in this case cross section (3.5) differs less than by 1% from the calculation taking into account all diagrams of the third order in α [42]. The contribution of radiative corrections must be small also [44].

The main physical background, kinematically indistinguishable from the effect, comes from the process first calculated by Landau and Lifshitz [48]

$$e^+e^- \rightarrow e^+e^-e^+e^- \qquad \text{(Landau – Lifshitz process)} \tag{3.6}$$

This process was for the first time observed at the VEPP-2 collider [49]. It was well studied theoretically [50, 51, 52] and was measured by many detectors [53, 54], as well as by the MD-1 [20, 214] (see Section 11).

The "effective" cross section of the process $\gamma e \rightarrow ee^+e^-$ and the cross section of $e^+e^- \rightarrow e^+e^-e^+e^-$ as a function of the beam energy E are shown in Fig.3.6. One can see that at the energy about 5 GeV these cross sections are comparable. The cross section calculation of the process $e^+e^- \rightarrow e^+e^-e^+e^-$ was performed using the main diagrams with the code [55].

The calculation of cross sections for Bethe-Heitler and Landau-Lifshitz processes at E = 5.14 GeV for the effective mass of e^+e^- -pair greater than a certain value showed that the "effective" cross section for $\gamma e \rightarrow ee^+e^-$ quickly decreases due to exponential decrease of the SR intensity at the energy above the critical energy ω_c (which is $\approx$ 22 keV in our case) [21]. The calculation of the distribution in SR photon energy under the detection conditions showed that SR photon energy lies in region $\omega \approx 1 - 20$ keV, the distribution is peaked at $\omega \approx 2$ keV and has average $< \omega > \approx 4$ keV. The distribution of detected events in the invariant mass of e^+e^- -pair is peaked at low masses and has average $< W > \approx 2$ MeV.

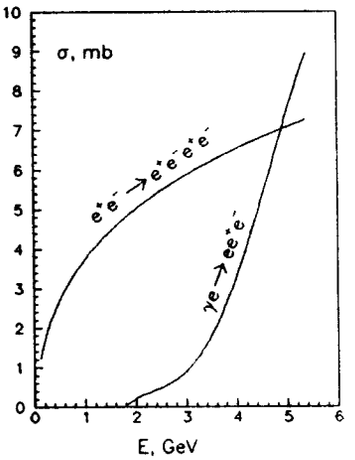

Fig. 3.6: Cross sections of the processes $\gamma e \rightarrow ee^+e^-$ and $e^+e^- \rightarrow e^+e^-e^+e^-$ vs beam energy. H, σ_z, σ_r change with the beam energy.

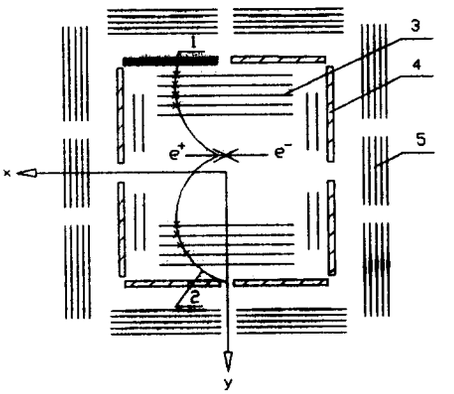

Fig. 3.7: View of an event in the MD-1 detector from above: 1, 2 – a detected e^+e^- -pair; 3 – coordinate chamber; 4 – scintillation counters; 5 – shower-range chambers.

The experiment was carried out at the energy 2E=2×5.14 GeV, the magnetic field during the experiment was 12.5 kG. Data from the coordinate chambers and scintillation counters were used in the trigger and for the analysis of events. For trigger the firing of one or more scintillation counter and several coordinate chambers from both sides of the beam were required.

For the luminosity measurement two processes were used: single bremsstrahlung and small angle Bhabha scattering. In the former the effect of impact parameters cut-off by transverse beam sizes as well as the Compton scattering of SR on the colliding beam were taken into account [56]. Systematic errors of the luminosity measurements in this experiment was about 10%. Typical luminosity in this experiment was $3 \cdot 10^{29}\, cm^{-2} sec^{-1}$.

Events were recorded in three runs. In total 74000 events were recorded for head-on beam collisions ("effect Δz=0"), 151000 events for beams, separated at several σ_z ("effect $\Delta z \neq 0$ ") and 15000 events for large displacement in vertical direction ("background"). The ratio of the recording time for the "effect" to that of the "background" was about 7. The integrated luminosity of 46 μb^{-1} was collected.

The radial beam size was 0.07 cm with error about 10%. The size σ_z was varied in different

runs in the range of 12 - 16 μm. The measurement of σ_z was performed by the dependence of the luminosity on the vertical displacement of the beams. In the experiment the currents of beams were chosen small ($\leq$ 3 x 3 mA^2) in order to avoid the collision effects. The absence of these effects was checked by the luminosity dependence on the vertical displacement of beams that was close to Gaussian.

Selection of the effect events was performed using criteria based mainly on the geometrical characteristics of the event (Fig.3.7). A a result, in the "effect Δz=0" measurements 324 events remained, 206 events were found in "effect $\Delta z \neq 0$" measurements, and no events were found in the "background" measurements,

The measured and calculated distributions of events in the particle momenta are shown in Fig.3.8. These distributions are in good agreement with each other. The distributions are normalized to the number of MC events. For the experimental points the statistical errors are shown.

The distribution in the effective mass of produced e^+e^- -pair obtained in experiment is also in agreement with the calculated one. But it is broader than the distribution in the original mass of pair in simulation because of the multiple scattering of the particles in the beam pipe.

The probability of firing scintillation counters (the inefficiency is due to 1.5 X_0 Fe in front of the counters) was 55±2 % in experiment, in good agreement with 56.7±1.6 % in simulation. This confirms that the detected particles are electrons.

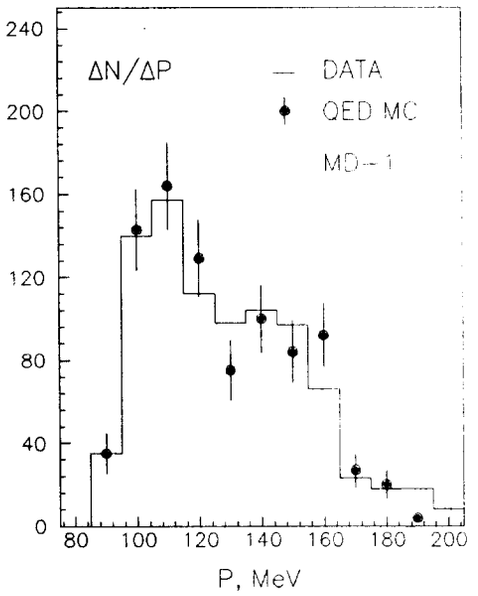

Fig. 3.8: Distribution in particle momenta.

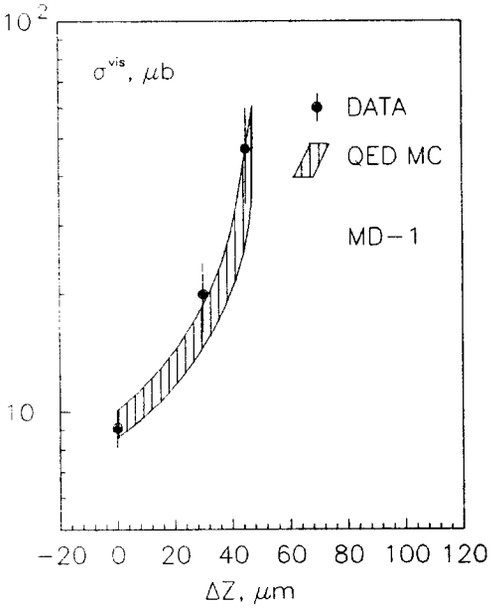

Fig. 3.9: Dependence of the visible cross section $\gamma e \to e e^+e^- + e^+e^- \to e^+e^-e^+e^-$ on the vertical displacement of beams for one experimental run. $\sigma_z = 13 \pm 0.5$ μm.

The effect of increase of "effective" cross section of the Bethe-Heitler process with the vertical displacement of the beams was measured in all experimental runs. The measured and calculated dependence of visible cross section $\sigma^{vis}(\Delta z) = \sigma_{B-H}(\Delta z) + \sigma_{L-L}$ on the displacement Δz in one

of the runs is shown in Fig.3.9. In the MC cross section the measured correction factor due to the inefficiencies of the coordinate chambers is taken into account. In the error bars we have included the statistical errors, the uncertainty of the luminosity measurements, and the errors due to uncertainties in the vertical beam size. The dashed area is the result of the calculation, the width of the shaded band equals two rms errors.

Calculations for Δz=0 showed that the cross section of the Bethe-Heitler process depends weakly on the vertical beam size. This allowed us to sum statistics of all runs. The obtained experimental cross section for Δz=0, corrected for the chamber inefficiencies, is equal to

$$\sigma^{vis} = 9.1 \pm 1.0\ \mu b,$$

where the error includes the statistical error (5.5%), the uncertainty of the luminosity measurement (10%) and the error in determination of the chamber efficiencies (2.6%). The errors are added in quadrature.

The calculated cross sections of the Bethe-Heitler and Landau-Lifshitz processes are equal to $\sigma^{MC}_{B-H} = 7.1 \pm 0.7\ \mu b$ and $\sigma^{MC}_{L-L} = 2.5 \pm 0.4\ \mu b$ respectively. The total Monte Carlo cross section is equal to

$$\sigma^{MC} = 9.6 \pm 0.8\ \mu b$$

Thus, the measured cross section is in agreement with the standard QED calculation, and we have not seen an influence of the photon formation length on the cross section. However a situation can arise, as for example at VLEPP [57], when coherent length of low energy synchrotron photons becomes of the order of the bunch length. In this case the discussed effect would play a noticeable role in interactions of such photons with colliding beam electrons and with each other.

4. Precise measurement of Υ masses

4.1. Storage ring energy calibration

In this subsection the calibration of the storage ring energy by the method of resonance beam depolarization is described, which is a basis of a series of precise experiments performed with MD-1. This method developed in our Institute [58, 59] was used at VEPP-2M storage ring for measurements of the ϕ -meson [60], charged [61] and neutral [62] kaon masses, and also at the VEPP-4 storage ring for the measurement of the Ψ, Ψ' [5], Υ [56, 63, 73, 74], Υ' [63, 64], and Υ'' -meson [63, 64] masses. This method was used also for the energy calibration of CESR and DORIS storage rings in the mass measurement of Υ [65] and Υ' -mesons [66].

The energy calibration by the resonance beam depolarization method is based on the measurement of the electron spin precession frequency Ω around the guiding magnetic field of the storage ring.

The precession frequency equals [67]:

$$\Omega = \omega_s(1 + \frac{\mu'}{\mu_0}\gamma), \tag{4.1}$$

where ω_s is the beam revolution frequency, μ'/μ_0 is the ratio of the anomalous and normal parts of the electron magnetic moment, γ is the relativistic factor of electrons. The resonant influence

of a weak high frequency electric field on the polarized beam is used for the measurement of the spin precession frequency. The beam becomes depolarized when the frequency of the external field coincides with that of the spin precession. Fixing the fact of depolarization and measuring the corresponding depolarizer frequency, one can thereby perform the absolute energy calibration of the storage ring.

The method allows to measure the average electron energy with an accuracy $\sim 10^{-5}$, much better than the beam energy spread. It is provided by the fact that particles undergo many energy oscillations during the depolarization time, i.e. the depolarization time should be much longer than the period of the synchrotron oscillations.

In the electron storage rings there exists the mechanism of the spontaneous beam polarization connected with the synchrotron radiation [68]. For a homogeneous magnetic field, the time dependence of the polarization degree $P(t)$ was calculated in the paper [69]:

$$P(t) = P_0[1 - \exp(-\frac{t}{\tau_p})], \tag{4.2}$$

$$P_0 = -\frac{8}{5\sqrt{3}} = -0.924, \tag{4.3}$$

$$\frac{1}{\tau_p} = \frac{5\sqrt{3}}{8}\alpha\left(\frac{\lambda_e}{\rho}\right)^2\gamma^5\omega_s, \tag{4.4}$$

where α is the fine structure constant, λ_e is the Compton wavelength of the electron, ρ is the orbit radius, γ is the relativistic factor, τ_P is the polarization time. For the VEPP-4 storage ring the polarization time τ_p is about 50 minutes in the Υ meson energy region.

Inhomogeneous storage ring fields have the depolarization influence on the beams. The degree of the equilibrium polarization P depends on the relative powers of the depolarizing and polarizing mechanisms τ_p/τ_d and is reached for the characteristic time τ [70]:

$$P(t) = P[1 - \exp(-\frac{t}{\tau})], \tag{4.5}$$

$$P = P_0\frac{\tau_d}{\tau_p + \tau_d}, \tag{4.6}$$

$$\tau = \tau_p\frac{\tau_d}{\tau_p + \tau_d}. \tag{4.7}$$

The main influence on the equilibrium beam polarization degree appears to be of the vertical orbit distortions and proximity of the spin precession frequency Ω to the resonance frequencies Ω_{res} [71],

$$K\Omega_{res} = K_s\omega_s + K_x\omega_x + K_z\omega_z + K_\gamma\omega_\gamma, \tag{4.8}$$

where ω_s is the revolution frequency, ω_x and ω_z are the radial and vertical betatron oscillations frequencies, ω_γ is the synchrotron oscillation frequency, K_i are the integer numbers.

In the $\Upsilon(1S)$ energy region the spin precession frequency for the electrons in VEPP-4 storage ring is far from the resonance frequencies, and the degree of the equilibrium beam polarization

depends only on the vertical orbit distortions. Using orbit corrections the mean square deviation of the orbit from the plane in VEPP-4 was decreased to the value of 1.3 ± 0.5 mm , that provides the degree of the equilibrium beam polarization 0.4 – 0.6.

The resonance beam depolarization was performed by the alternating electric field of 10 V/cm amplitude, created between the pair of the vertically spaced plates of 1.3 m length. The external field changes the spectrum of the resonance frequencies,

$$K\Omega_{res} = K_s\omega_s + K_x\omega_x + K_z\omega_z + K_\gamma\omega_\gamma + K_d\omega_d, \tag{4.9}$$

where ω_d is the external field frequency (the field of depolarizer). The following resonance conditions were chosen for the measurements: $K = 1$, $K_s = -11$, $K_x = K_z = K_\gamma = 0$, $K_d = 1$, i.e.

$$\Omega_{res} = -11\omega_s + \omega_d. \tag{4.10}$$

At the frequency $\omega_s = 818.78$ kHz the frequency of the depolarizer field is about $\omega_d \simeq 18.6$ MHz.

In our experiments the depolarizing resonance width was determined by the frequency band of the generator creating the depolarizing field and was about 0.3 kHz. At the chosen value of the field the calculated depolarization time was about 0.5 second. The search for the depolarization frequency was performed by the slow variation of the external generator frequency (4 Hz for 1 second).

The beam polarization in the storage ring was measured by the value of asymmetry in the angular distribution of the back-scattered circular-polarized photons. The cross section of the Compton scattering is [72]:

$$\frac{d\sigma}{d\Omega} = \frac{d\sigma_0}{d\Omega} + \frac{d\sigma_1}{d\Omega}\xi|\vec{\zeta}|\sin(\varphi), \tag{4.11}$$

where $d\sigma_0/d\Omega$ is the cross section on the unpolarized electrons, ξ is the degree of the photon circular polarization, $\vec{\zeta}$ is the vector of electron transverse polarization, φ is the angle between the scattering plane and the plane, perpendicular to the vector $\vec{\zeta}$. The sign of $d\sigma_1/d\Omega$ is opposite to the one of the value $\xi(\vec{k}\vec{\zeta})$, where $\vec{k}$ is a momentum of the scattered photon. This value has maximum at $\varphi = \pm\pi/2$, i.e. when the vector $\vec{\zeta}$ lies in the scattering plane. Thus, while the scattering of the circular polarized photons on the transverse polarized electrons, the "up-down" asymmetry appears with respect to the orbit plane. The asymmetry value A is given by the formula [72]:

$$A = \frac{d\sigma_1}{d\sigma_0} = -\frac{2\lambda n(1+n^2)}{2\lambda^2(1+n^2) + (1+n^2+2\lambda)(1+n^4)}, \tag{4.12}$$

where $\lambda = 2\omega E/m_e^2$, $n = \gamma\theta$, θ is the emission angle of the photon relative to the electron momentum $\vec{p}$, ω is the initial photon energy, E is the electron energy.

The asymmetry value reaches its maximum $A_{max} \simeq -1/3$ at $\lambda \simeq 1$ and $n \simeq 1$, i.e. at the initial photon energy $\omega \simeq m_e^2/2E$ that gives 25 eV at the electron energy E=5 GeV.

In the experiments with MD-1 the synchrotron radiation generated in the magnetic field of the detector by oppositely moving beam was used as a source of the circular polarized photons [46]. In the interaction region the electrons collide with the synchrotron radiation photons generated

by another beam. The polarization of the synchrotron radiation depends on the photon direction. In the orbit plane the photons are linearly polarized and out of it they have circular polarization with the opposite signs above and under the orbit. The degree of the circular polarization increases with increasing of the photon emission angle relative to the orbit plane. When the beams are separated in the vertical direction, the collision of the circular polarized photons with the transversely polarized electrons and positrons is provided in the interaction region. The method allows to measure the polarization of both beams simultaneously. The asymmetry value in the synchrotron radiation scattering on the colliding beam is considerably greater than that in the laser photons scattering. It is due to higher energies of the initial photons.

The equipment for the beam polarization measurement is shown in Fig.4.1. Two identical systems were located from the both sides of the interaction region and were intended for the polarization measurement of both beams. Each system for backscattered photons detection included two scintillation counters with the 13 mm lead plate installed in front of it. One counter was placed above the orbit plane and another one was under that plane. There was a gap of 1 mm between the counters. The asymmetry value was determined by the ratio:

$$A = \frac{N_u - N_d}{N_u + N_d - N_{ud}}, \tag{4.13}$$

where N_u and N_d are the counting rates of the upper and lower counters correspondingly, N_{ud} is the coincidence counting rate. The photon energy (higher than 0.5 GeV) was measured using the total absorption counter made of NaI(Tl) crystals.

For the stabilization of the vertical orbit position and the orbit angle in the vertical plane, the ionization chambers were installed from the both sides of the interaction region for measuring the "up-down" asymmetry of the straight synchrotron radiation of the beams. The results of the measurements were used for the continuous orbit correction in the interaction region that was carried out with the help of a computer controlling VEPP-4 storage ring.

During the polarization measurement the beams were separated vertically by 60 micrometers ($\sim 4\sigma_z$, where σ_z is the vertical size of the beam). For this separation the relative error of the asymmetry measurement is minimal.

For the beam polarization degree of 0.8 the asymmetry value is 5%. The statistical error in the asymmetry value equals 0.4% for the currents of $6 \times 6\,\mathrm{mA}^2$ and exposition time of 100 seconds.

The result of one of the beams polarization measurement is shown in Fig.4.2. The electron and positron depolarization frequencies were obtained by the maximum likelihood method. The dependence of the beam polarization degree on time (and hence on the depolarization field frequency) was approximated by three straight line segments. The accuracy of the measurement of the beam depolarization frequency is determined by the accuracy in the asymmetry measurement and by the size of asymmetry jump, i.e. depends on the beam currents and on the beam polarization degree.

The results of the energy calibration in our experiment on precise $\Upsilon(1S)$ mass measurement [73, 74] described in subsection 4.2 were the following. The typical statistical accuracy of the electron and positron energy measurements in this experiment was about 60 keV. The measured energy value is shifted. The shift depends on the depolarizer bandwidth, the rate of its frequency variation and on the depolarization time. The shift value of 63 ± 9 keV was obtained from 11 measurements done by opposite scanning direction with invariable conditions of the VEPP-4. It

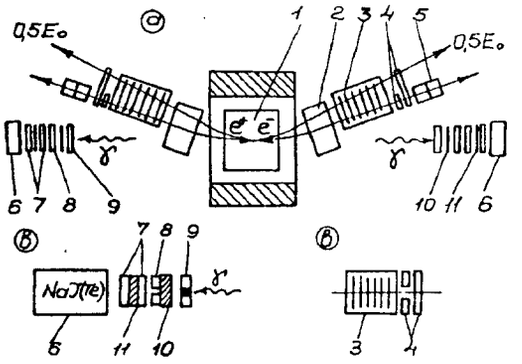

Fig. 4.1: Layout of the detector MD-1 (a - upper view, b - section by vertical plane): 1 - central part; 2 - additional bending magnets; 3 - system for detection of scattered electrons; 4 - counters for luminosity monitoring by small angle elastic scattering; 5 - lenses; 6,8 - counters for polarization measurement by SR; 7 - counters for luminosity monitoring by $e^+e^- \to e^+e^-\gamma$; 9 - doubled ionization chambers; 10 - lead plate of 13 mm thickness; 11 - lead plate of 5 mm thickness.

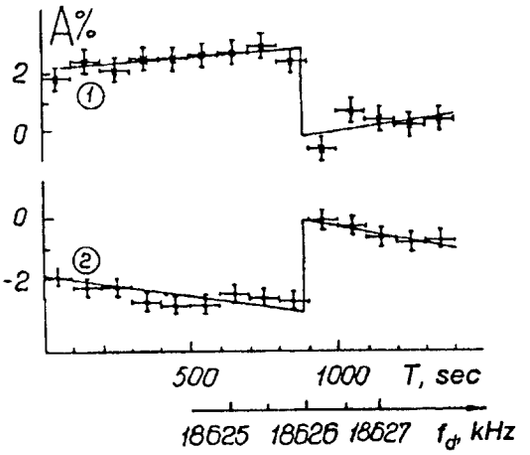

Fig. 4.2: Result of one of the depolarization frequency measurement. 1 and 2 - SR scattering on e^- and e^+ beams. A = (up-down)/(up+down) was averaged over 100 sec. Lower scale shows the depolarizer frequency f_d. Beam currents are I_-=5.8 mA, I_+=6.2 mA.

was also obtained that in the VEPP-4 storage ring the average electron energy is greater than that of the positrons by 24 ± 6 keV.

In the experiment [73, 74] the data taking time with the same beams was about 3 hours. The energy calibrations were done either before or after data taking. For the determination of the storage ring energy instability, the special measurements were performed in which several energy calibrations with the same currents were done with the time interval of about 40 minutes. Ten calibrations for three currents were done. The VEPP-4 energy instability obtained is $\sigma \simeq 40$ keV. This value was added in quadrature to the energy measurement error. No systematic variations of the storage ring energy during the data taking were found.

4.2. Measurement of the $\Upsilon(1S)$, $\Upsilon(2S)$ *and* $\Upsilon(3S)$ *masses*

The masses of the Υ-mesons were determined from the dependence of the measured hadronic cross section vs the beam energy. The calibration of the storage ring energy was carried out by the method of the resonance beam depolarization using backscattering of synchrotron photons.

4.2.1. Measurement of the $\Upsilon(1S)$ *mass*

Three independent measurements of the $\Upsilon(1S)$ mass have been done with the MD-1 [56], [63], and [73, 74]. The most precise one [73, 74] is described in more detail below.

In this experiment 4 scans of the $\Upsilon(1S)$ meson region were carried out. The sequence of the energy values in each scan was chosen accidentally. The integrated luminosity of 2.0 pb^{-1} was

collected. The energy calibrations took about 15% of time, and were accompanied by the simultaneous detection of background events, since during the calibrations the beams are separated in the vertical direction in the interaction point. During the data taking beams were kept unpolarized, in order to exclude the possible dependence of the detection efficiency upon the beam polarization.

The energy calibration procedure was described before. More than 80 energy calibrations were done during this experiment. The accuracy of the beam energy measurement was about 60 keV for runs with the energy calibration (65% of the statistics) and about 180 keV for runs between two calibrations.

The procedure of determination of the hadronic cross section and fitting of its dependence on the beam energy is described in the Section 5.1. The observed hadronic cross section is shown in Fig.5.1. The value of the $\Upsilon(1S)$ mass obtained in this fitting is $M = 9460.60 \pm 0.09(stat.)$ MeV.

Only statistical errors of the number of detected hadronic events were taken into account in the fit, the energy W (sum of the electron and positron energies) was fixed. The energy measurement errors were accounted in the following way: the energies in every experimental point were shifted independently near the average value according to the gaussian law with the standard deviation equal to the error in the value W at this point. For every set of the energy values the resonance mass was determined. The mean square spread of obtained mass values of 0.03 MeV was accepted as an error of the resonance mass value due to the energy measurement errors. This value was added in quadrature to the statistical error of the $\Upsilon(1S)$-meson mass.

Different effects that could contribute to the additional error in the Υ-meson mass value were considered. Below we list the most essential of them [73].

1. The spin precession frequency depends on $\gamma = E/m_e c^2$. The measured Υ mass is proportional to the electron mass. The uncertainty in the electron mass [75] results in an error of about ± 26 keV in the $\Upsilon(1S)$ mass.

2. The γ factor was determined by the ratio of the depolarization and beam revolution frequencies, their uncertainties lead to the error in the Υ-meson mass value of about ± 14 keV.

3. Vertical orbit distortions perturb the value of the spin precession frequency because rotations about different axes do not commute. This effect increases quadratically with the size of the distortions, and we estimate the correction to the Υ mass to be about -9 ± 7 keV for a 1.3 ± 0.5 mm vertical rms distortion.

4. Actually, the c.m. energy is not equal to the sum of electron and positron energies due to the motion of produced system. For energy spread in VEPP-4 this fact leads to the shift of the mass value by -4.1 ± 0.2 keV. Similar effect due to the beam angular spread is negligible.

5. The electron and positron energies at the interaction point differ from the average energy in the storage ring due to some effects: a) the interaction point is situated asymmetrically relative to the R.F. cavities (the shift value is $0.4 \cdot 10^{-2}$ of the circumference), b) since the synchrotron radiation intensity depends on the particle energy, the energy loss at the first half of the circumference is greater than that at the second one. The mass shift value associated with these effects appeared to be negligible.

6. There is some chromaticity of the VEPP-4 at the interaction point. This means that the vertical beta-function β_z and the transverse beam size depend on the particle energy and its radial coordinate. The effects has been studied experimentally, the data obtained agree with the

calculations and give the following form for the luminosity distribution:

$$G(W-W') = \left(1 + a\frac{W-W'}{W}\right)\frac{1}{\sqrt{2\pi}\sigma_W}\exp\left[-\frac{(W-W')^2}{2\sigma_W^2}\right], \tag{4.14}$$

where $a = -12 \pm 5$. This effect leads to the shift of the Υ mass value by -25 ± 10 keV.

7. From the check-up of the detector elements during the experiment the possible instability of the detection efficiency did not exceed $\pm 1\%$. The instability of the luminosity measurement was less than $\pm 2\%$. The variation of the background level in the detector did not exceed $\pm 20\%$. These instabilities resulted in the error of about ± 15 keV in the $\Upsilon(1S)$ mass.

8. Beam energy spread can be influenced by the phase instabilities, beam currents and collision effects. During the experiment special attention was paid to provide the absence of the phase instabilities. Separate fits of the data collected at small and large beam currents as well as at small and large specific luminosity showed that the beam energy spread was constant within $\pm 5\%$ at the operating current range. This uncertainty gives the error of ± 25 keV in the Υ mass.

9. The formula used for fitting of the observed hadronic cross section contained some approximations. The error in the Υ mass due to them is about ± 10 keV.

Different criteria were used to divide the experimental data on subsamples: different scans of the Υ region, small and large beam currents, small and large specific luminosity, small specific luminosity at the energy less than the resonance peak plus large specific luminosity at the energy greater than the peak and vice versa, presence and absence of the energy calibration, etc. Separate fits of the data subsamples agreed within statistical errors.

We conclude that the total shift of the mass value due to all effects mentioned above is about -0.04 MeV and the systematic uncertainty is about ± 0.05 MeV. So the final Υ mass value obtained in this experiment [74] is:

$$M(\Upsilon(1S)) = 9460.60 \pm 0.09 \pm 0.05 \text{ MeV} \qquad (1992).$$

This value agrees well with our previous results of 1982 [56] and of 1984 [63]. Averaging of these three independent results gives the $\Upsilon(1S)$ mass:

$$M(\Upsilon(1S)) = 9460.59 \pm 0.09 \pm 0.05 \text{ MeV}.$$

Our value of the $\Upsilon(1S)$ mass differs form the result of CUSB [65] by 3.8σ. We applied our algorithm to the data of CUSB [65]. In this case the difference is 2.3σ [73].

4.2.2. Measurement of the $\Upsilon(2S)$ mass

The integrated luminosity of 0.6 pb^{-1} was collected during 4 scans of the $\Upsilon(2S)$ energy region (W=9980÷10075 MeV) in this experiment [63, 64]. About 180 energy calibrations were done.

In this experiment the energy calibration procedure had some peculiarities. In the energy region of $\Upsilon(2S)$ the polarization degree of the beams in the VEPP-4 is small due to the coincidence of the frequency of spin precession with that of betatron oscillations. Therefore the calibrations were carried out at the point differed from the resonance one by 60 MeV (in the W scale) and the energy at the point of measurement was determined by extrapolation using the magnetic field value. The extrapolation curve has been obtained by the energy calibration below and above the resonance where the degree of polarization was sufficient for the energy calibration. The calibration curve was obtained several times during the experiment.

During the whole experiment the alteration of the magnetic field in the storage ring was carried out by one standard cycle. After injection, the energy was increased up to the point where the calibration was performed, then the energy was raised up to the point where the data were taken. After that, the energy was raised up to the fixed point much above the resonance and then lowered down to the injection energy. In some cycles two calibrations have been performed during the energy increase at the points placed below the resonance by 120 and 60 MeV. It was estimated that the error in the $\Upsilon(2S)$-meson mass due to the extrapolation procedure does not exceed 0.05 MeV.

Using the way described above, a half of the statistics has been taken. The remaining half of the statistics has been taken under somewhat different conditions of storage ring operation. Just after injection the energy was raised up to a maximum fixed point and then lowered to the point where the data were taken. After that, the energy was lowered by 60 MeV and the energy calibration was carried out. The calibration curve of the energy dependence on the magnetic field measured in this regime of the storage ring operation did not coincide with the first one. The mass error due to extrapolation in these series did not exceed 0.2 MeV.

The integrated luminosity of 0.6 pb^{-1} was collected during four scans of the $\Upsilon(2S)$ energy region (W=9980÷10075 MeV). About 180 energy calibrations were done. The observed hadronic cross section versus the center of mass energy is presented in Fig.4.3.

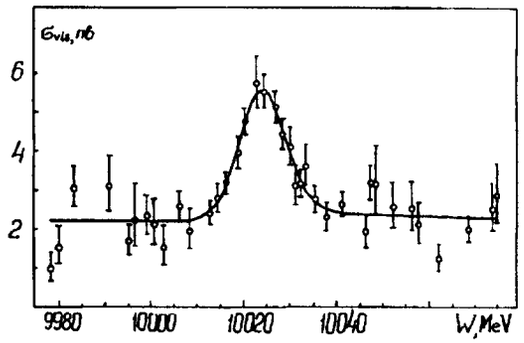

Fig. 4.3: Observed hadronic cross section in the $\Upsilon(2S)$ energy region

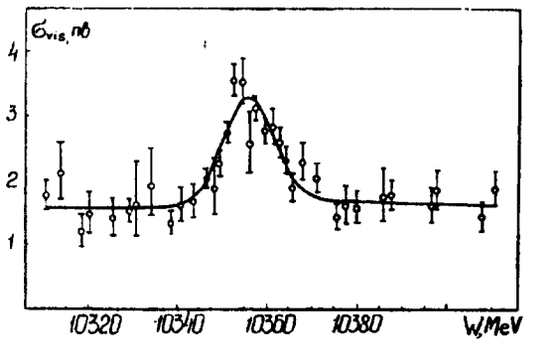

Fig. 4.4: Observed hadronic cross section in the $\Upsilon(3S)$ energy region

The fitting of the data gives the $\Upsilon(2S)$ mass

$$M(\Upsilon(2S)) = 10023.6 \pm 0.5 \text{ MeV}$$

and the energy spread $\sigma_W = 4.9 \pm 0.5$ MeV. The last value is in agreement with the estimated value of 4.5 MeV for the VEPP-4 at this energy. The systematic error in the $\Upsilon(2S)$ mass is less than 0.2 MeV according to our estimation. It's quadratic addition to the statistic error gives only small contribution to the total error. The $\Upsilon(2S)$ mass measured by ARGUS and Crystal Ball at DESY [66] agrees with ours.

4.2.3. Measurement of the $\Upsilon(3S)$ mass

The measurement of the $\Upsilon(3S)$ mass [63, 64] was similar to that of the $\Upsilon(1S)$. The integrated luminosity of 1.25 pb^{-1} was collected during 5 scans of the $\Upsilon(3S)$ energy region (W = 10310 ÷

10410 MeV). About 370 energy calibrations were done by the resonance beam depolarization method. The accuracy of the energy measurement depended on the beam polarization degree and was in the range 0.05÷0.2 MeV (in the W scale). The selection criteria for multihadronic events have been chosen using Monte Carlo simulation and background measurements. The result of the data processing is presented in Fig.4.4, where the detection cross section is plotted versus the center of mass energy.

The fitting formula and the fitting procedure were the same as in the $\Upsilon(1S)$ mass measurement and gave the $\Upsilon(3S)$ mass

$$M(\Upsilon(3S)) = 10355.3 \pm 0.5 \text{ MeV}.$$

The obtained value of the VEPP-4 energy spread in the $\Upsilon(3S)$ region $\sigma_W = 5.4 \pm 0.6$ MeV was in agreement with the estimated value of 4.8 MeV. The systematic error in the obtained $\Upsilon(3S)$ mass is less than 0.2 MeV according to our estimation. The total error obtained by quadratic addition of the statistical error and the systematic one is determined by the statistics and equals 0.5 MeV.

In conclusion note that in our experiments the mass of $\Upsilon(1S)$ meson was measured 100 times more precise and the masses of $\Upsilon(2S)$ and $\Upsilon(3S)$ were measured 20 times more precise than before [75].

5. Study of leptonic decays of Υ mesons

5.1. Measurement of the $\Gamma_{ee}(\Upsilon(1S))$

For the measurement of the $\Upsilon(1S)$ leptonic width [74], as well as for the mass measurement (subsection 4.2), we used the same statistics of 2.0 pb^{-1} collected during 4 scans of the $\Upsilon(1S)$ region ($E = 4710 \div 4745$ MeV). Additional 0.4 pb^{-1} continuum data collected with the same trigger and luminosity monitor conditions were employed for the data analysis. Energy calibration of the VEPP-4 was performed by the method of resonance depolarization.

The electronic width of a resonance can not be measured directly in an e^+e^--experiment. Fitting the resonance curve one can only extract the product $\Gamma_{ee} \cdot B_f$, where B_f is the branching ratio for the final modes selected in the experiment. In our work we did not suppress $\tau^+\tau^-$ decays: $\Upsilon \to \tau^+\tau-$ decays were taken into account with hadrons in calculation of the detection efficiency. Assuming $e - \mu$ universality one has $B_f = 1 - 2 \cdot B_{\mu\mu}$ in this case.

Two different sets of criteria were chosen to select the multihadronic and $\tau^+\tau^-$ events. The first set of criteria ("T-criterion") is based, mainly, on the information from the tracking system. The second one ("S-criterion") employs the information from the shower-range system. The number of charged particles and photons detected in the event had to be more than 3 and the number of background particles was required to be less than 4. Some additional cuts were used to suppress radiated Bhabha events and the cosmic background [74].

Detection efficiencies for hadronic events were about 90% (Table 5.1). The machine background contribution into the observed cross section in the continuum was about 2% for both selection criteria. The physical background (radiated Bhabha and two-photon processes) was about 20%. Both the machine and physical backgrounds were almost constant in the narrow region of the resonance and were automatically subtracted during the fitting procedure.

The numbers of events passed through *T.and.S*, *T.and..not.S* and *S.and..not.T* criteria are statistically independent and can be used in a joint fit. For the simulation of the $\Upsilon(1S)$ decays the

Table 5.1: Detection efficiencies (%) of the $\Upsilon(1S)$ decay modes for different selection criteria according to LUND 6.3

Decay mode	T	S	T.or.S
$\Upsilon(1S) \to 3g, 2g\gamma$	88.1	87.5	91.8 ± 0.4
$\Upsilon(1S) \to qq, qqg$	76.7	77.8	82.6 ± 1.0
$\Upsilon(1S) \to \tau\tau$	21.9	20.5	24.2 ± 2.0
$\Upsilon(1S) \to hadrons, \tau\tau$	85.2	84.7	89.0 ± 0.4

following branching ratios were used: $B(\Upsilon \to 3g, 2g\gamma) = 1-(R+3)\cdot B_{\mu\mu}$, $B(\Upsilon \to qq, qqg) = R\cdot B_{\mu\mu}$ and $B(\Upsilon \to \tau\tau) = B_{\mu\mu}$ with R = 3.55, $B_{\mu\mu} = 0.0257$.

The hadronic and $\tau^+\tau^-$ decays were generated with the LUND program version 6.3 [90].

Two main corrections were taken into account in the simulation of this experiment [74]. The first one is due to the probability of the true track reconstruction which depends on the chambers efficiencies. The second one corrected the hadron ranges in the shower-range system since ranges simulated in UNIMOD with the standard NUCRIN [16] were somewhat greater than in the experiment.

The systematic error in the detection efficiency due to uncertainty of the detector response were estimated to be about 0.5% for *T.or.S* selection criterion and about 1% for *T.and.S* criterion.

Comparison of the observed and simulated distributions in most important parameters has shown that LUND 6.3 satisfactory reproduces $\Upsilon(1S)$ decays though the observed charged particle momentum spectrum is somewhat harder than the simulated one. We tried to adjust the LUND **6.3** program parameters to generate harder momentum spectrum with the smallest possible variation of the mean multiplicity and sphericity. The agreement of the momentum spectra could be improved but at the price of disagreement in the sphericity distributions.

Having many sets of events simulated with the modified LUND 6.3 and LUND 4.3 parameters we have concluded that the systematic error due to model dependence of the detection efficiency does not exceed 1%.

The observed dependencies of the cross sections on the beam energy for events which passed the *T.and.S* (Fig.5.1), *T.and..not.S*, *S.and..not.T* selection criteria were fitted to the formula accounting radiative correction according to Kuraev and Fadin [85] with some small terms omitted.

Here one should note that before 1985 most of experiments in this field used the erroneous formula for the radiative corrections and used the definition of the Γ_{ee} inconsistent with the $\Gamma_{ee} = \Gamma_{tot} \cdot B_{\mu\mu}^{\rm exp}$ relation which is employed for the total width Γ_{tot} determination ($B_{\mu\mu}^{exp}$ is an experimentally measured muonic branching ratio) [76]-[81]. The situation was clarified by Kuraev and Fadin [85]. The new formula for the radiative correction was used in our works [73, 74, 84, 86], and then was employed in the Crystal Ball work [82]. Now it is generally accepted approach [87]. The results of all experiments on Γ_{ee} and Γ_{tot} of Ψ and Υ meson have been recalculated according to this formula [88, 89], it is the following:

$$\sigma_i^{obs} = \gamma_{ee,i} \cdot 6\pi^2/M^2 \cdot G(W-M) \cdot (1+\delta) + \sigma_{c,i}^{obs} \cdot (2 \cdot E_0/W)^2, \qquad (5.1)$$

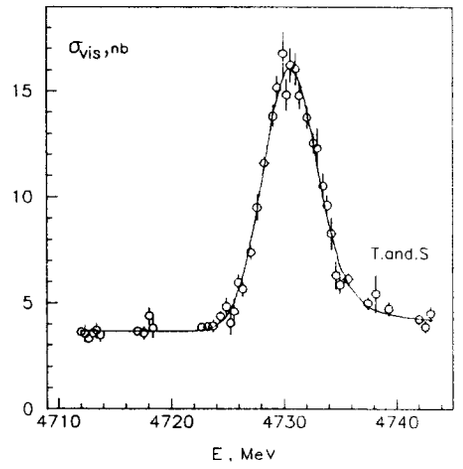

Fig. 5.1: The visible cross section for $e^+e^- \rightarrow$ *hadrons* with *T.and.S* selection criterion in the $\Upsilon(1S)$ region.

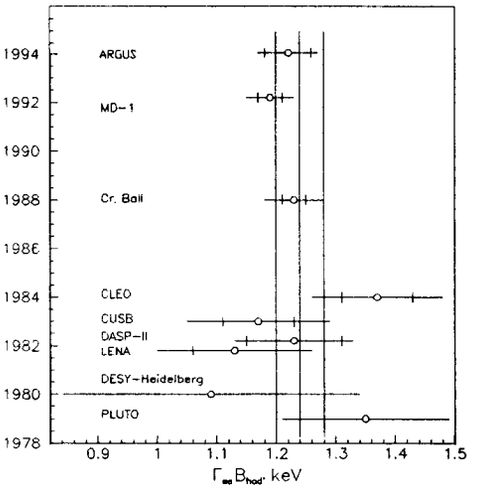

Fig. 5.2: Compilation of $\Gamma_{ee} \cdot B_{had}$ values for $\Upsilon(1S)$. The full error bars represent total errors, the small ones show statistical errors separately. The vertical lines illustrate the world average and its error (without this and ARGUS experiments).

$$G(x) = \left(\frac{2\sigma_W}{M}\right)^{\beta} \frac{\Gamma(1+\beta)}{\sqrt{2\pi}\sigma_W} \exp(-\frac{x^2}{4\sigma_W^2}) D_{-\beta}(-\frac{x}{\sigma_W}),$$

$$\delta = \frac{\alpha}{\pi}(\frac{\pi^2}{3} - \frac{1}{2}) + \frac{3}{4}\beta - \frac{1}{24}\beta^2(\frac{2}{3}\ln\frac{W}{m_e} + 2\pi^2 - \frac{37}{4}),$$

$$\beta = \frac{4\alpha}{\pi}(\ln\frac{W}{m_e} - \frac{1}{2}).$$

Here α is the fine structure constant, Γ is the gamma-function, $D_{-\beta}$ is the Weber parabolic cylinder function, m_e is the electron mass and $W = 2E$.

In the fitting there were 8 free parameters: M, σ_W, and $\sigma_{c,i}^{obs}$ and $\gamma_{ee,i}$ (i=1,2,3), where

M is the $\Upsilon(1S)$ mass,

σ_W is the machine energy spread,

$\gamma_{ee,i} = \Gamma_{ee} \cdot B_f \cdot \epsilon_i$, $B_f = 1 - 2 \cdot B_{\mu\mu}$,

ϵ_i is the detection efficiency of the selection i,

i=1,2,3: T.and.S, T.and..not.S, S.and..not.T,

$\sigma_{c,i}^{obs}$ is the nonresonant cross section at energy $E_0 = 4.7$ GeV for the selection i.

The accuracy of the approximation (5.1) is better than 0.1%. The β^2 terms, 0.0053 numerically, was not taken into account in the works [82, 88, 89].

The vacuum polarization is included in the definition of the Γ_{ee}, so that $\Gamma_{ee} = \Gamma_{tot} \cdot B_{\mu\mu}^{exp}$.

The experimental data and the fit for *T.and.S* selection criterion are shown in Fig.5.1.

The three values of $\gamma_{ee,i}$ with the known detection efficiencies and the $B_{\mu\mu}$ value from the PDG Tables [87] were used to calculate leptonic widths corresponding to *T*, *S* and *T.or.S* selection criteria. The last value was chosen as a resultant value of Γ_{ee} as having the smallest systematic error:

$$\Gamma_{ee} \cdot B_{had} = 1.187 \pm 0.023 \pm 0.031 \text{ keV}.$$

The full list of systematic errors is given in Table 5.2.

Table 5.2: Summary of systematic errors for the $\Upsilon(1S)$ electronic width measurement.

Contribution from	Value of error
luminosity absolute calibration	2.2%
luminosity monitor stability	0.5%
model dependence of detection efficiency	1.0%
uncertainty in the detector response	0.5%
Monte Carlo statistics	0.5%
background contribution	0.5%
beam energy uncertainty	0.5%

The published results of the experiments on the $\Upsilon(1S)$ leptonic width measurements [74]-[83] are shown in Fig. 5.2.

Our measurement is in a good agreement with others.

5.2. Measurement of the $\Gamma_{ee}(\Upsilon(2S))$

The same technique was employed for determination of the $\Upsilon(2S)$ leptonic width [92].

The data collected during the experiment [91] on the R-ratio measurement were used for the analysis. Three one-day scans of the $\Upsilon(2S)$ region were performed in two months period. The luminosity integral of 0.4 pb^{-1} was recorded for E = 5005 ÷ 5020 MeV. No energy calibrations by resonance depolarization method were done. The uncertainty in the beam energy turned out to be the main difficulty of the analysis.

From the previous experiments [73, 86, 56, 63] it was known that the VEPP-4 collider has two kinds of beam energy uncertainty: the fluctuations around the average level with the standard deviation of about 0.2 MeV and the sudden shifts of this level up to 2–3 MeV which occurred every few weeks. The probability of such shift during the short scan of the resonance region is small but it is very probable between the scans.

To take this into account, we considered the three scans of the $\Upsilon(2S)$ region as the three independent experiments. With each scan independent continuum data were used, 0.2 pb^{-1} per the scan. The three values of the $\Upsilon(2S)$ leptonic width obtained were weighted to produce the final result.

The multihadronic events (including τ-pairs) were selected with the *T.or.S* criterion. The $\Upsilon(2S)$ decay ratios used for the detection efficiency calculation are shown in the Table 5.3.

The simulation procedure was the same as for the $\Upsilon(1S)$. The additional decay modes were generated in the LUND 6.3 frame.

The observed dependencies of the visible cross sections on the beam energy for the three scans were fitted by the formula 5.1 with 3 free parameters: γ_{ee}, σ_c^{obs} and M. The machine energy spread

Table 5.3: Branching ratios and detection efficiencies (%) for the $\Upsilon(2S)$ decay modes

Decay mode	B_{mode}	ϵ_{mode}
$\Upsilon(2S) \to 3g, 2g\gamma$	46.6 ±2.2	94.9 ±0.5
$\Upsilon(2S) \to \Upsilon(1s)\pi\pi$	27.3 ±1.4	91.3 ± 1.4
$\Upsilon(2S) \to \chi, \gamma$	17.6 ±1.6	89.5 ± 1.4
$\Upsilon(2S) \to qq, qqg$	4.7 ± 0.7	91.4 ± 1.4
$\Upsilon(2S) \to \tau\tau$	1.3 ± 0.2	29.4 ± 2.0
$\Upsilon(2S) \to hadrons, \tau\tau$	97.4 ± 0.4	91.9 ± 0.5

$\sigma_{W,2S}$ was fixed: 5.25 ± 0.11 MeV. This value was calculated according to the formula:

$$\sigma_{W,2S} = \sigma_{W,1S} \cdot (M_{2S}/M_{1S})^2,$$

with the value $\sigma_{W,1S}$ and its error taken from the $\Upsilon(1S)$ experiment. The fit with all parameters free gives $\sigma_{W,2S} = 5.30 \pm 0.38$ MeV.

The experimental data and the fit are shown in Fig.5.3 (the scans are merged).

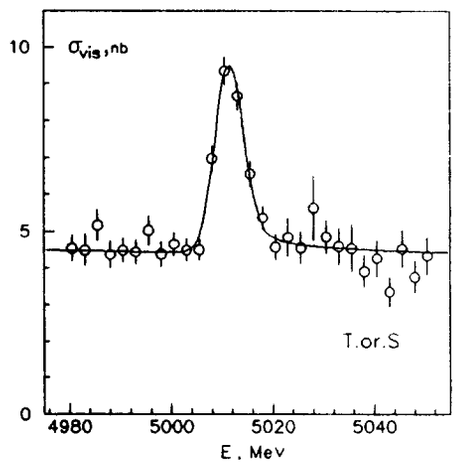

Fig. 5.3: The visible cross section for $e^+e^- \to$ *hadrons* with *T.or.S* selection criterion in the $\Upsilon(2S)$ region.

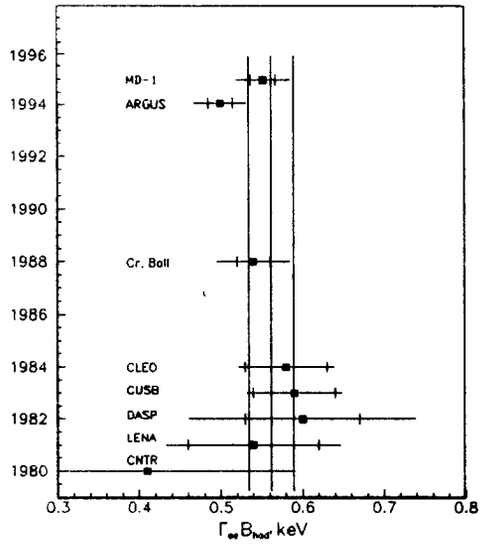

Fig. 5.4: Compilation of $\Gamma_{ee} \cdot B_{had}$ values for $\Upsilon(2S)$. The full error bars represent total errors, the small ones show statistical errors separately. The vertical lines illustrate the world average and its error (without this and ARGUS experiments).

The Γ_{ee} values obtained for all three scans are in a good agreement, the $\chi^2 = 1.68$ for 2 degrees of freedom. Averaging of them gives

$$\Gamma_{ee} \cdot B_{had} = 0.552 \pm 0.031 \pm 0.017 \text{ keV}.$$

The resonance mass for the second scan is shifted by about 3 MeV relative to the masses of the other two scans. If energy shift between scans is ignored, the resulting Γ_{ee} value decreases by 2.4%.

The factors contributing to the systematic errors are given in Table 5.4.

Table 5.4: Summary of systematic errors for the $\Upsilon(2S)$ leptonic width measurement.

Contribution from	Value of error
luminosity absolute calibration	1.9%
luminosity monitor stability	1.5%
model dependence of detection efficiency	1.0%
uncertainty in the detector response	0.5%
Monte Carlo statistics	0.5%
background contribution	0.5%
beam energy uncertainty	0.9%
uncertainty in the σ_W	0.8%

The results of experiments on $\Upsilon(2S)$ leptonic width measurement [77, 93, 78],[80]-[83] and this one are shown in Fig.5.4.

All measurements are in agreement.

5.3. Measurement of the $B_{\mu\mu}(\Upsilon(1S))$

In this experiment [22] the collinear and multihadronic events were selected from the statistics collected in the $\Upsilon(1S)$ and nearby continuum.

Experimental data were taken during two runs. The total integrated luminosity is 20.4 pb^{-1}. During the first run 3.4 pb^{-1} in the continuum and 5.1 pb^{-1} on the resonance were collected. At the second run the energy was scanned in the mass region $\sqrt{s}$ = 7.6 – 10 GeV. The data collected in the nonresonant region have been used for the continuum subtraction.

For $B_{\mu\mu}$, assuming the $e-\mu-\tau$ universality, we have

$$B_{\mu\mu} = \overline{B}_{\mu\mu}/(1+3\overline{B}_{\mu\mu}), \tag{5.2}$$

where $\overline{B}_{\mu\mu} = \sigma_r^{\mu}/\sigma_r^{h}$, σ_r^{μ} and σ_r^{h} are the total resonance cross sections for muons and hadrons respectively.

The calibrations of the storage ring energy were carried out by the method of resonance depolarization (subsection 4.1).

Two types of the trigger logic (T_1, T_2) were used during the experiment which correspond to two data sets. In the trigger firing of at least one scintillation counter and two proportional chambers (T_1) or two shower-range units (T_2) situated on both sides from the beam axis were required. The trigger efficiency for the QED process $e^+e^- \to \mu^+\mu^-$ is 35.7 % and 44.9 % for T_1 and T_2 respectively.

The *collinear events* were selected from the low multiplicity events with some additional cuts [22]. Contributions of the main background processes are shown in Table 5.5. They are given compared to the QED process $e^+e^- \to \mu^+\mu^-$ at $\sqrt{s}$=9.46 GeV.

The *hadronic events* were selected using the multiplicity and the momenta of the particles [22].

The detection efficiencies $\epsilon_c^\mu, \epsilon_\tau^\mu, \epsilon_\tau^h$ were determined by the Monte Carlo simulation for the reactions $e^+e^- \to \mu^+\mu^-$, $e^+e^- \to \Upsilon \to \mu^+\mu^-$, $\Upsilon \to$ *hadrons* respectively.

For the QED process $e^+e^- \to \mu^+\mu^-$ the simulation with the radiative corrections up to order α^3 [99, 100] was used. The total cross section for this process was calculated using the formula from the paper of E.Kuraev and V.Fadin [85] where the radiative corrections up to order α^4 have been accounted.

Table 5.5: Summary of background and systematic errors in the experiment on determination $B_{\mu\mu}$.

The source of background	Background (%)	Systematic error (%)
Cosmic rays (CR)	4.9	0.5
$e^+e^- \to e^+e^-$	2.1	0.4
CR and $e^\pm$ of single brems. coincidence [22]	0.7	0.3
$e^+e^- \to$ hadrons (simul.)	0.6	0.2
$e^+e^- \to \tau^+\tau^-$ (simul.)	0.4	0.4
$e^+e^- \to e^+e^-\mu^+\mu^-$ (simul.)	3.2	0.7
Sum	11.9	1.1

For the reaction $e^+e^- \to \Upsilon \to \mu^+\mu^-$ the photon emission by the initial state particles is suppressed. Therefore the detection efficiency ϵ_τ^μ was obtained from the same simulation as for $e^+e^- \to \mu^+\mu^-$ but with the photon emission in the final state only. The obtained detection efficiencies for the two data sets T_1 and T_2 are 32.9±0.9% and 41.4±0.8% respectively.

The simulation of the hadronic decays of the Υ was carried out with the LUND 6.3 computer code [90]. The detection efficiency ϵ_τ^h was determined to be $(87 \pm 2)\%$. The contamination of the decays $\Upsilon \to \tau^+\tau^-$ was estimated to be 0.3 %.

The visible cross section $\sigma_v(s)$ is shown in Fig.5.5.

The experimental data in the continuum were fitted to the 1/s dependence with one free parameter: the visible continuum cross section σ_{vc} at $\sqrt{s} = 9.46$ GeV. After correction for the detection efficiency $(23.2 \pm 0.4)\%$ for T_1 and $(29.2 \pm 0.4)\%$ for T_2 the total cross section for the reaction $e^+e^- \to \mu^+\mu^-$ in the continuum at $\sqrt{s} = 9.46$ GeV was obtained:

$$\sigma_c = 1.372 \pm 0.0018 \pm 0.035 \text{ nb}.$$

The systematic error includes uncertainties in the detection efficiency (1.2%), background subtraction (Table 5.5), and absolute luminosity calibration (2.1%). The measured cross section is in a good agreement with the theoretical calculation (1.404 nb).

The cross section for the reaction $e^+e^- \to \mu^+\mu^-$ in the Born approximation is [101]:

$$\sigma_t(s) = \frac{4\pi\alpha^2}{3s}(1 + 2 \cdot Re\{B(s)\} + |B(s)|^2); \tag{5.3}$$

$$B(s) = \frac{\beta \cdot s}{s - M^2 + i \cdot \Gamma_{tot} \cdot M}; \qquad \beta = \frac{3 \cdot \Gamma_{ee}}{\alpha \cdot M},$$

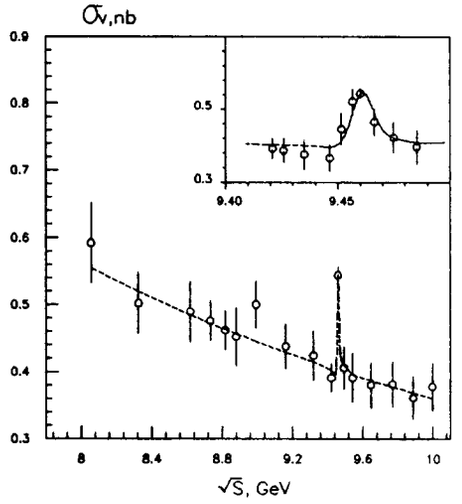

Fig. 5.5: The visible cross section for $e^+e^- \rightarrow \mu^+\mu^-$.

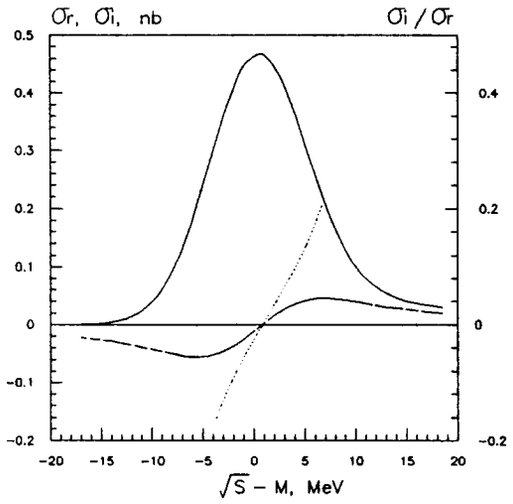

Fig. 5.6: The calculated cross sections σ_r (solid line), σ_i (dashed line) and the ratio σ_i/σ_r (dotted line).

where M is mass of resonance, Γ_{tot} is the total, and Γ_{ee} is the leptonic width of $\Upsilon(1S)$ meson. The three terms in (5.3) give the QED (σ_0), the interference (σ_i) and the resonance (σ_r) cross section. The experimental cross section is quite different from the cross section σ_t because the machine energy has certain width σ_W and also the energy of the initial state electrons is degraded by the bremsstrahlung emission [102, 103].

The visible muon cross section (Fig.5.5) was approximated by the following formula:

$$\sigma_v^\mu(W) = \sigma_{vc}\left(\frac{M}{W}\right)^2 + \sigma_r^\mu \epsilon_r^\mu \sigma_\mu(W)/\sigma_\mu(M), \tag{5.4}$$

where W is the center of mass energy. Two parameters were free: the observed cross section at the continuum σ_{vc} and the resonance's excess above the continuum σ_r^μ. The ratio $\sigma_\mu(W)/\sigma_\mu(\mathrm{M})$ gives the shape of the resonance curve. $\sigma_\mu(W)$ was calculated by the formulae:

$$\sigma_\mu(W) = \int_0^\infty dW'' F(W, W'')[\sigma_r(W'') + \sigma_i(W'')](1+\delta_a) = \sigma_r(W) + \sigma_i(W), \tag{5.5}$$

$$F(W, W'') = \frac{1}{\sigma_W}\left(\frac{2\sigma_W}{W}\right)^t \frac{\Gamma(1+t)}{\sqrt{2\pi}} \times exp(-\frac{x^2}{4}) D_{-t}(-x),$$

$$x = \frac{(W - W'')}{\sigma_W};\ t = \frac{2\alpha}{\pi}(2\ln(\frac{W}{m_e}) - 1);\ \delta_a = \frac{\alpha}{\pi}(\frac{\pi^2}{3} - \frac{1}{2}) + \frac{3}{4}t,$$

where m_e is the electron mass, α is the fine structure constant, $\Gamma(1+t)$ is a gamma-function, $D_{-t}(-x)$ is a Weber's parabolic cylinder function.

The hadronic cross section was approximated by the same way as the muonic cross section (5.4) The continuum and resonance interference for multihadronic events is negligible and the shape of the hadronic resonance curve was calculated without the interference term in (5.5).

The results of the data analysis are summarized in Table 5.6, where the cross sections σ_r^μ and σ_r^h, the measured number of μ-pairs from the resonance decays ($N_{\mu\mu}$), and $\overline{B}_{\mu\mu}$ are shown. The errors are statistical and were obtained by fitting with the fixed value of the continuum σ_c^μ.

Table 5.6: The resonance cross sections for muons and hadrons, $N_{\mu\mu}$ and $\overline{B}_{\mu\mu}$ for two different data sets T_1 and T_2

	σ_r^μ, nb	σ_r^h, nb	$N_{\mu\mu}$	$\overline{B}_{\mu\mu}$, %
T_1	0.348±0.045	15.8±0.13	276±36	2.20±0.28
T_2	0.357±0.042	15.4±0.14	339±40	2.32±0.27

Using (5.2) and adding the statistical error due to the continuum subtraction we obtain the branching ratio: $B_{\mu\mu} = 2.12\% \pm 0.20\%\,(stat.)$.

The following contributions were taken into account in the systematic error of the branching ratio $B_{\mu\mu}$: the accuracy of detection efficiencies ϵ_r^μ (2.2%), ϵ_r^h (2.0%), the luminosity uncertainty (3.2%), the background from the Υ decays into hadrons (1.2%±0.7%), and the storage ring energy instability (0.8%). The last effect for the first time was taken into account in our experiment. It is described below.

Table 5.7: Compilation of results for the branching ratio of the decay $\Upsilon(1S) \to \mu\mu$.

$B_{\mu\mu}$,%	Experiment	Reaction
2.2 ±2.0	PLUTO [76]	$\Upsilon(1S) \to \mu^+\mu^-$
$1.4\ ^{+3.4}_{-1.4}$	DESY-HD [77]	$\Upsilon(1S) \to \mu^+\mu^-$
3.8 ±1.5 ±0.2	LENA [79]	$\Upsilon(1S) \to \mu^+\mu^-$
3.2 ±1.3 ±0.3	DASP [78]	$\Upsilon(1S) \to \mu^+\mu^-$
2.7 ±0.3 ±0.3	CLEO [80]	$\Upsilon(1S) \to \mu^+\mu^-$
2.70±0.28±0.14	CUSB [94]	$\Upsilon(1S) \to \mu^+\mu^-$
2.84±0.18±0.20	CLEO [95]	$\Upsilon(2S) \to \Upsilon(1S)\pi^+\pi^-;\ \Upsilon \to \mu^+\mu^-$
2.30±0.25±0.13	ARGUS [96]	$\Upsilon(2S) \to \Upsilon(1S)\pi^+\pi^-;\ \Upsilon \to \mu^+\mu^-$
2.61±0.09±0.11	CUSB [97]	$\Upsilon(1S) \to \mu^+\mu^-$
2.52±0.07±0.07	CLEO [98]	$\Upsilon(1S) \to \mu^+\mu^-$
2.12±0.20±0.10	MD-1 [22]	$\Upsilon(1S) \to \mu^+\mu^-$

The ratio of the muon and hadron yields in the Υ decays gives the branching ratio $B_{\mu\mu}$ when the center-of-mass energy W is equal to the resonance mass M (without radiative correction). If W is not equal to M, the interference between resonance and continuum should be taken into account. The calculated cross sections σ_i, σ_r and their ratio are shown in Fig.5.6. In the calculation the leptonic width Γ_{ee}=1.34 eV [87] and the VEPP-4 energy spread σ_W=4.62 MeV were used. The ratio σ_i/σ_r gives the alteration of the $B_{\mu\mu}$ value dependent on the center-of-mass

energy if the interference is omitted:

$$\frac{1}{B_{\mu\mu}}\frac{dB_{\mu\mu}}{dW} = \frac{d}{dW}(\sigma_i/\sigma_r) = 3.2\%/MeV.$$

Therefore the absolute energy calibration of the storage ring is necessary to measure the $B_{\mu\mu}$. The energy calibration with the resonance depolarization technique was carried out during all the experiment. The accuracy of this calibration gives contribution to the systematic error of the $B_{\mu\mu}$ equal to 0.8 %.

Finally, the probability of the reaction $\Upsilon(1S) \to \mu^+\mu^-$ is

$$B_{\mu\mu} = (2.12 \pm 0.20 \pm 0.10)\%.$$

In Table 5.7 the result obtained with the MD-1 detector for the branching ratio of the decay $\Upsilon(1S) \to \mu^+\mu^-$ as well as results of other measurements are presented. Our measurement agrees with the results of the previous experiments.

6. Search for rare decays of $\Upsilon(1S)$ meson

6.1. Upper limit on $B(\Upsilon \to \pi^+\pi^-)$, $B(\Upsilon \to K^+K^-)$

For these upper limits determination [22] we used the same data sample as for the measurement of $B_{\mu\mu}$. The collinear events with angle of track to the beam axis $\theta > 45°$ were selected. The μ -pairs rejection have been performed using the muon chambers. The particles were classified as muons if at least one chamber inside the yoke (5.5 nucl. int. lengths) or behind the yoke (7.5 nucl. int. lengths) was fired. Events where muons were not revealed were selected as candidates for the decays under study. To reduce the background from the reaction $e^+e^- \to e^+e^-\mu^+\mu^-$ the additional cuts were used.

Finally, we have obtained 5 events in the resonance region (interval $\pm\sigma_W$, $\int$ Ldt=5.1 pb^{-1}) and 21 events at the continuum ($\int$ Ldt=15.0 pb^{-1}). The measured number of events is in a good agreement with expected background from the reactions $e^+e^- \to \mu^+\mu^-$, $e^+e^- \to e^+e^-\mu^+\mu^-$, $e^+e^- \to e^+e^-$. From MC simulation the background was estimated to be 2.5±1.0, 3.0±3.0, 2.3±1.5 events respectively for integrated luminosity 5.1 pb^{-1}. The contamination of the multi-hadronic events is negligible. The data fitting was carried out for two different energy dependencies of the continuum cross section: const and $\sim 1/s$. Less than 4.3 (90 % CL) two-hadron decays of the Υ have been obtained and the result doesn't depend on the fitting method.

The detection efficiencies for $\Upsilon \to \pi^+\pi^-$ and $\Upsilon \to K^+K^-$ were obtained from the MC simulation and were estimated to be 11±2%. The angular distribution of the collinear pseudoscalar mesons was simulated as $\sin^2(\theta)$.

The obtained upper limit on branching ratio for the decays $\Upsilon \to \pi^+\pi^-$ or K^+K^- is:

$$B(\Upsilon \to \pi^+\pi^- \text{ or } K^+K^-) < 5 \cdot 10^{-4}\,(90\%\,CL).$$

The calculation with QCD sum rules gives: $B_{\pi\pi} \sim 5 \cdot 10^{-8}$, $B_{KK} \sim 10^{-7}$ [104].

In this experiment upper limit on the branching ratio for the decays $\Upsilon \to \pi^+\pi^-, K^+K^-$ have been obtained for the first time.

6.2. Upper limit on $B(\Upsilon \to p\bar{p})$

In the same manner as for the decay $\Upsilon \to \pi^+\pi^-, K^+K^-$ the upper limit was obtained for the decay $\Upsilon \to p\bar{p}$. For this process the calculated detection efficiency equals $6 \pm 1\%$. The limit obtained is $B(\Upsilon \to p\bar{p}) < 9 \cdot 10^{-4}$ at 90% CL [22].

For more effective search for $\Upsilon(1S) \to p\bar{p}$ decay we used particle identification in the MD-1 by the gas Cherenkov counters with threshold value of Lorentz factor of $\gamma_{th} = 5$ [105]. The γ-factor of p and $\bar{p}$ from the $\Upsilon(1S)$ decay is less than γ_{th}, and therefor the Cherenkov counters were very effective in background suppression.

The integrated luminosity of 5.7 pb^{-1} collected at the $\Upsilon(1S)$ resonance was used in this analysis. This sample of data contained 80800 Υ mesons.

The events with two collinear charged particles were selected. The cuts on the momenta and time of flight of particles were used to suppress the cosmic background. The selected sample of events consisted mainly of muon pairs and Bhabha events.

The information from Cherenkov counters was employed to search for $p\bar{p}$ events. For this aim we selected the events where each of two particles crossed only one Cherenkov counter and had the path in the radiator more than 17 cm. So, both particles crossed two Cherenkov counters with 8 photomultipliers (PM). The events with fired PM number $N_{PM} < 2$ were considered as the $p\bar{p}$ candidates. There was no events with $N_{PM} = 0$, and only 18 events with $N_{PM} = 1$ remained. Using the information from muon chambers we found that all of these 18 remained events had the sum of ranges of particles larger than 8 nuclear absorption lengths, and we concluded that these events are the muon pairs. So we did not find any events satisfied to our selection criteria for $p\bar{p}$.

The detection efficiency of $p\bar{p}$ selection criteria was determined by the Monte Carlo simulation. In the simulation the angular distribution of $p\bar{p}$ was proportional to $(1 + \cos^2\vartheta)$ and could differ from the real one estimated in [106]. The relative error in the efficiency due to this reason did not exceed 1.5%.

The apparatus parameters used in the simulation were determined experimentally. For this aim the selected cosmic muons, muon pairs, and Bhabha events were used. The apparatus parameters that were important in this experiment are listed below. The dependence of the photoelectron number in Cherenkov counters versus the inverse square of the cosmic muons velocity and the fitted curve are shown in Fig.6.1. The probability distributions on number of the fired PMs in Cherenkov counters for Bhabha events, muon pairs, and simulated $p\bar{p}$ events are presented in Fig. 6.2. The probability of PM firing in the uncrossed counters was less than 2.3%. The average muon chamber efficiency was equal to $97.0 \pm 0.5\%$, but two chambers were installed in each layer. The firing of muon chambers determined by Bhabha events did not exceed 0.9%.

The $p\bar{p}$ detection efficiency found by the simulation was equal to $6.7 \pm 1.4\%$ and was determined mainly by the chosen acceptance.

The estimated upper limit is

$$B(\Upsilon(1S) \to p\bar{p}) < 5 \cdot 10^{-4} \text{ at } 90\% \text{ CL.}$$

The theoretical estimation [104] gives about 4 orders smaller branching ratio: $B_{p\bar{p}} \sim 10^{-7}$.

6.3. Upper limit on $B(\Upsilon \to \gamma\xi(2.2)) \times B(\xi \to K^+K^-)$

Investigation of the radiative decays of the heavy vector mesons (J/ψ, Υ etc.) is one of the most promising ways to search for new particles. Radiative decays produce a system of two

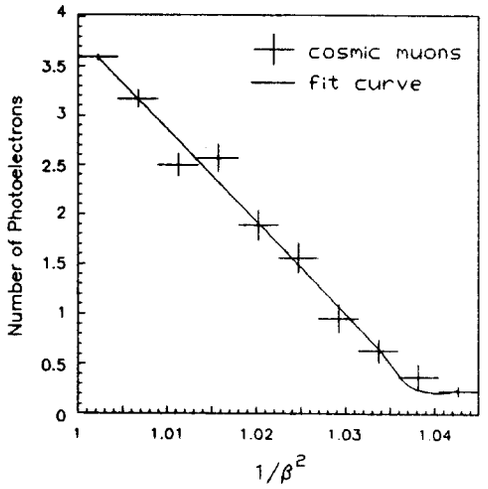

Fig. 6.1: The dependence of the photoelectron number in Cherenkov counters versus the inverse square of the cosmic muons velocity and the fitted curve

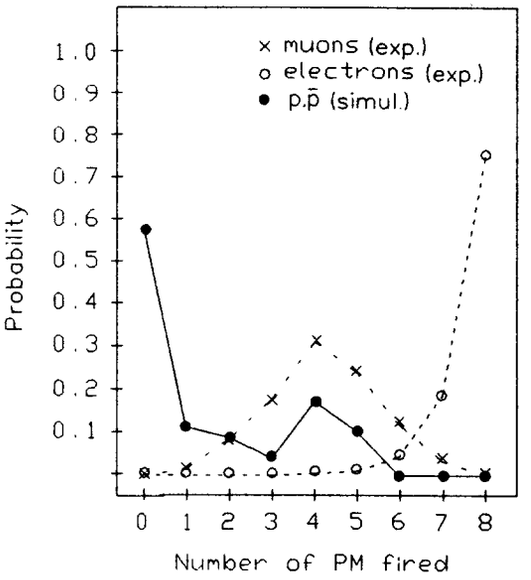

Fig. 6.2: The distributions of probability versus the fired PM number in Cherenkov counters for Bhabha events, muon pairs, and simulated $p\bar{p}$ events. The lines are drown to guide eye.

gluons with a positive charge parity. These gluons can form ordinary mesons as well as new states. Another interesting task is a search for possible light Higgs bosons.

In 1983 the MARK III detector discovered the resonance $\xi(2.2)$ in the spectrum of K^+K^- in the decay $J/\psi \to \gamma K^+K^-$ [107]. Later this resonance was observed also in other experiments [108]-[113]. The discovery of $\xi(2.2)$ by MARK III in J/ψ radiative decays stimulated its search in radiative decays of the Υ meson. The interpretation of $\xi(2.2)$ as a Higgs boson was the most popular and it was important to check this hypothesis [114]. The $\xi(2.2)$ can only have the quantum numbers $J^{PC} = 0^{++}, 2^{++}, \ldots$. Analysis of decay $\xi \to K_sK_s$ [109] assigned to $\xi(2.2)$ a minimum spin of 2.

At the present time the nature of $\xi(2.2)$ still remains unclear. For an explanation of this resonance, various hypotheses have been suggested: Higgs boson [114], gluonium and hybrid state [115], meson with high spin [116], and others [117]. Since the zero spin of $\xi(2.2)$ seems to be excluded, the hypothesis that this particle is a Higgs boson is probably ruled out.

In this experiment [118] the integrated luminosity of 6.5 pb^{-1} at the Υ resonance and 2.7 pb^{-1} off the peak of the resonance was used. For study the decay $\Upsilon \to \gamma K^+K^-$ we selected events with at least one photon reconstructed in the shower-range system and only two charged particles found in the coordinate system. Besides, information from the Cherenkov counters was used. In the vicinity of $\xi(2.2)$ no events were found, that yields an upper limit for the product branching ratio:

$$B(\Upsilon \to \gamma\xi(2.2)) \times B(\xi \to K^+K^-) < 2 \cdot 10^{-4} \quad (90\%CL)$$

The cited upper limit on the branching ratio is obtained under the assumption that the spin of $\xi(2.2)$ equals zero. In this case the decay $\Upsilon \to \gamma\xi \to \gamma K^+K^-$ is described by one amplitude. For

Table 6.1: Upper limits on $B(\Upsilon \to \gamma\xi(2.2)) \times B(\xi \to K^+K^-)$ and $B(\Upsilon \to \gamma\xi(2.2))$ obtained in different experiments.

Detector	Upper limit (90% CL)	Experiment
Cr.Ball [123]	$\sim 5 \cdot 10^{-4}$	incl.
CUSB [121, 122]	$\sim 2 \cdot 10^{-4}$	incl.
CLEO [119]	$2 \cdot 10^{-4}$	excl.
CUSB [121]	$\sim 1 \cdot 10^{-3}$	excl.
MD-1 [118]	$2 \cdot 10^{-4}$	excl.
ARGUS [124]	$2.9 \cdot 10^{-5}$	excl.
CLEO [120]	$\sim 1.5 \cdot 10^{-5}$	excl.

$J \neq 0$ the detection efficiency depends on the decay dynamics. For example, for $J = 2$ when the amplitude with $\lambda_\xi = 0$ or 2 is dominant (here λ_ξ is the helicity of $\xi(2.2)$), the difference of the upper limit from the case of $J = 0$ is less than 10%; when the amplitude with $\lambda_\xi = 1$ is dominant, the upper limit is 20% smaller.

Upper limits for the decay $\Upsilon \to \gamma\xi \to \gamma K^+K^-$ obtained with different detectors as well as results of search for $\xi(2.2)$ in inclusive channel $\Upsilon \to \gamma\xi$ are given in Table 6.1.

6.4. Upper limit on $B(\Upsilon \to \gamma X(2.2)) \times B(X \to \phi\phi)$

At the DM2 detector in the decay $J/\psi \to \gamma\phi\phi$ a narrow state in the $\phi\phi$ system was discovered with a mass 2.2 GeV/c^2 and probable $J^P = 0^-$, though $J^P = 2^\pm$ is not excluded [125]. Later MARK III also reported results on the observation of a pseudoscalar structure $X(2.2)$ in radiative decays of J/ψ with a mass 2.2 GeV/c^2 decaying to $\phi\phi$. The resonance width is $\Gamma = 132 \pm 46 \pm 35 MeV$ [126]. It seems that the resonance observed by DM2 is narrower than that in the MARK III observation.

We have searched for the decay $\Upsilon \to \gamma X \to \gamma\phi\phi \to \gamma K^+K^-$ at the MD-1 [118]. The same statistics as in the search for the decay $\Upsilon \to \gamma\xi(2.2) \to \gamma K^+K^-$ was used. In this experiment the main selection criteria were: at least one reconstructed photon in shower-range system and four particles reconstructed in the coordinate system. After these criteria some others (based mainly on Cherenkov counters) were applied to suppress the hadron background. No events were found in the vicinity of the X(2.2). The upper limit is

$$B(\Upsilon \to \gamma X)B(X \to \phi\phi) < 3 \cdot 10^{-3} \quad (90\% CL).$$

Since the number of remaining events is zero, our upper limit for this decay does not depend on the assumption about the resonance width.

This result was obtained under the assumption that the spin of X(2.2) equals 0. The variations of the upper limit due to uncertainties in the dynamics of the $X \to \phi\phi$ decay are less than 10%. For $J = 2$ the detection efficiency depends strongly both on the dynamics of the decays $\Upsilon \to \gamma X$ and $X \to \phi\phi$. Depending on the assumption of the dominance of various amplitudes the upper limit varies in the range $2 \cdot 10^{-3}$ to $4 \cdot 10^{-3}$.

We are not aware of other experiments on the search for this decay.

Table 6.2: The numbers of the experimental events and the events of the simulated processes $e^+e^- \to \rho^0\gamma$ and $e^+e^- \to \mu^+\mu^-\gamma$.

	Resonance	Continuum
experiment	19 ± 4.4	71 ± 8.4
$e^+e^- \to \rho^0\gamma$	5.2 ± 0.7	18.6 ± 2.1
$e^+e^- \to \mu^+\mu^-\gamma$	11.3 ± 1.2	37.2 ± 2.2

6.5. Upper limit on $B(\Upsilon \to \rho^0\pi^0)$

One of the interesting questions of the Υ physics is the search for the Υ meson decays with low multiplicity. The theoretical estimate gives the value $B(\Upsilon \to \rho\pi)/B(J/\psi \to \rho\pi)\ (M_{J/\psi}/M_\Upsilon)^6 \sim 10^{-3}$ [104, 127]. Using the known experimental value of $B(J/\psi \to \rho\pi) = 1.28 \cdot 10^{-2}$ [128] one obtains $B(\Upsilon \to \rho\pi) \sim 10^{-5}$. The experimental limit for $B(\Upsilon \to \rho^0\pi^0) < 6.9 \cdot 10^{-4}$ $(90\%\, CL)$ was obtained with LENA detector [129].

In this experiment [130] the same statistics as in our search for the decay $\Upsilon \to \gamma\xi(2.2) \to \gamma K^+K^-$ was used.

The energy of π^0 in the decay $\Upsilon \to \rho^0\pi^0$ is equal to 4.5 GeV. The resolution of our detector did not allow to reconstruct both photons in this decay, so the events were detected as two charged particles and one photon.

The same final state can be produced in the following processes: $e^+e^- \to \rho^0\gamma$, $e^+e^- \to \mu^+\mu^-\gamma$, $e^+e^- \to e^+e^-\gamma$, and $e^+e^- \to \gamma\gamma$ (with conversion of one γ quantum to the e^+e^- pair at the beam pipe). These are the main background processes for the decay under investigation.

For the simulation of the decay $\Upsilon \to \rho^0\pi^0$ we used the following dependence of the decay probability on the final particles momenta:

$$\frac{dw}{dR} \sim |F_\pi(m^2_{\pi^+\pi^-})|^2[\vec{q}_+(\vec{n}\vec{q}_-) - \vec{q}_-(\vec{n}\vec{q}_+)]^2, \tag{6.1}$$

where R is the phase space of three particles (π^+, π^-, π^0), $\vec{q}_+$, $\vec{q}_-$ are π^+ and π^- momenta, $\vec{n}$ is the direction along the beam line, $m_{\pi^+\pi^-}$ is the invariant mass of the $\pi^+\pi^-$ system. F_π is the π meson form factor, the expression for which could be found in [131].

The cross section of the process $e^+e^- \to \rho^0\gamma$ $(\rho^0 \to \pi^+\pi^-)$ was derived, using the formulae for the photon emission from the initial state obtained in [132]. For a simulation of the process $e^+e^- \to \mu^+\mu^-\gamma$ the computer code [100] was used, and for $e^+e^- \to e^+e^-\gamma$ – the computer code [133]. The process $e^+e^- \to \gamma\gamma$ was simulated according to the known cross section [134]. For all these processes we took into account the radiative corrections [135]. The value of these corrections is about 20% for our experimental conditions.

For the search of decay $\Upsilon \to \rho^0\pi^0$ we used the same selection criteria as in the search for decay $\Upsilon \to \gamma\xi(2.2) \to \gamma K^+K^-$. The only difference is the assumption about the charged particles masses. The charged particles were assumed to be pions.

The number of events having passed these selection criteria and having $m_{\pi^+\pi^-} < 4\ GeV/c^2$ is given in Table 6.2. The resolution on the invariant mass of charged particles in this region of $m_{\pi^+\pi^-}$ is equal to 35 MeV/c^2. In this Table the number of events obtained by the simulation of the background processes $e^+e^- \to \rho^0\gamma$ and $e^+e^- \to \mu^+\mu^-\gamma$ is also given.

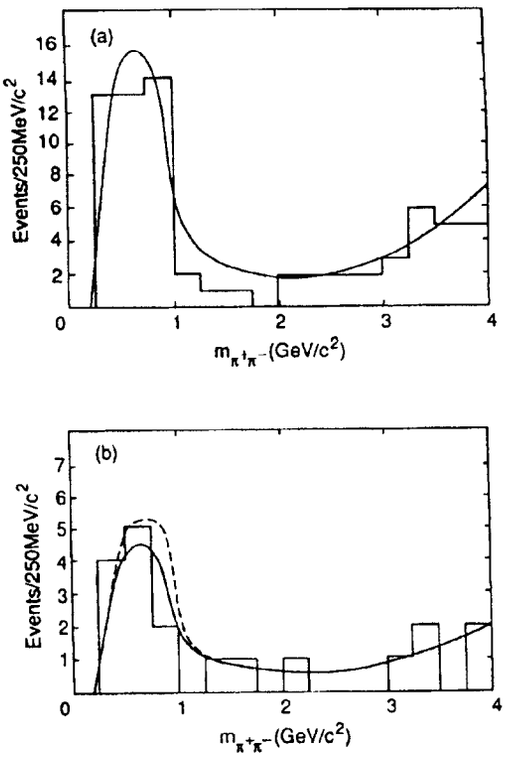

Fig. 6.3: Distribution of experimental events in $m_{\pi^+\pi^-}$ and fitted curves. (a) Events outside the resonance region are shown. (b) Events in the resonance region are shown. The dashed line displays the fitted curve including the decay $\Upsilon \to \rho^0\pi^0$ with probability $B(\Upsilon \to \rho^0\pi^0 = 3.3 \cdot 10^{-4}$ in addition to the background processes.

Other background processes contribute less than the processes mentioned above. We estimated the number of background events of the processes $e^+e^- \to e^+e^-\gamma$ to be about 30% of that due to the process $e^+e^- \to \mu^+\mu^-\gamma$. The process $e^+e^- \to \gamma\gamma$ with the conversion of one photon at the beam pipe of the detector into an e^+e^- pair is also one of the possible background sources. The number of events of this process is about 20% of that due to the process $e^+e^- \to \rho^0\gamma$.

As one can see in Table 6.2, the background processes $e^+e^- \to \rho^0\gamma$, $e^+e^- \to \mu^+\mu^-\gamma$ do not describe entirely the experiment. Therefore we tried to fit the experimental events with the sum of the contributions from the decay $\Upsilon \to \rho^0\pi^0$, two background processes, $e^+e^- \to \rho^0\gamma$, $e^+e^- \to \mu^+\mu^-\gamma$, and an unknown background.

We assumed that the cross section of the unknown background is $\sigma_B \sim s^{-1}$. The validity of this assumption was checked on the statistics collected outside the resonance region. The dependence of σ_B on $m_{\pi^+\pi^-}$ was approximated in two ways: independent of $m_{\pi^-\pi^+}$ with $\sigma_{B1} = a/s$ or quadratic on $m_{\pi^+\pi^-}$ with $\sigma_{B2} = b(m_{\pi^+\pi^-} - c)^2/s$, where a, b, c are free parameters fitted to the experimental data. Using this parametrization we obtained for the fitted events of the continuum a value of $P(\chi^2)$ equal to 2.5% and 30% for the uniform and quadratic dependence on the $m_{\pi^+\pi^-}$ background, respectively. In Fig. 6.3 the continuum and resonance events are shown with the quadratic parametrization σ_B of $m_{\pi^+\pi^-}$.

We obtained the following upper limit for the decay probability $\Upsilon \to \rho^0\pi^0$:

$B(\Upsilon \to \rho^0\pi^0) < 3.3 \cdot 10^{-4}$ (90% CL).

We checked the dependence of this result on a shape of the unknown background and on the range of beam energies used in the experiment. The difference from the cited result does not exceed 20%.

At the same time as ours, the upper limit for the $B(\Upsilon \to \rho^0\pi^0) < 6.6 \cdot 10^{-5}$ was obtained by detector CLEO [120] on larger statistics.

7. Measurement of inclusive production of hadrons

7.1. Inclusive production of the Λ in $\Upsilon(1S)$ decays and continuum

One of the interesting experimental facts of Υ physics is that a baryon yield in direct Υ decays is enhanced by a factor of more than 2.5 in comparison with the continuum. The study of inclusive baryon production is important for investigating the difference between the fragmentation of quarks and gluons.

We measured the inclusive Λ production in direct $\Upsilon(1S)$ decays and in the continuum [136]. The event sample used corresponds to the integrated luminosity of 5.6 pb^{-1} on the $\Upsilon(1S)$ resonance and 16.6 pb^{-1} in the continuum.

The suppression of background is described in sec.5.1. Detection efficiencies of 92 % and 83 % were achieved for the multihadronic $\Upsilon(1S)$ decays and the continuum events respectively.

Our Λ selection used the fact that $\sim$ 85 % of the events from the decay $\Lambda \to p\pi^-$ (in this Section references to specific states also imply the charge conjugate state) contain a proton and a pion with the momenta larger and smaller than 400 MeV/c respectively. Besides this, we required the distance from the secondary Λ-vertex to the beam axis in the plane transverse to the orbit to be larger than 3 cm, the minimum half-distance between tracks in the Λ candidate decay vertex to be smaller than 0.6 cm [137], and some other cuts on the geometry of the decay.

The detection efficiency was calculated using the LUND Monte Carlo [90, 138] and determined as a function of scaled momentum x_p ($x_p = p_\Lambda/p_{max}$, $p_{max} = \sqrt{E^2 - m_\Lambda^2}$). After application of the above mentioned cuts it is equal to 2.5 % for the x_p range 0.2-0.6. In the continuum the dependence of the detection efficiency on beam energy was taken into account.

The total number of events in our $\Upsilon(1S)$ sample was 98200. It decreased by 28 % after continuum subtraction. In this analysis the data with cms continuum energies of 8.8÷10.0 GeV were used. The corresponding integrated luminosities and the s-dependence of the continuum cross section were taken into account. Afterwards the number of Υ-mesons was decreased by (8.8 ± 0.5)% that is the fraction of observable $\Upsilon(1S)$ electromagnetic decays through qq pairs.

The integrated luminosities at different cms energies and the corresponding numbers of produced multihadronic events in the continuum are listed in Table 7.1. The background from two-photon (1%), tau- tau (2%), beam-gas (1%), radiative Bhabha (2%) and Υ decay events (21%) was subtracted.

Fig.7.1 shows the $p\pi^-$ mass spectrum for the $\Upsilon(1S)$ data after the above mentioned cuts. The contribution of the continuum was subtracted. For the data fit we used the resonance shape taken from the Monte Carlo model. The background was described by a second order polynomial with three free parameters. The results of the fit for the $\Upsilon(1S)$ data are:

$M_\Lambda = 1116.2 \pm 0.4$ MeV, $\qquad N_\Lambda = 228 \pm 21.$

Table 7.1: The luminosity integrals and the number of produced multihadronic events in the continuum.

Cms energy (GeV)	Luminosity int. (pb^{-1})	Number of events
7.2 - 8.0	1.02	6172
8.0 - 8.8	4.06	19022
8.8 - 9.42	4.42	19095
9.42 - 9.44	1.66	8237
9.47 - 10.0	4.89	22531

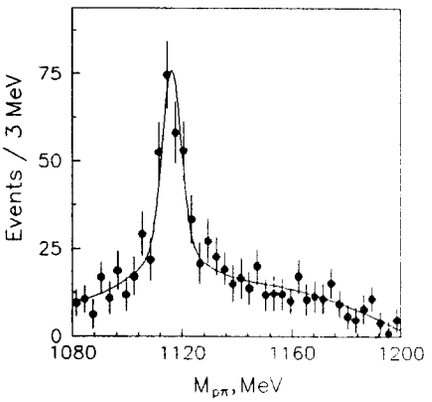

Fig. 7.1: $p\pi^-$ invariant mass distribution for the $\Upsilon(1S)$ data (the continuum contribution is subtracted).

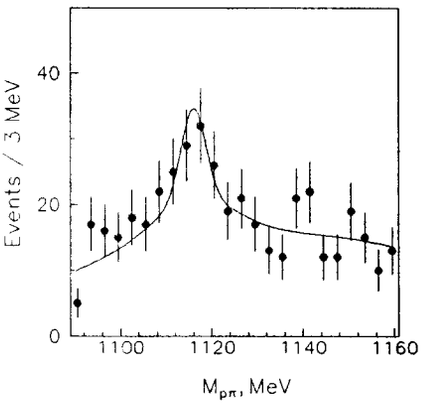

Fig. 7.2: $p\pi^-$ invariant mass distribution for the continuum.

Fig.7.2 shows the $p\pi^-$ mass distribution for the continuum. In this case both the resonance and the background shapes were taken from the Monte Carlo model. The results of the fit are :

$$M_\Lambda = 1116 \pm 2 \text{ MeV}, \qquad N_\Lambda = 77 \pm 18.$$

The fit with free background parameters gives almost the same values [136].

The Λ spectrum $(1/N)dn/dx_p$ in direct $\Upsilon(1S)$ decays is shown in Table . (N is total number of multihadronic events). It agrees with other measurements [139, 140].

The estimation of the different sources of systematic errors is given in Table 7.3.

Our estimation of the error due to the uncertainty in the Λ momentum distribution in the continuum is based on known experimental information on the Λ momentum spectrum [139, 140].

Taking into account systematic errors we have obtained the following Λ yield per multihadronic event in direct Υ decays and in the continuum

$$< n_\Lambda(\Upsilon(1S)_{dir}) >= 0.194 \pm 0.018 \pm 0.017,$$

$$< n_\Lambda(cont) >= 0.076 \pm 0.018 \pm 0.015.$$

Our results on the Λ yield in the direct $\Upsilon(1S)$ decays and in the continuum (for two different cms energy intervals) are presented in Table 7.4. Our measurements agree with the data of

Table 7.2: Λ spectrum in direct $\Upsilon(1S)$ decays.

x_p interval	$(1/N)dn/dx_p$
0.1-0.2	$0.82 \pm 0.14 \pm 0.09$
0.2-0.3	$0.57 \pm 0.09 \pm 0.06$
0.3-0.4	$0.29 \pm 0.07 \pm 0.04$
0.4-0.6	$0.053 \pm 0.016 \pm 0.011$

Table 7.3: Summary of systematic errors (in %) in the measurement of inclusive production of the Λ.

Source of systematic error	$\Upsilon(1S)$	Continuum
Efficiency of the tracking system	5	5
Background subtraction and efficiency calculation	3	7
Λ momentum distribution	3	7
Λ decay length distribution	2	2
Monte Carlo statistics	5	5
Resonance and background shapes	3	16
Total systematic error	9	20

detectors CLEO and ARGUS. In the range of cms energies 7.2÷9.4 GeV the Λ yield was measured for the first time.

7.2. Inclusive production of Ξ^- in $\Upsilon(1S)$ decays

Using data sample for the Λ production measurement we studied the $\Lambda\pi^-$ combinations to extract the Ξ^- signal. For this purpose we restricted the Λ-mass to be in the range of 1108 to 1124 MeV and imposed some cuts on the geometry of decay. Fig.7.3 shows the $\Lambda\pi^-$ mass distribution for the $\Upsilon(1S)$ data after these cuts.

The continuum was subtracted analogously to the Λ case. For the fit we have used the resonance shape from the Monte Carlo and a linear energy dependence for the background. The

Table 7.4: The results of the inclusive production of the Λ in direct $\Upsilon(1S)$ decays and continuum

Experiment	$< n_\Lambda(\Upsilon_{dir}) >$	$\sqrt{s}$, GeV	$< n_\Lambda(cont) >$
CLEO (85) [139]	0.19 ± 0.02	10.4 - 10.6	0.066 ± 0.010
ARGUS (88) [140]	$0.228 \pm 0.003 \pm 0.021$	9.4 - 10.6	$0.092 \pm 0.003 \pm 0.008$
MD-1 (94) [136]	$0.194 \pm 0.018 \pm 0.017$	7.2 - 10.0	$0.076 \pm 0.018 \pm 0.015$
		7.2 - 9.4	$0.070 \pm 0.027 \pm 0.020$

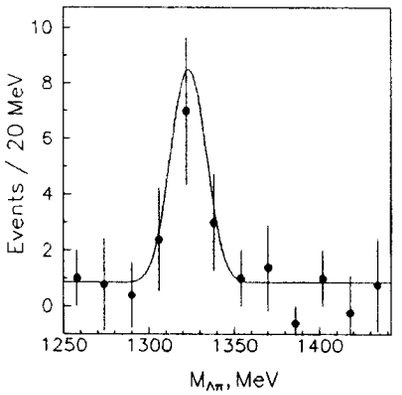

Fig. 7.3: $\Lambda\pi^-$ invariant mass distribution for the $\Upsilon(1S)$ data (the continuum contribution is subtracted).

fit results are :

$$M_{\Xi} = 1323 \pm 5 \text{ MeV}, \qquad N_{\Xi} = 9.9 \pm 4.0.$$

The sources of systematic errors are the same as in the Λ analysis. But the uncertainty in the Ξ^- momentum distribution gives larger error (16%). As a result we have obtained the Ξ^- yield per multihadronic event at the $\Upsilon(1S)$ decay:

$$< n_{\Xi}(\Upsilon(1S)_{dir}) >= 0.038 \pm 0.015 \pm 0.009.$$

The result of MD-1 on Ξ^- yield and results of other measurements are presented in Table 7.5

Table 7.5: The results of the inclusive production of the Ξ^- in direct $\Upsilon(1S)$ decays

Experiment	$< n_{\Xi} >$
CLEO (85) [139]	0.016 ± 0.04
ARGUS (88) [140]	$0.0206 \pm 0.0017 \pm 0.0023$
MD-1 (94) [136]	$0.038 \pm 0.015 \pm 0.009$

8. Measurement of Bose-Einstein correlations

An enhancement in the production of pairs of pions of the same charge and similar momenta was first observed in $p\bar{p}$ annihilation and attributed to Bose-Einstein statistics appropriate to identical pion pairs [141]. Later this phenomenon has been proposed in Refs. [142]-[144] as a tool to study the space-time structure of particle sources in high-energy reactions. Since then Bose-Einstein (BE) correlations have been extensively studied in various reactions. A comprehensive review has been given in [145].

Description of the theoretical basis for BE correlations can be found in a number of sources [142]-[147]. The BE correlation function is usually determined as

$$r(k_1, k_2) = P(k_1, k_2)/P_0(k_1, k_2), \tag{8.1}$$

where k_1, k_2 are particle four-momenta, $P(k_1, k_2)$ is the measured two-particle density for a like-charged pairs, and $P_0(k_1, k_2)$ denotes the two-particle density for a "reference sample", which, ideally, resembles the data in all respects except for the BE correlations.

Assuming gaussian distribution of the pion source density in the pair rest frame, the BE correlation function can be parametrized as

$$r(Q^2) = 1 + \lambda \cdot \exp(-r_0^2 \cdot Q^2) \tag{8.2}$$

where $Q^2 = -(k_1 - k_2)^2$, r_0 is the radius of the pion source and the parameter λ measures the strength of the correlations between pions. For chaotic source of identical bosons $\lambda = 1$. Taking both particles as pions $Q^2 = M_{\pi\pi}^2 - 4 \cdot m_\pi^2$, where $M_{\pi\pi}$ is the invariant mass of the pair.

An expression often used to analyze the experimental data is:

$$r(Q^2) = N \cdot (1 + \delta \cdot Q) \cdot (1 + \lambda \cdot \exp(-r_0^2 \cdot Q^2)), \tag{8.3}$$

where the factor $(1 + \delta \cdot Q)$ is introduced to take into account possible long-scale differences between $P(Q^2)$ and $P_0(Q^2)$, and N is a normalization factor. Although this expression is purely empirical, it has been shown to describe e^+e^- annihilation data well over a wide range of energies [148]-[155].

The event sample used in our experiment [156] corresponds to an integrated luminosity of 6.6 pb^{-1} on the $\Upsilon(1S)$ resonance and 19.1 pb^{-1} in the continuum in the energy region 7.2-10.3 GeV. Multihadronic final states in the continuum are produced via quark and antiquark fragmentation, those from the direct $\Upsilon(1S)$ decays originate from the hadronization of $3g$ and γgg states. Therefore studying these processes allows us to compare space-time properties of quark and gluon fragmentation.

The event selection procedure is described in subsection 9.1. The total number of selected continuum events is 39200. The total number of selected events in the $\Upsilon(1S)$ sample is 59300. It transforms to 48700 after background and continuum subtraction. After accounting for electromagnetic $q\bar{q}$-decays of the $\Upsilon(1S)$ the number of direct decays is 44600.

The like-sign pairs from these events are used for calculation of two-particle probability densities $P(Q^2)$, supposing all particles are pions.

One of the simplest ways to obtain a reference density $P_0(Q^2)$ is to use the unlike-sign pairs in the events. Their distribution contains much of the same physics as the like-signed distribution (i.e. phase space, momentum and angular distributions), but does not contain BE correlations. However, differences exist due to resonance decays, detector effects, and some other phenomena.

To the extent that the failings of the reference sample are correctly simulated by the Monte Carlo, one can overcome them by dividing the data by the Monte Carlo, i.e. studying the double ratio:

$$R = r_{data}/r_{MC} \tag{8.4}$$

The direct $\Upsilon(1S)$ decays and $q\bar{q}$ events were generated by the LUND 6.3 Monte Carlo code [157] which does not contain the BE correlations. Several corrections have been applied to remove residual differences between the data and simulation. A most substantial of them is correction of the resonance multiplicities in LUND 6.3, which are higher than give the recent measurements of ARGUS [158]-[160].

The correlation functions R as a function of $M_{\pi\pi}$ are shown for the direct $\Upsilon(1S)$ decays and continuum in Figs. 8.1, 8.2. Fits to these spectra by parametrization (8.3) yields the following parameters for $\Upsilon(1S)$ and continuum respectively:

$\lambda = 0.52 \pm 0.10$, $r_0 = 0.69 \pm 0.10$ fm, $\delta = 0.07 \pm 0.07$ GeV^{-1}.

$\lambda = 0.37 \pm 0.13$, $r_0 = 0.82 \pm 0.22$ fm, $\delta = 0.03 \pm 0.07$ GeV^{-1}.

The region of $0.46 < M_{\pi\pi} < 0.535$ GeV/c^2 was excluded from the fits to remove sensitivity to the production rate of K_s.

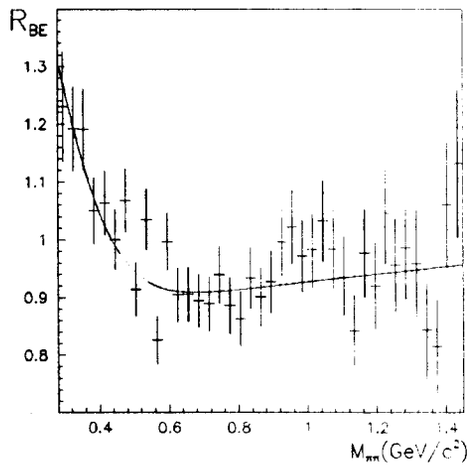

Fig. 8.1: $\Upsilon(1S)_{dir}$: r_{data}/r_{MC}, corrected.

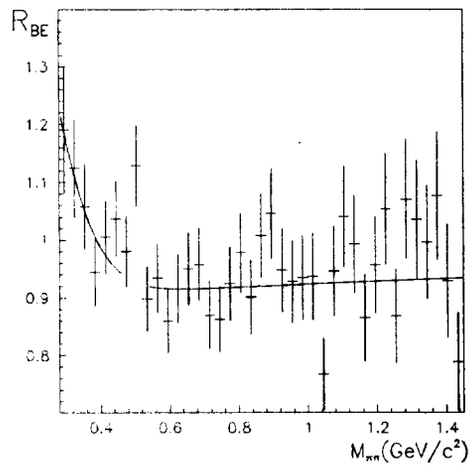

Fig. 8.2: Continuum: r_{data}/r_{MC}, corrected.

The following sources of systematic errors have been studied: 1) the finite momentum resolution of the detector, 2) $q\bar{q}$-contamination of the Υ-sample, 3) errors of the resonance multiplicities, 4) parametrization of long-range correlations. Combining these errors in quadrature we obtain the systematic errors of λ and r_0 0.06 and 0.04 fm for direct $\Upsilon(1S)$ decays and 0.06 and 0.05 fm for continuum.

Our values of λ as well as results of most previous e^+e^- experiments [148]-[155] are below of unity which is expected for chaotic source of identical bosons. Some factors responsible for it and related modifications of the correlation parameters are discussed below.

The first factor is admixture of unidentical (e.g., Kπ-) pairs in our like-sign sample. Assuming absence of BE correlations for these pairs parameters of correlations for identical pions can be derived by fitting to $R(Q^2)$ with a slightly modified version of (8.3) [152]:

$$R(Q^2) = N \cdot (1 + \delta \cdot Q) \cdot (1 + P_\pi(Q) \cdot \lambda \cdot \exp(-r_0^2 \cdot Q^2)), \tag{8.5}$$

where $P_\pi(Q)$ is a fraction of identical pions among all like-sign pairs obtained using the LUND 6.3. This yields parameters given below

$\Upsilon(1S)_{dir}$: $\lambda = 0.68 \pm 0.14$, $r_0 = 0.69 \pm 0.09$ fm,

continuum : $\lambda = 0.48 \pm 0.17$, $r_0 = 0.80 \pm 0.22$ fm.

Another λ-decreasing factor is the final-state pions originated from decays of long-lived particles (e.g., K_s, Λ, c-hadrons). BE enhancement, for pairs separated by the decay-lengths of weakly decaying particles, is unobservably narrow. Therefore parameters of BE correlations for remaining pairs can be derived similarly to previous case replacing in (8.5) $P_\pi(Q)$ by $P_\pi^{near}(Q)$, which is a fraction of such pairs among all like-sign pairs obtained using the LUND 6.3 MC simulation. Fits to $R(Q^2)$ by this modification of (8.5) yield the following parameters

$$\Upsilon(1S)_{dir}: \lambda = 0.77 \pm 0.16,\ r_0 = 0.69 \pm 0.09 \text{ fm},$$

$$\textit{continuum}: \lambda = 0.79 \pm 0.28,\ r_0 = 0.80 \pm 0.22 \text{ fm}.$$

Thus, if λ-decreasing contributions of unidentical pairs and weakly decaying particles are accounted, λ for remaining pairs becomes close to the theoretical expectation of unity.

However analysis [161] shows that contribution of the final state pions originated from decays of resonances to the observed BE enhancement is also suppressed. Accurate description of this effect is absent up to now. A rough estimate is obtained from analysis of the string fragmentation in LUND 6.3, assuming pions are effectively interfering only if distance between their production points don't exceed a decay-lengths of ρ-mesons. It is motivated by the fact that ρ-mesons are the only resonances included in the LUND 6.3 whose decay-length in the rest frame of the daughter pion ($\gamma c\tau \simeq 3\ fm$) is comparable with the measured size of the pion source. Similarly to previous cases $\lambda \simeq 2.6$ for direct $\Upsilon(1S)$ decays and $\lambda \simeq 2.8$ for continuum are obtained for such pairs. Although it's not a quantitative estimate we can see, that contribution of resonances is big and its account can move λ far above unity. Similar conclusions were obtained in Refs.[151, 153].

The correlation function is distorted also by the final-state interactions which are ignored by simulation. While hadronic final-state interaction is poorly known, the Coulomb correction can be applied through modification of $R(Q^2)$ as:

$$R(Q^2) \rightarrow R(Q^2) \cdot (1 - P^{cul}(Q^2) + P^{cul}(Q^2) \cdot \exp(2\pi\alpha m_\pi/Q)), \tag{8.6}$$

where P^{cul} is a fraction of pairs of the same type particles produced closely enough for substantial modification of their wave function by Coulomb interaction. Since Coulomb correction is relatively small, P^{cul} can be estimated as average between λ and P_π^{near}. It gives $P^{cul} = 0.58 \pm 0.07$ for the direct $\Upsilon(1S)$ decays and $P^{cul} = 0.41 \pm 0.05$ for continuum. Related correction to λ is equal to $+(8 \pm 1)\%$, while r_0 remains almost unchanged. In previous analyses Coulomb correction has been applied with $P^{cul} = 1$ [146], which leads to overcompensation of this effect.

There are several measurements of BE correlations in e^+e^- experiments in the continuum between $\sqrt{s}$=4 and 91 GeV, $J/\Psi(3.1)$- and $\Upsilon(9.46)$- decays [148]-[155].

Different experiments use different sets of corrections. Most papers contain corrections for non-pion track contamination and Coulomb effect but don't take into account contribution of long-lived particles. Therefore we shall take for comparison MD-1's as well as other results, corrected only for these two effects, with Coulomb correction recalculated according to (8.6). A summary of results is shown in Table 8.1.

There is no evidence of variation of the BE correlation parameters in the continuum in the energy range of Table 8.1. The constancy of r_0 confirms statement of the color string model [162]-[164], that r_0 represents the size of the local region responsible for production of pions of similar momenta rather than the size of the entire source. Taking into account $c\bar{c}$-contamination

Table 8.1: Compilation of BE correlation measurements corrected for non-pion tracks and Coulumb interaction only.

Experiment	$\sqrt{s}(GeV)$	Reference sample	λ	r_0 (fm)
MARK-2 [151]	4.1-6.7	unlike-signed	0.59 ± 0.06	0.71 ± 0.05
		event mixing	0.68 ± 0.07	0.78 ± 0.06
CLEO [149]	10.5	unlike-signed	0.46 ± 0.07	0.86 ± 0.15
	10.8	unlike-signed	0.44 ± 0.04	0.86 ± 0.08
MARK-2 [151]	29	unlike-signed	0.47 ± 0.05	0.84 ± 0.08
		event mixing	0.43 ± 0.05	1.01 ± 0.11
TPC [148]	29	event mixing	0.57 ± 0.07	0.65 ± 0.07
TASSO [150]	34	unlike-signed	0.57 ± 0.09	0.80 ± 0.06
AMY [152]	57.2	unlike-signed	0.56 ± 0.12	1.18 ± 0.17
OPAL [153]	91	unlike-signed	0.84 ± 0.14	0.93 ± 0.15
ALEPH [154]	91	unlike-signed	0.58 ± 0.04	0.81 ± 0.04
		event mixing	0.38 ± 0.02	0.49 ± 0.02
DELPHI [155]	91	unlike-signed	0.41 ± 0.03	0.82 ± 0.03
		event mixing	0.33 ± 0.03	0.42 ± 0.04
MD-1 [156]	7.2-10.3	unlike-signed	0.52 ± 0.19	0.80 ± 0.22
MARK-2 [151]	$J/\Psi(3.1)$	unlike signed	0.98 ± 0.09	0.81 ± 0.05
		event mixing	0.95 ± 0.09	0.79 ± 0.05
CLEO [149]	$\Upsilon(9.46)$	unlike-signed	0.54 ± 0.10	0.99 ± 0.14
MD-1 [156]	$\Upsilon(9.46)$	unlike-signed	0.73 ± 0.16	0.69 ± 0.10

of the continuum sample, we don't see any difference between parameters of BE correlations in the direct $\Upsilon(1S)$ decays and in the continuum nearby. Results of our experiment are in agreement with previous measurements.

9. Study of the reaction $e^+e^- \to$ hadrons

9.1 Search for narrow resonances

The energy region $2E$ =7.23–10.34 GeV (excluding Υ-mesons) in e^+e^- collisions has not been studied much before our experiment [165]. The region below 7.5 GeV has been investigated with MARK-1 at SPEAR [166]. Scanning has also been done using the detector LENA at DORIS in the regions 7.4–7.48 GeV and 8.47–9.43 GeV [79].

To some extent our interest in this region was connected with experiments on search of the $\zeta(8.3)$ performed by Crystal Ball and ARGUS [167, 168]. According to some models, if scalar quarks exist the new bound states can be predicted [169, 170]. Some of these states can be observed as narrow resonances in e^+e^- annihilation.

In this experiment the scan was performed in the range of cms energies $7.23 \div 10.34$. An integrated luminosity of 16 pb^{-1} was taken. The luminosity integral distribution over the energy is given in Table 9.1.

The energy region scan was done in steps of $\Delta(2E)$ =4–5 MeV (this value is close to the c.m.s. energy spread in VEPP-4). The data in each energy point were taken in several runs. The different energy regions were scanned 2 to 4 times. The regions 8.67–8.88 GeV and 9.420–9.445

GeV were scanned with increased luminosity per point in order to search for the $\zeta(P)$ predicted in the Tye and Rosenfeld model [169].

In selecting the multihadronic events the information from coordinate and shower-range chambers was used. The criterion more than 1 charged particle and some cuts on geometrical parameters of tracks and particle momenta reduced contamination from the processes $e^+e^- \to e^+e^-$, $e^+e^- \to \mu^+\mu^-$, $e^+e^- \to \tau\tau$ and $e^+e^- \to e^+e^- + hadrons$ to about 6%. The beam-gas background was about 0.3%, as determined by visual scan. The total number of selected multihadronic events was $4.8 \cdot 10^4$. The observed multihadronic cross-section is presented in Ref.[165].

The parameters of possible resonances were determined using the procedure described in subsection 5.1. The fitting of the experimental data were carried out with two parameters: $\sigma_{con} \cdot \varepsilon_{con}$ and $\sigma_{res} \cdot \varepsilon_{res}$, where σ_{con} and σ_{res} are the production cross-sections of the hadronic events for the continuum and resonance, and $\varepsilon_{con}, \varepsilon_{res}$ are the corresponding efficiencies. The visible width of a narrow resonance is determined by the c.m.s. energy spread of the colliding beam. For the VEPP-4 it is

$$\sigma_{2E} = (4.48 \pm 0.12)\left(\frac{2E}{M_\Upsilon}\right)^2 (\text{MeV}),$$

where M_Υ is the $\Upsilon(1S)$ meson mass, the value 4.48 ± 0.12 MeV was determined in our experiment on precise measurement of the $\Upsilon(1S)$ mass (subsection 4.2.).

The efficiency ε_{res} was calculated using the Lund 6.3 code [90]. We proposed that resonances decay like Υ mesons. The efficiency equals 0.72 for $\Upsilon(1S)$ meson decays and 0.62 for a resonance with a mass of 7.3 GeV. (A calculation using version 4.3 of the code differs by less than 2%). The energy dependence of the efficiency was approximated by a linear fit $\varepsilon_{res} = 0.24 + 0.051 \cdot 2E(\text{GeV})$.

No new resonances were observed in the energy region 7.23–10.34 GeV. The upper limits on leptonic width Γ_{ee} at a 90% confidence level are presented in Table 9.1 and Fig.9.1. The energy range 7.23–10.34 GeV is divided into several regions, for each region the maximum Γ_{ee} is taken.

Table 9.1: Upper limits on Γ_{ee} (at 90% CL) in the region 7.23–10.34 GeV

$2E$ (GeV)	$\Delta(2E)$ (MeV)	$\int Ldt\, pb^{-1}$	Upper limit (eV)
7.23–7.99	5	1.15	98
7.99–8.67	5	1.4	123
8.67–8.88	4	3.87	27
8.88–9.23	5	2.28	54
9.23–9.42	5	1.19	58
9.42–9.445	5	0.65	15
9.50–10.00	5	4.3	51
10.00–10.34	5	1.12	120

The experimental upper limit of 27 eV on Γ_{ee} in the region 8.67–8.88 GeV is close to the predicted value Γ_{ee} from Tye and Rosenfeld model [169]. The upper limit of 15 eV in the region 9.420–9.445 GeV is lower than the predicted value of 30 eV.

9.2. Measurement of the R

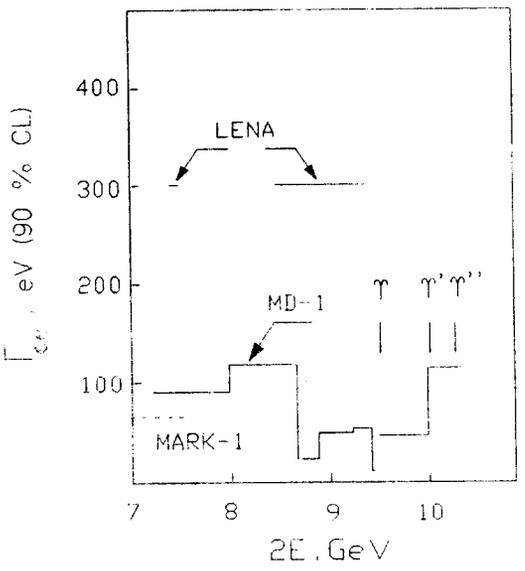

Fig. 9.1: Upper limits on Γ_{ee} for narrow resonances (90% CL). Data from MARK-1 [165] (dashed line), LENA [79], and MD-1 [165]

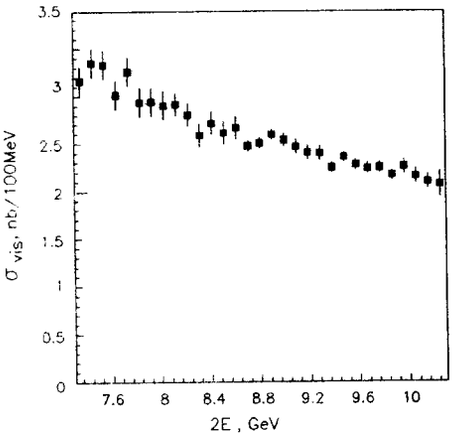

Fig. 9.2: The visible cross section of $e^+e^- \rightarrow$ *hadrons* versus center-of-mass energy.

The ratio R is defined as $\sigma(e^+e^- \rightarrow hadrons)/\sigma(e^+e^- \rightarrow \mu^+\mu^-)$, where non-resonant hadronic cross section does not include QED corrections and τ -pair decays, for μ -pair the Born cross section is taken. In the quark-parton model the process $e^+e^- \rightarrow hadrons$ proceeds via quark-pair which fragments into hadrons. In Born approximation R is a sum of the squares of the quark charges. The high order QCD corrections increase the R value calculated in Born approximation. In the third order of QCD [171] the R value is given by :

$$R = 3\sum_{i=1}^{n_f} Q_i^2 \cdot f_i^0 \cdot \{1 + f_i^1 \cdot [(\alpha_s/\pi) + r_1 \cdot (\alpha_s/\pi)^2 + r_2 \cdot (\alpha_s/\pi)^3]\}, \tag{9.1}$$

where Q_i is the quark charge, n_f is the number of active quark flavours, the factor 3 is due to the number of quark colors. The factors f_i^0 and f_i^1 are connected with the threshold dependence of the cross section [172]:

$$f_i^0 = \beta_i \cdot [1 + \frac{1}{2}(1 - \beta_i)^2],$$

$$f_i^1 = \frac{4\pi}{3}[\frac{\pi}{2\beta_i} - \frac{3 + \beta_i}{4}(\frac{\pi}{2} - \frac{3}{4\pi})],$$

where $\beta_i = v_i/c$, v_i is the quark velocity, c is velocity of light. The coefficients r_1 and r_2 obtained in the $\overline{MS}$ renormalization scheme are given in Ref.[171]:

$$r_1 = 1.9857 - 0.1153 \cdot n_f,$$

$$r_2 = -6.639 - 1.2001 \cdot n_f - 0.0052 \cdot n_f^2 - 1.2395 \cdot (\sum Q_i)^2/(3\sum Q_i^2).$$

The expression (9.1) for R is valid at center-of-mass energies far below Z^0 -mass where electroweak effects are negligible.

After the pioneering experiments in Frascatti [173, 174] and in Novosibirsk [175], the process $e^+e^- \to hadrons$ was investigated in many experiments at different energies [176]. The interest to this process is connected with possibility of the test of QCD calculations and determination of the strong coupling constant in the way independent of fragmentation models.

In our experiment [91] we performed a measurement of R at the center-of-mass energy region $7.25 \div 10.34$ which was not studied much before.

Two different sets of criteria ("S" and "T", see subsection 5.1) were used to select hadronic events and to suppress backgrounds. The detection efficiencies of about 70% were obtained both with T and S-criterion for hadronic events in the continuum with the background level about 25%. For further suppression of the two-photon, Bhabha, and $e^+e^- \to \tau^+\tau^-$ background we required T and S-criteria simultaneously and applied some additional cuts on number of particles in the tracking and shower-range systems, and on energy deposition in the shower-range system. As a result the detection efficiency of 52% was obtained at $2E = 9.46$ GeV for the continuum events with the background at the level of 5%.

The following processes were considered as the sources of background: 1) Beam-wall and beam-gas interactions, 2) $e^+e^- \to \mu^+\mu^-\gamma$, 3) $e^+e^- \to e^+e^-\gamma$, 4) $e^+e^- \to e^+e^- + e^+e^-(\mu^+\mu^-, \tau^+\tau^-)$, 5) $e^+e^- \to e^+e^- + hadrons$, 6) $e^+e^- \to \tau^+\tau^-$, 7) $e^+e^- \to \Upsilon(1S), \Upsilon(2S)$. The processing of the runs with the separated beams has shown that after the event selection procedure the contribution from the process 1 is negligible. The contaminations from the processes $2 \div 6$ were estimated using the Monte Carlo simulation. The contribution from the processes 2,3,4 was found to be negligible. The background from the process $e^+e^- \to e^+e^- + hadrons$ was estimated to be 1.5% at $2E = 9.4$ GeV and 1% at $2E = 7.4$ GeV. The contamination from the process $e^+e^- \to \tau^+\tau^-$ was 3.5% and it does not depend on the beam energy. The total background in the nonresonant region was estimated to be 5% at $2E = 9.4$ GeV and it slightly depends on the c.m.s. energy. The background from the $\Upsilon(1S)$ and $\Upsilon(2S)$ mesons was determined by fitting of the experimental data using procedure described in subsection 5.1 with 4 parameters: the masses and the cross section of the Υ mesons, the energy spread in the machine and the cross section in the continuum. The visible cross section after background subtraction is shown in Fig.9.2.

From the visible cross section after background subtraction the R value is obtained using the expression:

$$R = \frac{\sigma_{vis}}{\varepsilon(1+\delta)} \cdot \frac{1}{\sigma_{\mu\mu}}, \tag{9.2}$$

where ε is the detection efficiency for the multihadronic events with radiative effects included and $(1+\delta)$ is the radiative correction factor due to QED processes up to order α^3.

To determine the radiative corrections to the hadronic cross section and the detection efficiency, events in continuum were generated using the LUND 6.3 code [90]. In this version the radiative corrections are included according to [177]. The value obtained is $(1+\delta) = 1.234$ at $2E = 9.4$ GeV. It depends on cut-off for hard photons, but product $\varepsilon \cdot (1+\delta)$ is insensitive to these cuts since the detection efficiency for events with hard photons emitted is small. The systematic error in product $\varepsilon \cdot (1+\delta)$ due to uncertainty in the multihadronic cross section at low energies and low lying resonances is about 0.1%.

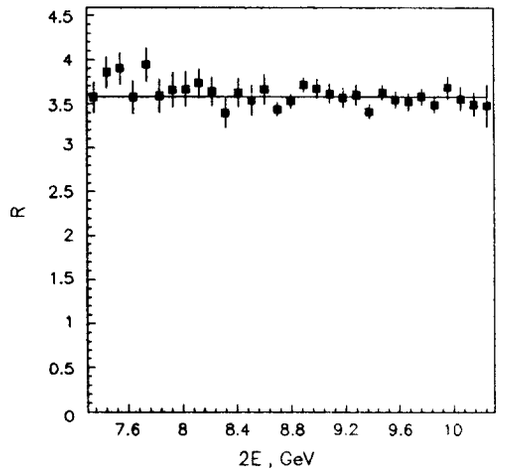

Fig. 9.3: The R value versus center-of-mass energy. The errors shown are statistical only. The solid line is the constant fit.

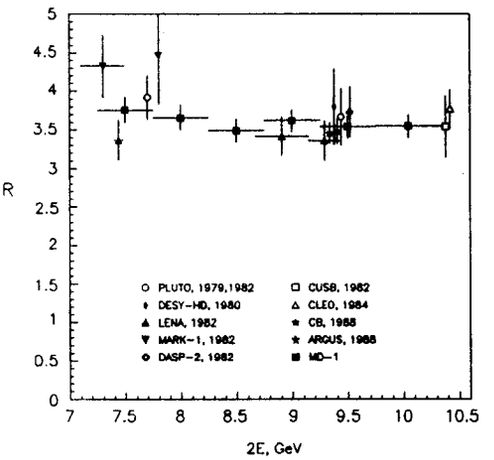

Fig. 9.4: Compilation of the results for R in the energy region between $7.0 \div 10.5$ GeV. The combined errors (statistical and systematic errors summed in quadrature) are shown.

The calculated efficiencies of the detector were corrected by both the measured efficiencies of chambers and the inadequate simulation of hadron ranges in NUCRIN. These corrections are equal to 10.5% and 1.2% respectively. After these corrections the simulated and observed distributions in such important parameters as the multiplicity, the sphericity, and the momentum distribution are in a good agreement.

The R value was determined using eq.(9.2). Its dependence on the c.m.s. energy is shown in Fig.9.3. The errors shown are statistical only (the systematic errors are given in Table 9.2). The data are presented in Table 9.3. There is no evidence for resonances (except Υ mesons). The data are fitted very well by constant ($\chi^2 = 28$ for 30 degrees of freedom) and we have found $\overline{R} = 3.578 \pm 0.021$.

Table 9.2: Summary of systematic errors to R

Source of systematic error	Error (%)
luminosity measurement	1.9
detector response	1.7
model dependence of efficiency	2.5
Monte Carlo statistics	0.5
$e^+e^- \rightarrow e^+e^- + hadrons$	0.4
$e^+e^- \rightarrow \tau^+\tau^-$	0.5
$e^+e^- \rightarrow e^+e^-\gamma$	0.6
radiative corrections	1.0

The systematic error in R is determined by several factors which are described below.

The error due to the detector response (1.7%) was estimated from the variation of chamber efficiencies and nuclear interaction parameters within acceptable limits.

The error arising from hadronization model was estimated by the following way. The comparison of the data and simulated observed multiplicities shows that they are in agreement within the error of $2.0 \div 3.0\%$. We adjusted the LUND 6.3 program parameters so that the observed multiplicity was changed by 2.7% and found the efficiency variation of 2.5%. This value was taken as an estimate of the error due to hadronization model.

The error due to the gamma-gamma background subtraction (0.4%) was estimated using our measurement of the total cross section of gamma-gamma into hadrons (subsection 10.2), where the total cross section was measured with error about 25%.

The errors due to subtraction of $e^+e^- \to \tau^+\tau^-$ (0.5%) and $e^+e^- \to e^+e^-\gamma$ (0.6%) processes were determined by Monte Carlo statistics.

We varied most significant cuts to check the stability of the R value. When the detection efficiency was increased by a factor of 1.12 and background by a factor of 2.5, the value of R was shifted only by $-0.5 \pm 0.7\%$.

The error due neglecting higher order QED contribution to the radiative corrections was estimated to be 1%.

The full list of systematic errors is given in Table 9.2.

Combining these errors in quadrature we obtained the systematic error of 3.9% for the measured R value. Our result for the average value in the energy region $7.25 \div 10.34$ GeV is

$$\overline{R} = 3.578 \pm 0.021 \pm 0.140$$

This value is in a good agreement with QCD prediction $R_{QCD} = 3.602 \pm 0.014$ at average scaling parameter $\Lambda = 260^{+54}_{-46}$ MeV [176].

The data (Table 9.3 and Fig.9.3) are also fitted very well by linear fit ($\chi^2 = 25$ for 29 degrees of freedom). This fit gives the value of slope

$$K = [R(7.2\,GeV) - R(10.34\,GeV)]/\overline{R} = 0.039 \pm 0.025\,(stat).$$

The systematic uncertainty in this value due to Monte Carlo statistics of efficiency calculation is 0.026. We summed the statistical and systematic errors in quadrature and obtained $K < 0.08$ at 90% CL.

We divided the energy region $7.25 \div 10.34$ GeV in 6 parts. In the Table 9.4 and Fig.9.4 our data on R are compared to the previous experiments in the region between 7.0 and 10.5 GeV.

The averaging of results collected in the Table 9.4 gives the value for $\overline{R}$ in the energy region $7.0 \div 10.5$ GeV:

$$\overline{R} = 3.579 \pm 0.066$$

(all errors were summed in quadrature). Using the formula (9.1) we obtain:

$$\alpha_s = 0.174 \pm 0.039 \quad (2E \approx 8.9\,GeV,\ n_f = 4,\ \beta_4 = 0.908).$$

Although the average $\overline{R}$ value has a good accuracy (1.8%), the corresponding error on α_s is about factor $2 \div 3$ worse than it was obtained from study of the direct QCD effects [176].

Our results are the most precise ones (only ARGUS measurement at 9.36 GeV has the same systematic error). The R value was not measured before in the energy intervals of $7.8 \div 8.7$ GeV and $9.5 \div 10.34$ GeV.

Table 9.3: The value of R in the region $7.25 \div 10.34$ GeV. The presented errors are statistical only. Systematic point-to-point error is 1.5%. The total systematic error in each point and for the average value of R is about 4%.

$2E$, GeV	R	ΔR (stat)	$2E$, GeV	R	ΔR (stat)
$7.25 \div 7.35$	3.57	0.175	$8.75 \div 8.85$	3.53	0.080
$7.35 \div 7.45$	3.86	0.178	$8.85 \div 8.95$	3.71	0.081
$7.45 \div 7.55$	3.89	0.181	$8.95 \div 9.05$	3.67	0.109
$7.55 \div 7.65$	3.57	0.184	$9.05 \div 9.15$	3.63	0.110
$7.65 \div 7.75$	3.94	0.187	$9.15 \div 9.25$	3.57	0.112
$7.75 \div 7.85$	3.59	0.189	$9.25 \div 9.35$	3.60	0.113
$7.85 \div 7.95$	3.66	0.192	$9.35 \div 9.45$	3.41	0.079
$7.95 \div 8.05$	3.67	0.195	$9.45 \div 9.55$	3.63	0.080
$8.05 \div 8.15$	3.73	0.158	$9.55 \div 9.65$	3.55	0.092
$8.15 \div 8.25$	3.64	0.161	$9.65 \div 9.75$	3.52	0.093
$8.25 \div 8.35$	3.40	0.163	$9.75 \div 9.85$	3.58	0.094
$8.35 \div 8.45$	3.63	0.165	$9.85 \div 9.95$	3.49	0.095
$8.45 \div 8.55$	3.54	0.168	$9.95 \div 10.05$	3.68	0.130
$8.55 \div 8.65$	3.66	0.170	$10.05 \div 10.15$	3.56	0.131
$8.65 \div 8.75$	3.44	0.079	$10.15 \div 10.25$	3.49	0.133
			$10.25 \div 10.34$	3.48	0.239
			$7.25 \div 10.34$	3.578	0.021
				Average	

10. Study of tagged $\gamma\gamma$ reactions

The two photon reaction

$$e^+e^- \to e^+e^- + X \tag{10.1}$$

is described by the diagram shown in Fig.10.1 where X is a system produced by two photons. The kinematics of $\gamma\gamma$ system X is determined by the four-momenta of the incoming and scattered electron and positron (usually below for brevity – scattered electrons). In Fig.10.1 $p_{1,2}$ and $p'_{1,2}$ are four-momenta of incoming and scattered electrons respectively, $\vartheta_{1,2}$ are angles of scattering of electrons, $q_{1,2}$ are four-momenta of the virtual photons, and $k_1, ..., k_n$- four-momenta of produced particles. In the $\gamma\gamma$ reaction (10.1) photons are predominantly emitted at small angles to the axis of beam. Therefore they are almost real ($q_i \approx 0$). The scattered electrons also emerge very close to the beam axis. As far as the momentum transfers q_1 and q_2 in this reaction are small, the system X has a very small transverse momentum. This feature of the reaction is usually used to extract two photon events from the data, especially in experiments without tagging of scattered electrons.

The $\gamma\gamma$ experiments can be defined depending on detection conditions of scattered electrons: 1) double-tag – the detection of both scattered electrons is required; 2) single-tag – one of the scattered electrons is detected, another escapes at zero angle; 3) anti-tag – both scattered electrons escape at zero angles; 4) no-tag – the experiment without detection of scattered electrons.

Our studies of $\gamma\gamma$-reactions in double-, single-, and no-tag modes performed with MD-1 are described in this Section and Section 11.

Table 9.4: Compilation of R measurement at center-of-mass energies between $7.0 \div 10.5$ GeV.

Experiment	$2E$ (GeV)	R
PLUTO, 1979 [178]	7.7	$3.92 \div 0.28$
DESY -Hidelberg, 1980 [77]	9.4	$3.80 \div 0.27 \div 0.42$
PLUTO, 1982 [179]	9.4	$3.67 \div 0.23 \div 0.29$
MARK-1, 1982 [166]	$7.0 \div 7.5$	$4.31 \div 0.04 \div 0.43$
	7.8	$4.47 \div 0.53 \div 0.45$
DASP II,1982 [78]	9.5	$3.73 \div 0.16 \div 0.28$
LENA, 1982 [79]	$7.40 \div 7.48$	$3.37 \div 0.13 \div 0.23$
	$8.67 \div 9.15$	$3.42 \div 0.10 \div 0.23$
	$9.15 \div 9.43$	$3.34 \div 0.09 \div 0.23$
CUSB, 1982 [180]	10.4	$3.54 \div 0.05 \div 0.40$
CLEO, 1984 [81]	10.4	$3.77 \div 0.06 \div 0.24$
Crystal Ball, 1988 [82]	9.4	$3.48 \div 0.04 \div 0.16$
ARGUS, 1991 [181]	9.36	$3.46 \div 0.03 \div 0.13$
MD-1, 1993 [91]	$7.25 \div 7.75$	$3.76 \div 0.10 \div 0.15$
	$7.75 \div 8.25$	$3.66 \div 0.10 \div 0.14$
	$8.25 \div 8.75$	$3.49 \div 0.08 \div 0.14$
	$8.75 \div 9.25$	$3.62 \div 0.07 \div 0.14$
	$9.25 \div 9.75$	$3.54 \div 0.07 \div 0.14$
	$9.75 \div 10.34$	$3.54 \div 0.07 \div 0.14$
Average	$\cong 8.9$	3.579 ± 0.066

10.1. Study of the reaction $\gamma\gamma \to \mu^+\mu^-$

Study of the reaction

$$e^+e^- \to e^+e^-\mu^+\mu^- \tag{10.2}$$

allows to check the calculation for α^4 order QED processes. During last 10 years this reaction was measured in many experiments [182]. The measurements were carried out in no-, single- and double-tag modes. In all experiments the number of the double-tagged events was small (less than 100) because the scattered electrons were detected at large emission angles (usually more than 20 mrad).

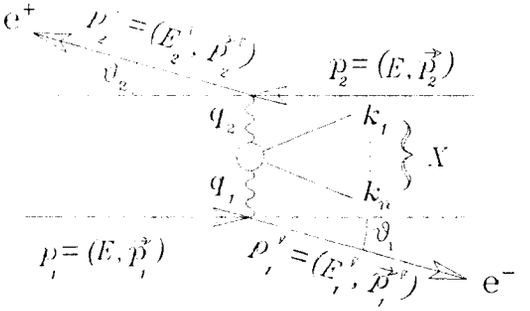

Fig. 10.1: The diagram for the two-photon reaction $e^+e^- \to e^+e^- + X$.

The reaction (10.2) in single- and double-tag modes was studied with the MD-1 detector [8]. With the aim of the tagging system (TS) calibration this process was also studied in the central detector (CD) without tagging of scattered electrons (no-tag mode). The data sample used for this analysis corresponds to the integrated e^+e^- luminosity of 23.6 pb^{-1} collected at 2E=7.2÷10.6 GeV. Results of our measurements are given below.

10.1.1. The no-tag mode

The total cross section of the process (10.2) calculated with the code [52], where the radiative corrections are taken into account, is equal to 61.8±0.2 nb at the beam energy E=4.73 GeV. The main physical background comes from the two-photon reactions:

$$e^+e^- \to e^+e^-\pi^+\pi^-, \tag{10.3}$$

$$e^+e^- \to e^+e^-e^+e^-. \tag{10.4}$$

The cross section of the process (10.4) is by a factor of 10^5 larger than that of (10.2), but most of the e^+e^--pairs are not detected in the detector.

We used the same selection criteria in the central part of the detector for the reaction $\gamma\gamma \to 2$ ***charged***, as described in subsection 11.2, with exception cuts based on the Cherenkov counters. The additional suppression of the processes with electrons in the final state ($e^+e^- \to e^+e^-$, $\gamma\gamma \to e^+e^-$, beam-gas interaction) was done using the pulse height information from both the scintillation counters and the shower-range chambers. Final sample contained N_0=12334 events.

The contributions of the background processes in the final event sample were estimated using the experimental data as well as the MC simulation. The events of the process (10.2) were generated with the code described in Ref. [52]. The processes (10.3) and (10.4) were simulated as it is described in subsection 11.2. Due to the lack of computing time the Monte Carlo statistics was about the same as the experimental one. The systematic error due to simulation of the detector is about 3%. The contributions of the background processes in the final sample of events are listed in Table 10.1.

Table 10.1: Process $\gamma\gamma \to \mu^+\mu^-$ in the no-tag mode. Background contributions in central detector.

Source of background	N_b/N_0 (%)
$\gamma\gamma \to \pi\pi$ (MC)	14.9 ± 2.2
$\gamma\gamma \to ee$ (MC, exp)	3.3 ± 1.2
$\gamma\gamma \to K\bar{K}, \tau\tau$ (MC)	0.5 ± 0.1
$ee \to ee, \mu\mu$ (MC)	0.5 ± 0.4
cosmic muons (exp)	0.5 ± 0.2
$ee \to$ *hadrons* (exp)	0.5 ± 0.3
beam-gas (exp)	2.5 ± 1.0

The invariant mass distribution for the selected $\mu^+\mu^-$ pairs is shown in Fig.10.2a. All particles are considered as muons. The spectrum shown is obtained after subtraction of contamination from $\gamma\gamma \to \pi^+\pi^-$, e^+e^- and other backgrounds (Table 10.1). It agrees with the calculated one within 5% error.

The number of the $\gamma\gamma \to \mu^+\mu^-$ events in the no-tag mode after the background subtraction is given in Table 10.2. The visible cross section of the $e^+e^- \to e^+e^-\mu^+\mu^-$ in the no-tag mode is

$$\sigma_{nt}^{vis}(ee \to ee\mu\mu) = 0.404 \pm 0.005 \pm 0.018\, nb.$$

In the simulation the number of selected events equals $7028 \pm 84 \pm 120$ for the integrated luminosity of 17.9 ($\pm 0.3\%$) pb^{-1}. The ratio of the measured cross section to the calculated one is

$$\sigma_{nt}^{exp}/\sigma_{nt}^{MC} = 1.021 \pm 0.013(stat) \pm 0.055(syst)$$

where the statistical error of the MC simulation is included into the systematic error of the ratio. The systematic error for the experiment is determined by the background subtraction procedure and simulation of detector response.

So, we have obtained a sample of 12334 events, mainly $\gamma\gamma \to$ *2 charged.* This sample is clean enough and was used for selection of the single- and double-tagged events $\gamma\gamma \to \mu^+\mu^-$.

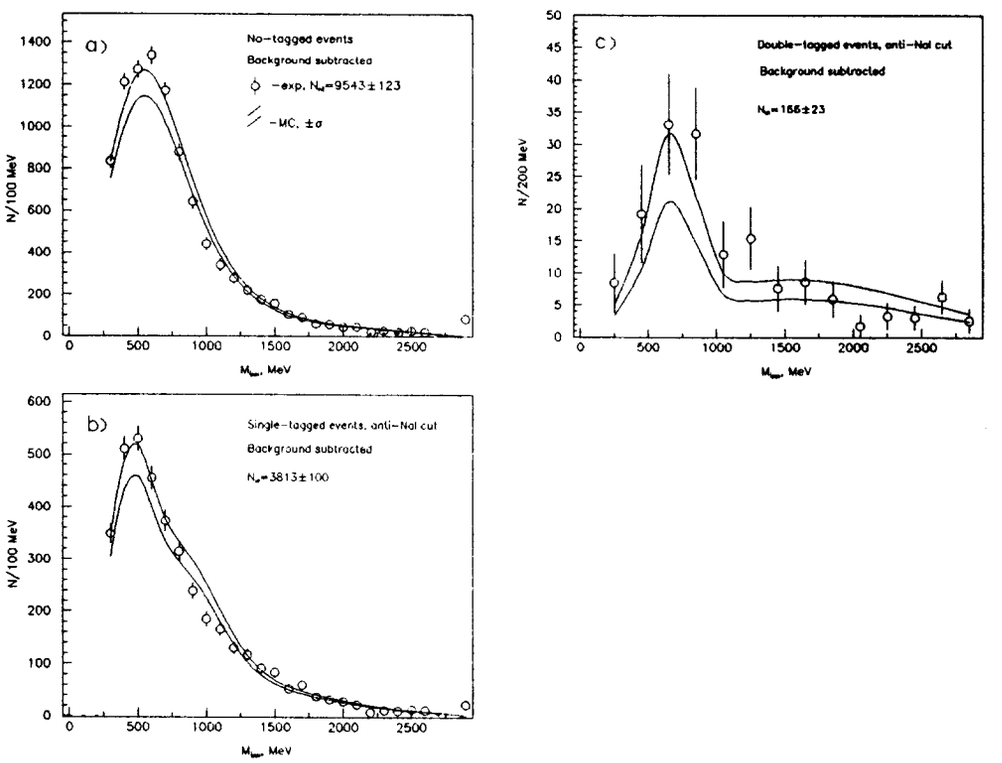

Fig. 10.2: Invariant mass spectra of selected pairs after subtraction of backgrounds. Particles are considered as muons. a) All events. b) Single-tag, anti-NaI cut. c) Double-tag, anti-NaI cut.

10.1.2. The single-tag mode

Each block of TS of the MD-1 detector measures emission angles of scattered electrons in radial and vertical directions (ϑ_Y, ϑ_Z), that allows to determine the energy E_e^{TS} with resolution of 1.75%. For selection of the tagged $\gamma\gamma$-events one should take into account the background in the TS. For one block of TS the probability of faked tagging is about 20%.

Main background comes from the single bremsstrahlung process (SB) where secondary electron is detected in TS. It can be effectively suppressed with the veto signal from the NaI detector, which detects the photons of the SB (anti-NaI cut).

Using the momenta of muons measured in the central detector one can calculate the energies (E_e^{CD}) of both scattered $e^{\pm}$ with additional assumption that at undetected electron was emitted with zero angle. This assumption is reasonable for our TS. The resolution on E_e^{CD} is about 1.5%. This allows to check the tagged electrons and to reject the background ones. The misidentification of the events $\gamma\gamma \to e^+e^-$ and $\gamma\gamma \to \pi^+\pi^-$ as $\gamma\gamma \to \mu^+\mu^-$ gives small effect on the calculated E_e^{CD}.

To determine the number of the single-tagged two-photon events we used the parameter $\Delta=(E_e^{TS} - E_e^{CD})/E$. The distributions in Δ for all events with tagged e^- and that after the SB background suppression are presented in Fig.10.3a,b. Fitting the distributions in Δ gives the number of real single-tagged $\gamma\gamma$-events (where all particles are properly reconstructed). The signal was approximated by the Gaussian with a tail. The width of the Gaussian was a free parameter. The tail $\sim 1/\Delta$ for $\Delta < -2\sigma$ was taken from the MC calculation. The background in the TS was described with the third degree polynomial. The results of the fitting are shown in Fig.10.3 too. The efficiency of the anti-NaI cut for the $\gamma\gamma$-events was about 0.85, whereas the background events were suppressed by a factor of about 7. The peak position and its width are close to the MC calculation. The efficiency of single-tagging is about 40%.

The distribution in the $\mu^+\mu^-$ invariant mass for the single-tagged $\gamma\gamma$-events is shown in Fig.10.2b. The distribution is obtained after the anti-NaI cut and subtraction of the known backgrounds including anti-tagged events $\gamma\gamma \to \mu^+\mu^-$ (plus background electron). The latter contribution was estimated directly by fitting the data (curve 3 in Fig.10.3b).

The detailed results are presented in Table 10.2. After the anti-NaI cut and backgrounds subtraction the visible cross section of the single-tagged $e^+e^- \to e^+e^-\mu^+\mu^-$ process is equal to

$$\sigma_{st}^{vis}(ee \to ee\mu\mu) = 0.162 \pm 0.004 \pm 0.007\ nb$$

and its ratio to the calculated one is

$$\sigma_{st}^{exp}/\sigma_{st}^{MC} = 0.988 \pm 0.026 \pm 0.061.$$

The systematic error is increased as compared to the no-tag case due to the background in the TS.

10.1.3. The double-tag mode

The background situation in this case is essentially worse compared to that for the single-tagged events. The reason is a small double-tag efficiency which is about 2% for the detected region of $M_{\mu\mu}$. Whereas the probability of the accidental coincidence of electron from the single-tagged $\gamma\gamma$-event with electron from the SB in the opposite block of TS is about 6% and that for the no-tagged $\gamma\gamma$-event with electrons from the SB in both blocks of TS is about 4%.

In the case of double-tagging we can determine the parameters of the $\mu^-\mu^+$ system from the TS information independently from the central part of MD-1. We used the distributions in $\Delta M_{\mu\mu} = M_{\mu\mu}^{CD} - M_{\mu\mu}^{TS}$ to obtain the number of the real double-tagged $\gamma\gamma$-events. The $\mu^+\mu^-$ invariant mass $M_{\mu\mu}^{CD}$ is calculated using the central detector data whereas $M_{\mu\mu}^{TS}$ – using the TS information.

Table 10.2: The results on the $\gamma\gamma \to \mu^+\mu^-$ process with and without tagging. Errors are statistical and systematic respectively.

	No-tag mode	Single-tag mode	Double-tag mode
Observed events	12334	5203	**385**
Background in TS	-	337 ± 87	177 ± 23
Background in CD	$2791 \pm 53 \pm 366$	$1052 \pm 44 \pm 144$	$42 \pm 9 \pm 6$
$N_{exp}(\gamma\gamma \to \mu\mu)$	$9543 \pm 123 \pm 366$	$3813 \pm 100 \pm 169$	$166 \pm 23 \pm 12$
$N_{MC}(\gamma\gamma \to \mu\mu)$	$9347 \pm 163 \pm 348$	$3857 \pm 86 \pm 143$	$135 \pm 16 \pm 6$
σ^{exp}/σ^{MC}	$1.021 \pm 0.013 \pm 0.055$	$0.988 \pm 0.026 \pm 0.061$	$1.23 \pm 0.18 \pm 0.16$

For the background suppression the anti-NaI cut was employed too. Additional suppression of the background electrons from SB can be done exploiting the fact that angular distribution of the SB electrons is more narrow than that for electrons from $\gamma\gamma$-processes. Rejecting the electrons with $\vartheta_Z < 5 \cdot 10^{-4}$ rad (ϑ_Z cut) we can increase the effect/background ratio.

The distribution in $\Delta M_{\mu\mu}$ after anti-NaI cut is shown in Fig.10.4a. This distribution was used to find the number of double-tagged events for comparison with the Monte Carlo calculation. The shape of the signal was approximated by the sum of two Gaussians. The fraction, location, and width of the broad Gaussian were taken from the simulation (fraction is about 0.20, width is about 1.2 GeV). Other parameters of the signal were free. The presence of the background events below the peak greatly increases the errors of the signal parameters. To decrease these errors the following fitting procedure was used. The sample of double-tagged events (Fig. 10.4a) was divided to two independent parts: the first - obtained after ϑ_Z cut (Fig. 10.4b) and the second which contained all the rest events. Both histograms were fitted simultaneously. In this case the second histogram having good signal/background ratio determines the shape of the signal. The shape of the signal was assumed to be the same for both samples. The background in the TS was described with the polynomial.

The parameters of the signal are Δ_{max}=-30±50 MeV/c^2 and FWHM/2.36=280±30 MeV/c^2. The width is determined equally by the central detector and the TS. The number of the double-tagged events equals 208 ± 23 at $M_{\mu\mu}$ around 1.0 GeV/c^2. This gives $166 \pm 23 \pm 12$ $\gamma\gamma \to \mu^+\mu^-$ events after the CD background (of $42 \pm 9 \pm 6$ events) subtraction. The detailed information about the double-tagged events is given in Table 10.2. The distribution in $M_{\mu\mu}$ for the double-tagged $\gamma\gamma$-events after anti-NaI cut with subtracted background is shown in Fig.10.2c. The visible cross section of the double-tagged $e^+e^- \to e^+e^-\mu^+\mu^-$ process is equal to

$$\sigma_{dt}^{vis}(ee \to ee\mu\mu) = 7.3 \pm 1.0 \pm 0.5\ pb,$$

its ratio to expected one is

$$\sigma_{dt}^{exp}/\sigma_{dt}^{MC} = 1.23 \pm 0.18 \pm 0.16.$$

The systematic error is mostly determined by the limited statistics of the MC simulation.

In summary, in the energy region of Υ-mesons we compared the measured cross section of the $e^+e^- \to e^+e^-\mu^+\mu^-$ process with the QED expectation in the no-, single- and double-tag modes. An order α^4 QED calculation (plus radiative corrections for the multiperipheral diagrams) shows

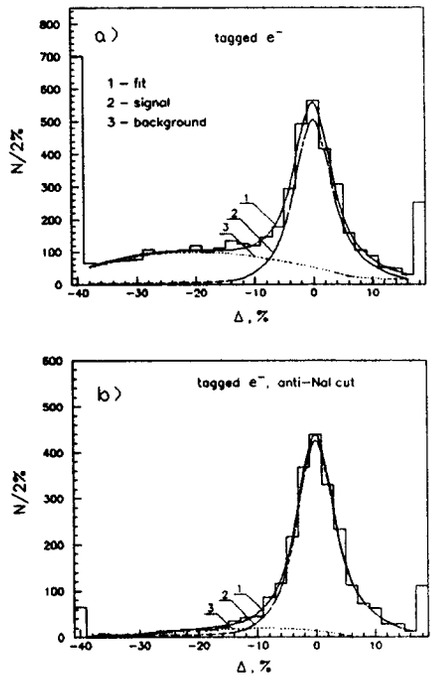

Fig. 10.3: Events with tagged electrons (e^-). Distributions in $\Delta = (E_e^{TS} - E_e^{CD})/E$ for selected $\mu\mu$-pairs. a) All events. Effect/background ratio equals 0.9. b) Events with anti-NaI cut. Effect/background ratio equals 5.7.

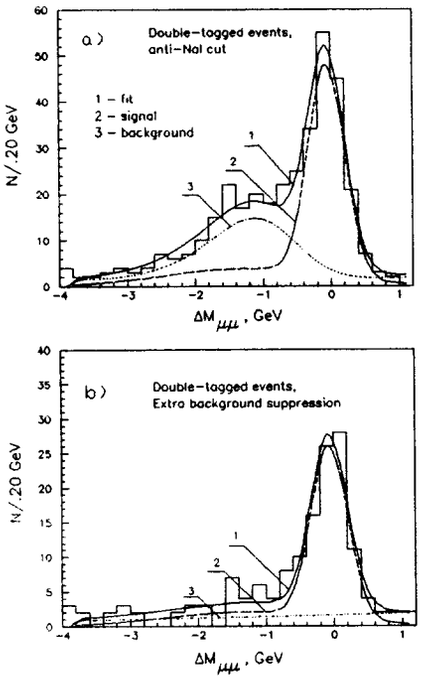

Fig. 10.4: Double-tagged events. Distributions in $\Delta M_{\mu\mu} = M_{\mu\mu}^{CD} - M_{\mu\mu}^{TS}$. a) Events with anti-NaI cut. Effect/background equals 1.1. b) Events with anti-NaI and $\vartheta_Z < 0.5$ mrad cuts. Effect/background ratio equals 2.3.

no discrepancy with the experimental results at the level of $(5 \div 6)\%$ for the no-tag and single-tag modes. We observed 166 events (the largest value among all experiments) for the double-tag mode at average $M_{\mu\mu} \simeq 1.0$ GeV/c^2. This measurement has an accuracy of 23% and agrees with the expectation.

10.2. Measurement of the total cross section $\gamma\gamma \to$ hadrons

The information on the two photon reaction $\gamma\gamma \to$ *hadrons* is extracted from the data on the reaction

$$e^+e^- \to e^+e^- + hadrons \tag{10.5}$$

Using the energy–momentum conservation laws at small scattering angles and omitting the terms of the order m_e^2/E^2, one can find the invariant mass W of the produced system and the photon masses squared q_i^2:

$$W^2 = 4(E - E_1')(E - E_2'), \tag{10.6}$$

$$q_i^2 = -EE_i'\vartheta_i^2, \tag{10.7}$$

where variables are shown in Fig.10.1.

In $\gamma\gamma$ experiments at e^+e^- colliders the double-tag mode with the detection of both scattered electrons is the most attractive due to the possibility of the direct measurement of the invariant mass of the produced system. Usually tagging systems can detect scattered electrons with emission angles greater than 20 - 30 mrad. However in this case the extrapolation of cross section to zero q^2 is required that results in some model dependence of the cross section data.

The first experiments on the total cross section measurement were performed in 1979 – 1981 by PLUTO [183] and TASSO [184] collaborations both in the single-tag mode. It was shown that these results can be well described by GVDM extrapolation to zero q^2 [185]. But further TASSO analysis with the larger data sample has shown that determination of the total cross section was impossible without assuming some a priori knowledge of the model parameters ([54], page 117).

The last results of PLUTO [186] obtained in a single-tag mode appeared in 1984, in 1984 – 1986 the results of the TPC/2γ double-tag experiment [187] and PLUTO [188] anti-tag data were published. Several years ago TPC/2γ published the results of their single-tag analysis [189]. The preliminary results of the MD-1 double-tag experiment were reported in 1985-1990 [190]. Final results of this experiment were published in 1992 [191].

The first theoretical calculation of the W dependence of the total cross section was performed by J.L.Rosner [192] in 1972 and slightly corrected by I.F.Ginzburg and V.G.Serbo in the paper [185] mentioned above. During the next few years some new calculations of the total cross section have been published [193]-[195].

The main advantage of the MD-1 detector for the study of two photon reactions gives the magnetic field transverse to the orbit plane of the colliding beams. The tagging system of the MD-1 provides a possibility to detect scattered electrons in a wide energy region with extremely small emission angles including ϑ_i=0. It makes possible a measurement of the invariant mass in the double-tag mode for practically real intermediate photons.

This experiment was performed at the VEPP-4 collider during 1984 - 1985. The center-of-mass energy of the colliding beams was varied in the region 7.7 – 9.7 GeV, and the integrated luminosity was 19.7 pb^{-1}.

The scattered electrons emitted at zero angles are detected by the tagging system in the range 0.5 – 0.85 of the beam energy. The elastically scattered electrons are detected if the emission angles are 12 – 100 mrad. The energy resolution measured with the Bhabha events is 1.75% and slightly depends on the energy. It results in an invariant mass resolution σ = 200 – 100 MeV at invariant masses W = 1.25 – 4.0 GeV (see Fig.2.5).

To suppress the single bremsstrahlung background in the tagging system each detected scattered electron was required to have the angle to the orbit plane greater than 0.5 mrad. This leads to the averaged $< q^2 >$ -value $-5 \cdot 10^{-3}$ GeV^2. Besides that it was required to have not more than one detected bremsstrahlung photon in the event. The tagging efficiency is shown in Fig.2.6. versus the invariant mass of the produced system. In order to select multihadronic events we required no less than 3 particles detected in the central part of the detector. Also some cuts on topology of events and hits in the shower system were used [191].

Finally 448 events in the W region 1.25 – 4.25 GeV were selected. The efficiency in the central part of the detector is shown in Fig.10.5. The main efficiency loss in comparison to the trigger efficiency is connected with the requirement to have not less than three detected particles.

The residual background contains beam-gas events, multi-hadron annihilation, two photon production of e^+e^- and $\mu^+\mu^-$ pairs, $\pi\pi$ – pair production (including $f_2(1270)$ meson contribution)

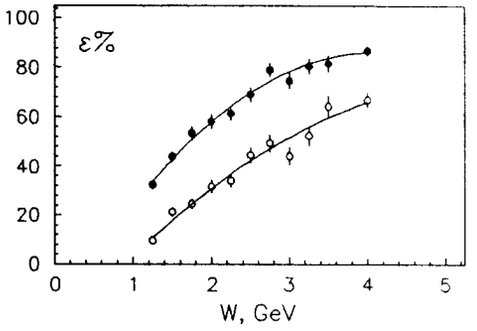

Fig. 10.5: Detection efficiency in the central part of the detector versus the invariant mass. Black circles — the trigger efficiency, open circles — the resulting efficiency of the event selection (curves — the quadratic fit).

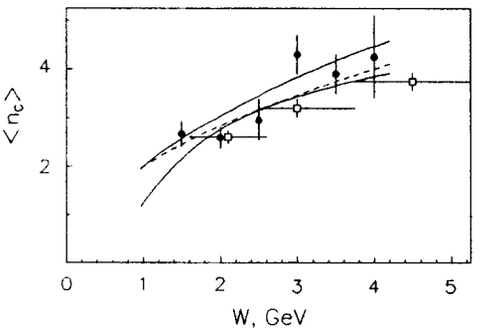

Fig. 10.6: Mean charged multiplicity versus invariant mass. Black circles - MD-1 data [191], solid lines — $\pm 1\sigma$ logarithmic fit, squares — TPC/2γ data [187], dashed line — PLUTO data [183, 186].

as well as the C-even resonances $a_2(1320)$ and $f_2'(1525)$. The beam - gas background was estimated using special background runs with vertically separated beams with a proper normalization as well as by visual scanning of selected events and was about 3%. The other background sources were determined by the Monte Carlo simulation. The total background level is 12% and was subtracted statistically.

As it was shown in [50] the cross section of the reaction (10.5) in the general case contains 6 invariant quantities corresponding to the various helicities of the virtual photons. But when the photons are close to the mass shell (small q^2) and the detector is symmetric with respect to the orbit plane the general formula can be considerably simplified and the differential cross section takes the following form:

$$E_1' E_2' \frac{d\sigma}{d^3p_1' d^3p_2'} = \frac{4\alpha^2((q_1q_2)^2 - q_1^2q_2^2)^{1/2}}{32\pi^4 E^2 q_1^2 q_2^2} \rho_1 \rho_2 \sigma_{\gamma\gamma}(W), \tag{10.8}$$

where $\rho_{1,2}$ are elements of the photons density matrix:

$$2\rho_1 = (2p_1q_2 - q_1q_2)^2/X + 1 + 4m_e^2/q_1^2, \quad \rho_2 = \rho_1(1 \leftrightarrow 2), \tag{10.9}$$

$$X = (W^2 - q_1^2 - q_2^2)^2/4 - q_1^2 q_2^2,$$

$\sigma_{\gamma\gamma}(W)$ - cross section for real photons.

This differential cross section was used for the simulation of the scattered electrons.

The produced hadronic system was sampled under the assumption that all produced particles are pions and the distribution in the transverse momenta of the produced pions is described by isotropic phase space (more details are in Ref.[191]).

The requirement of at least 3 particles in the central part of the detector leads to the loss of the experimental information about two pion production. Thus the cross section reported here excludes final states of two hadrons and we prefer to make no assumptions concerning them.

In order to determine the W-dependence of the cross section all statistics was divided into 6 bins on the W with a width of 0.5 GeV, as it is shown in the first line of the Table 10.3.

Table 10.3: Data on the charged multiplicity and the total cross section

W, GeV	1.5	2.0	2.5	3.0	3.5	4.0
χ^2/n_D	7.0/11	10.5/13	16.2/13	23.8/12	6.2/11	4.2/ 5
$< n_C >$	$2.67 \pm .26$	$2.59 \pm .21$	$2.95 \pm .42$	$4.30 \pm .40$	$3.90 \pm .40$	$4.25 \pm .85$
fit	$2.36 \pm .21$	$2.89 \pm .14$	$3.30 \pm .15$	$3.63 \pm .20$	$3.91 \pm .26$	$4.16 \pm .31$
σ, nb	606	352	356	260	352	214
stat. er., nb	100	49	42	37	59	64
syst. er., nb	61	35	33	22	42	28
total er., nb	117	59	53	43	72	70

The mean charged multiplicity $< n_c >$ and the estimation of its accuracy were found by the maximum likelihood method in the following way. The distributions of the number of charged particles and photons as well as the mean squared momentum of the charged particles were built for the experimental and Monte Carlo samples for each W-bin. All these histograms gave contribution to the χ^2-value which was minimized as a function of $< n_c >$.

To vary the $< n_c >$-value for the simulated sample the statistical weight was ascribed to each event. The weight was defined as a ratio of the desired and the initial probability to have the given number of the charged particles in the event. The charged multiplicity distribution was chosen of the KNO [196] shape that seems to be proper for the hadronic reactions [54], p.112. The ratio of the mean value and dispersion was fixed at the value 2.8 similar to that for the e^+e^- annihilation [197].

The results of the optimization are shown in the second line of the Table 10.3 in terms of χ^2-values for n_D degrees of freedom, the optimal $< n_c >$ values and estimated errors are shown in the third line. The W-dependence of the mean charged multiplicity was fitted by the function:

$$< n_c >= a + b \ln(W/GeV). \tag{10.10}$$

The optimal values of parameters are:

$$a = 1.62 \pm 0.37, \; b = 1.83 \pm 0.15.$$

Correlation coefficient is r=-0.93 and $\chi^2/n_D = 6.9/4$. The results of this fit are shown in the fourth line of the Table 10.3 and in Fig.10.6.

The radiative corrections connected to the photon emission by electrons and positrons were estimated in accordance with the radiation probabilities calculated in [85]. These corrections are 2 – 10% and were taken into account.

The obtained values of the cross section and their statistical and systematic errors as well as these errors added in quadrature are shown in the last four lines of the Table 10.3.

The systematic errors caused by the $< n_c >$ dependence of the efficiency, the uncertainties of the radiative corrections, simulation of nuclear interactions, acceptance of the tagging system, beam orbit instability, and the luminosity monitoring are about 10% in each W bin.

As it was mentioned above, we have excluded from our data the processes of two pion production (including $f_2(1270)$ meson) as well as $a_2(1320)$ and $f_2'(1525)$ mesons. Their calculated total contribution to the bin 1.25 – 1.75 GeV is 190 nb and does not exceed 5 nb for the others.

Fitting our cross section by the function

$$\sigma = A + B/W, \tag{10.11}$$

we found

$$A = 63 \pm 96\ nb,\ \ B = 670 \pm 246\ nb \cdot GeV.$$

The correlation coefficient is r=-0.97, $p(\chi^2)$ = 44%. However, because of the almost complete negative correlation, the values of A and B are very sensitive to the variations of the experimental points. The comparison of A and B values tends to exaggerate the differences between various experiments. The similar conclusion was made also in the work [189]. Therefore we prefer to compare the values of the cross section themselves rather than the obtained values of A and B.

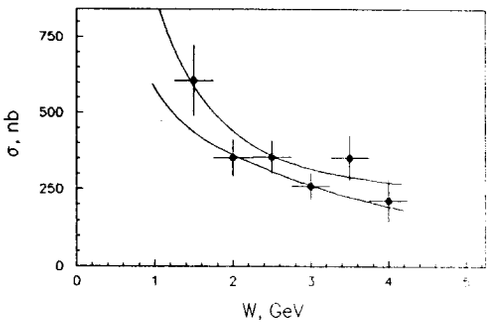

Fig. 10.7: Total cross section of the reaction $\gamma\gamma \to$ *hadrons* versus the invariant mass. Points — experimental data, vertical bars — statistical and systematic errors added in quadrature, horizontal — intervals of the cross section averaging. Lines — A+B/W - fit $\pm 1\sigma$.

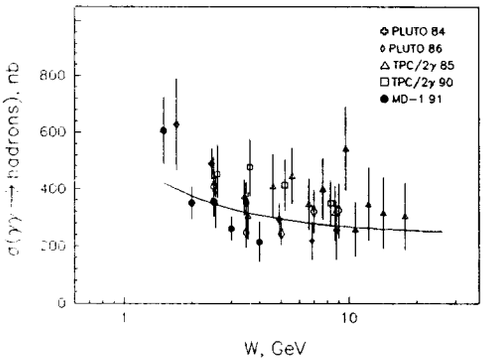

Fig. 10.8: Data of various experiments on the total cross section. Systematic errors are added in quadrature. PLUTO 1984 - single-tag data [186], PLUTO 1986 - anti-tag data [188], TPC/2γ 1985 - double-tag data [187], TPC/2γ 1990 - single-tag data [189], MD-1 1991 - this double-tag experiment. Line — σ=240+270/W(GeV).

The results on the total cross section measurement presented in the Table 10.3 and Fig.10.7 are in a good agreement with the early prediction [192] - σ(nb)=A+B/W(GeV) with A=240 nb, B=270 nb·GeV (p(χ^2)=29%), and apparently do not contradict to the calculation [185] A=255 - 300 nb, B=315±55 nb· GeV, $p(\chi^2)$ = 1.4% for average values of A and B.

The other theoretical expectations [193]–[195] predict a larger cross section for small W and do not agree with our results (the values of $p(\chi^2)$ are below 10^{-5}).

Our data on the charged multiplicity are in a good agreement with PLUTO [183], [186] approximation and are slightly higher than TPC/2γ [187]. The total cross section data of the experiments [186]–[189] and our results are shown in Fig.10.8. Our results are in a reasonable agreement with the other four experiments if the systematic errors are taken into account.

For a more detailed comparison of the data on the cross section we have averaged our data over W intervals as it is shown in Table 10.4. One can see that our data are in a good agreement with the PLUTO anti-tag [188] and TPC/2γ double-tag data [187], the differences are inside one standard deviation. The single tag data of PLUTO [186] and TPC/2γ [189] give the cross section values larger by 100 – 200 nb, the maximal difference is 2.5 standard deviations.

In conclusion, we outline the following. The total cross section of $\gamma\gamma \to$ *hadrons* in the invariant mass range 1.25 – 4.25 GeV was measured for the first time in the double-tag mode for almost real photons ($< -q^2 >= 5 \cdot 10^{-3}$ GeV^2) with a good W resolution (σ_W =100 – 200 MeV).

Table 10.4: Comparison of the experimental data on the total cross section. Cross sections are in *nb*.

Experiment.	W intervals, GeV		
	1.5-2	2-3	3-4
PLUTO 1984, single-tag [186]	627 ± 163	489 ± 54	369 ± 55
PLUTO 1986, anti-tag [188]		408 ± 104	247 ± 53
TPC/2γ 1985, double-tag [187]		353 ± 91	305 ± 82
TPC/2γ 1990, single-tag [189]		452 ± 104	476 ± 102
MD-1 1992, double-tag, zero angles [191]	448 ± 56	334 ± 29	257 ± 34

It allowed us to avoid any model dependence of the results due to the q^2 -extrapolation of the cross section and to keep the summary systematic error from other sources at the level of 10%. In the same W region the data on the charged multiplicity are obtained.

Our cross section data are compatible with the calculation of J.L.Rosner [192], do not contradict to the calculation of I.F.Ginzburg and V.G.Serbo [185], but disagree with the predictions [193]–[195].

10.3. Measurement of the $\Gamma_{\gamma\gamma}(\eta')$ *and* $\Gamma_{\gamma\gamma}(a_2)$

In this subsection results of studies of the two-photon production of the $\eta'(958)$ and $a_2(1320)$ with MD-1 in the reactions

$$e^+e^- \to e^+e^-\eta' \to e^+e^-\pi^+\pi^-\gamma \tag{10.12}$$

and

$$e^+e^- \to e^+e^-a_2 \to e^+e^-\pi^+\pi^-\gamma\gamma \tag{10.13}$$

are presented [198].

In this experiment integrated luminosity of 20.8 pb^{-1} collected at energy 2E=7.2–10.4 GeV was used. In the analysis events with two oppositely charged particles with momenta between 0.1 and 2.5 GeV/c, one or two photons and at least one tagged electron were selected. As a background in this experiment were processes of the type $ee \to eell\gamma$, $ee \to ll\gamma$ $(l = e, \mu, \pi)$, and $ee \to eell$, $ee \to ll$, which are accompanied by a fake photon or photon produced on the vacuum chamber, as well as non-resonant hadron continuum. To suppress these backgrounds some cuts in the main on geometrical features of events were used [198].

Then the events were kinematically reconstructed under the assumptions that the final state is $e^+e^-\pi^+\pi^-\gamma$ and undetected scattered electron has zero transverse momentum [198]. By reconstruction the photon energy was determined with an accuracy of 40 MeV, whereas the shower range system gives 100 MeV.

When two photons are present in an event (as in the decay of the a_2) the photon which is more coplanar to the system of charged particles was taken. The second photon is ignored in the analysis. That leads to some broadening of the a_2 mass spectrum and shift to lower masses, but the resonance structure subsists.

The method of equivalent photons (subsection 11.2) was used in calculation of the detection efficiency. About 11 % of scattered electrons emit photons with the energy greater than 50 MeV [199]. We took into account this process in calculations, since it decreases the energy of the tagged electron and shifts the reconstructed resonance mass.

For the process (10.13) we assume that it goes via $a_2 \to \rho\pi$ and the interference between the $\rho^+\pi^-$ and $\rho^-\pi^+$ decay modes was taken into consideration. The a_2 can be produced with helicities 0 and ± 2. The simulation was performed for both cases, since the difference in angular distributions has an influence on the detection efficiency.

The results of the analysis are shown in Fig.10.9, where the invariant mass spectrum of $\pi^+\pi^-\gamma$ system is presented after all cuts.

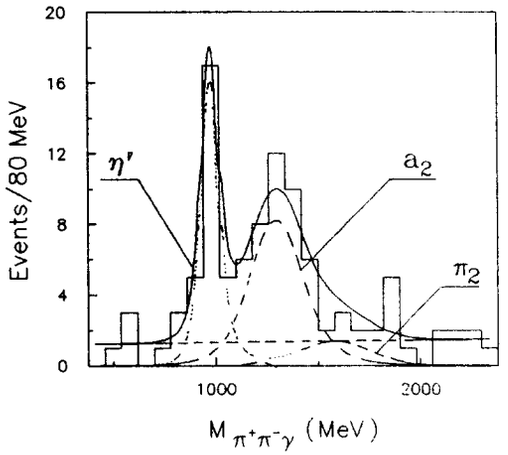

Fig. 10.9: $\pi\pi\gamma$ invariant mass distribution. Solid line is the fit of the data, dashed curves show separately the contributions of resonances and background

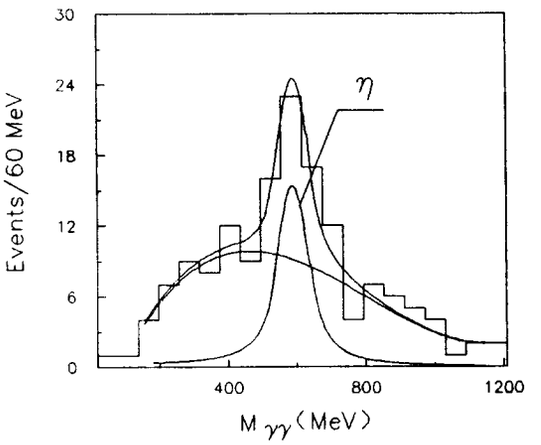

Fig. 10.10: $\gamma\gamma$ invariant mass distribution and the fit of the data. Separately the contributions of resonance and background are shown.

For the fit we have used the shapes of the a_2 and η' resonance curves taken from the Monte Carlo and parametrized by Gaussians with power-law tails. The background was described by a third degree polynomial with four free parameters. The η' and a_2 masses were also free. The fitting gave practically linear shape of the background, therefore the final results were obtained for linear background. The results of the fit for the data of Fig.10.9 are :

$$M_{a_2} = 1311 \pm 29 \text{ MeV}, \qquad M_{\eta'} = 974 \pm 15 \text{ MeV},$$

$$N_{a_2} = 38.8 \pm 7.5, \qquad N_{\eta'} = 23.3 \pm 5.6,$$

$$\chi^2/N_D = 7.2/10.$$

Contributions of the following background two-photon processes were calculated:

$$e^+e^- \to e^+e^-\eta \to e^+e^-\pi^+\pi^-\pi^0, \tag{10.14}$$

$$e^+e^- \to e^+e^-f_1(1285) \to e^+e^-\pi^+\pi^-\gamma\gamma, \tag{10.15}$$

$$e^+e^- \to e^+e^-\eta' \to e^+e^-\eta\pi^+\pi^-, \tag{10.16}$$

$$e^+e^- \to e^+e^-\pi_2(1670) \to e^+e^-\pi^+\pi^-\pi^0. \tag{10.17}$$

Only 9 ± 4 events of the reaction (10.17) passed selection criteria (we used $\Gamma_{\gamma\gamma}(\pi_2) = 1.4 \pm 0.4$ keV [200]). The fit with this process taken into account gives :

$$N_{a_2} = 36.3 \pm 7.5,\ N_{\eta'} = 23.3 \pm 5.6,\ N_{\pi_2} = 7 \pm 3,$$

$$\chi^2/N_D = 8.8/10.$$

By comparing these results with the simulation we obtained :

$$\Gamma_{\gamma\gamma}(a_2) = 1.26 \pm 0.26 \text{ keV},\ \Gamma_{\gamma\gamma}(\eta') = 4.6 \pm 1.1 \text{ keV}.$$

The known in 1990 experimental result on the helicity of the a_2 in two photon production [202] was used :

$$\sigma(J_z = 2) = (0.81 \pm 0.22) \cdot \sigma_{tot}.$$

Using the assumption of pure ± 2 helicity of the a_2 , our result on its two-photon width should be increased by 8 %.

The corrections connected with non-zero masses of colliding photons are negligible (less than 1 %) as soon as in our case $< -q^2 >$ is less than 0.001 GeV^2.

The detection efficiencies for the reactions under study are 0.8 % for the a_2 and 0.5 % for the η' where the efficiency of the detection of scattered electrons (55%) is included.

The estimation of systematic errors is presented in Table 10.5.

Table 10.5: Summary of systematic errors (in %) in the measurement of the two photon widths of the a_2 and η'

Source of systematic error	Contribution to $\Gamma_{\gamma\gamma}(a_2)$	Contribution to $\Gamma_{\gamma\gamma}(\eta')$
Trigger efficiency	3	3
Luminosity [19]	2.5	2.5
Branching [128]	4	5
Detection efficiency of coordinate chambers	3	3
Detection efficiency of tagging system	4	4
Uncertainty in resonance shape	4	3
Uncertainty in helicity of a_2	10	-
Statistical error of simulation	5.5	8
Total systematic error	14	12

Finally our measurements give the following two-photon widths of the a_2 and η' :

$$\Gamma_{\gamma\gamma}(a_2) = 1.26 \pm 0.26 \pm 0.18 \text{ keV},$$

$$\Gamma_{\gamma\gamma}(\eta') = 4.6 \pm 1.1 \pm 0.6 \text{ keV}.$$

These results are in good agreement other experiments [201].

10.4. Measurement of the $\Gamma_{\gamma\gamma}(\eta)$

The two-photon production of the $\eta(549)$ was studied in the reaction

$$e^+e^- \to e^+e^-\eta \to e^+e^-\gamma\gamma. \tag{10.18}$$

The same collected statistics was used as in the above experiment. The events without charged particles with two photons of energy less than 2 GeV each and at least one tagged electron were selected. To reject the cosmic rays background a time coincidence between the signals of scintillation counters and the beams collision moment (RF phase) within 6 ns was required. Background events from reactions of the type $ee \to eell, ee \to ll(l = e, \mu, \pi$ detected by the shower range system) and from the beam gas interactions were rejected by some cuts on the geometrical features of events [198].

Then the events were kinematically reconstructed under the assumption that the final state is $ee\gamma\gamma$ [198]. The measurement of the scattered electron momentum and the photon angles allowed us to reconstruct the η mass with an accuracy about 60 MeV.

The detection efficiency for the process (10.18) is equal to 0.8%. It was determined by the Monte Carlo simulation of the two photon production of the η using the same approach as in the case of the a_2 and η' production.

The resulting spectrum of $\gamma\gamma$ invariant masses is presented in Fig.10.10.

For the fit we have used the shape of the resonance curve from the Monte Carlo model parametrized by a Gaussian with power-law tails and a third degree polynomial with 4 free parameters for the background. The mass of the η was free parameter.

The result of the fit is:

$$N_\eta = 36.5 \pm 8.8,\ M_\eta = 588 \pm 17 \text{ MeV},$$

$$\chi^2/N_D = 7.8/13.$$

The comparison with the simulation gives

$$\Gamma_{\gamma\gamma}(\eta) = 0.51 \pm 0.12 \text{ keV}.$$

For the estimation of contributions of other two-photon reactions the following reactions were simulated (two-photon widths were taken from [128]):

$$e^+e^- \to e^+e^-\eta' \to e^+e^-\gamma\gamma, \tag{10.19}$$

$$e^+e^- \to e^+e^-\pi^0. \tag{10.20}$$

Only 2 ± 1 events from the process (10.19) passed our cuts. Due to the difference in masses they do not contribute to the measurement of two photon width of the η.

The sources of systematic errors in our measurement of $\Gamma_{\gamma\gamma}(\eta)$ are the trigger efficiency (3 %), the luminosity measurement (2.5 %), the uncertainty in the branching of (10.18) (1 %) [128], the detection efficiency of the tagging system (4 %), the uncertainty in the resonance shape (6 %), the statistical error of the simulation (5 %). The total systematic error is 10 %.

Our final result is

$$\Gamma_{\gamma\gamma}(\eta) = 0.51 \pm 0.12 \pm 0.05 \text{ keV}.$$

It is in a good agreement with other experiments [201].

10.5. Search for narrow resonances

During last 10 years many groups studied the two-photon production of C-even mesons at e^+e^- colliders [203]. Most of the results was obtained in the no-tag mode when the resonances were completely reconstructed in the detector. This requirement greatly reduces the efficiency and allows to study only resonances with the known decay modes.

For the double-tag measurement the invariant mass of the produced system $W_{\gamma\gamma}$ can be calculated as a missing mass from the parameters of scattered $e^{\pm}$. The narrow resonances would be presented as peaks in the spectrum of $W_{\gamma\gamma}$. The TPC/2γ collaboration has presented the result of such analysis [204]. Using the tagged electrons (emission angles $26 \div 90$ mrad) the missing mass resolution $\sigma(W) = 0.45 \div 0.20$ GeV/c^2 was obtained for $W_{\gamma\gamma} = 4.0 \div 20.0$ GeV/c^2. The double-tag efficiency ϵ_{dt} was about 1%. The upper limits for $(2J+1)\Gamma_{\gamma\gamma}$ of the possible resonances were established at the level of 30 keV$\div$10 MeV. This result seems to be preliminary but we are not aware of other publications.

In our double-tag experiment [205] the integrated luminosity of about 23 pb^{-1} collected in the energy region $2E = 7.2 \div 10.6$ GeV was used. The TS of the MD-1 detector was described in Section 2. The invariant mass resolution vs $W_{\gamma\gamma}$ for the double-tag mode is shown in Fig.2.5. It is $\sigma(W) = 0.2 \div 0.1$ GeV/c^2 for $W_{\gamma\gamma} = 1.0 \div 4.5$ GeV/c^2. The double-tag efficiency ϵ_{dt} vs $W_{\gamma\gamma}$ is shown in Fig.2.6. For the 100% efficiency in the central detector (CD) it reaches 20% at $W_{\gamma\gamma} \approx 2.5$ GeV/c^2. The real efficiency was 2–5 times smaller due to background in the TS and CD.

The selection criteria for the central detector were chosen to be relatively simple to provide a high efficiency for all hadronic events. It was required no less than 3 particles with at least 1 charged originating from the interaction region. Some additional cuts were applied to suppress the background from the two-prong events, cosmic muons, beam-gas and beam-wall events. Using these criteria about $3 \cdot 10^4$ events with two scattered electrons were selected, while the expected number of $\gamma\gamma$–events was about $2 \cdot 10^3$.

The events with one or two scattered electrons of non-$\gamma\gamma$ origin were considered as the background ones. The main background in the TS comes from the single bremsstrahlung process. Two independent methods were used for the background suppression: the anti-NaI cut and the ϑ_Z cut (see subsection 10.1). The efficiency of both cuts was measured directly with the $\gamma\gamma \to \mu^+\mu^-$ events for the effect and with the $e^+e^- \to hadrons$ events for the background. The efficiency of the anti-NaI cut is 0.78 ± 0.02 for the true event and 0.03 ± 0.005 for the fake event with two background electrons. For the ϑ_Z cut these values are 0.37 ± 0.015 and 0.02 ± 0.005 respectively. After the anti-NaI cut we had 2120 events with estimated background of 1200 ± 170 events. After applying both cuts we obtained 470 double-tagged events with residual background of 130 ± 45 events.

The resulting distributions in $W_{\gamma\gamma}$ are shown in Fig. 10.11a,b. For the case of anti-NaI cut we have high efficiency for the effect with the large level of background. In the case of combined cut we have good signal to background ratio for the price of the essential loss of the efficiency.

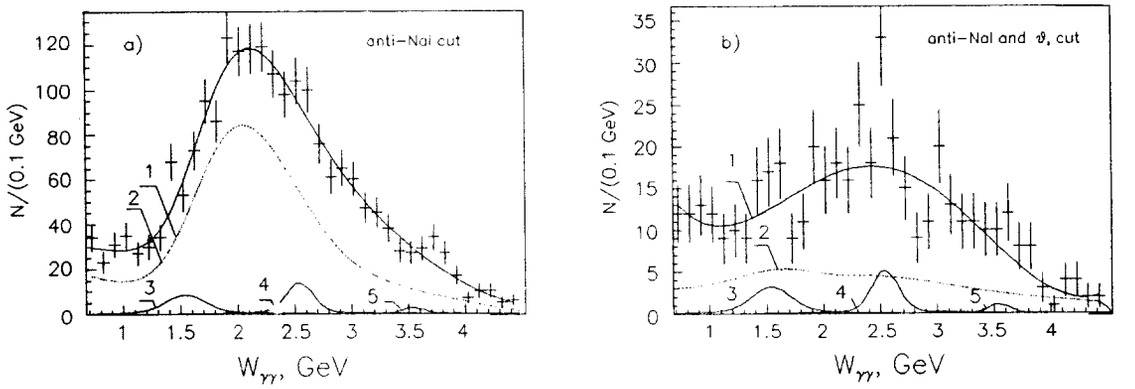

Fig. 10.11: The spectrum in $\gamma\gamma$ invariant mass of the selected events. a) Events passing anti-NaI cut, b) events after additional ϑ_Z cut. 1 – fitting curve, 2 – estimated background, 3,4,5 – expected signals of resonances corresponding to $\Gamma_{\gamma\gamma} = 20$ keV.

To estimate the selection efficiency for the unknown resonance the MC events $\gamma\gamma \to hadrons$ were used. The resulting total efficiencies for the anti-NaI and for both cuts are shown in Fig. 10.12. For the resonance with $\Gamma_{tot} < 50$ MeV/c^2 its width is determined by the resolution of the TS only. The resolution function of the TS was approximated by the sum of two Gaussians: about 20% with $\sigma = 500\ MeV/c^2$ and 80% with $\sigma = 90 \div 160\ MeV/c^2$. The influence of the radiative corrections on the value of the total cross section calculated according to Ref. [206] is small. The emission of hard photons gives the tail in the region $W_{\gamma\gamma} > M_{res}$. In the case of small angle tagging there is destructive interference between the electron radiation from initial and final lines [182]c. This effect essentially decreases the radiation tail for resonances.

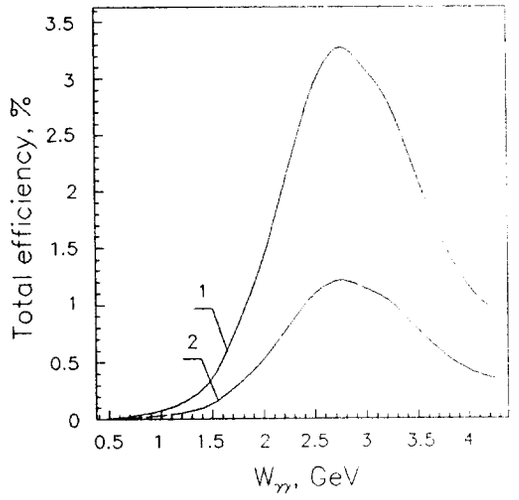

Fig. 10.12: The total selection efficiency in the double-tag mode for narrow resonances vs resonance invariant mass. 1– anti-NaI cut, 2– anti-NaI cut and ϑ_Z cut.

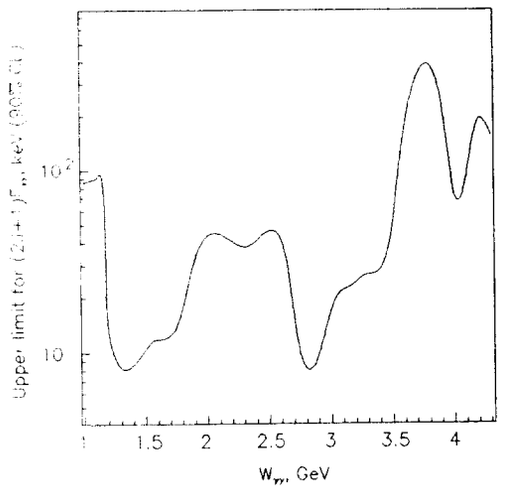

Fig. 10.13: The result of the upper limit analysis of search for narrow two-photon resonances.

To search for the resonance structure the spectrum in $W_{\gamma\gamma}$ was fitted as follows. The shape

was described by the sum of two parts:

1) resonance in the form of Breit-Wigner convoluted with the resolution function of the TS;

2) smooth line in a form $e^{p(W)}$, where $p(W)$ is a polynomial up to 4-th degree.

For the fitting we can use any of two spectra shown in Fig. 10.11. To achieve the best accuracy the following procedure was applied. The events selected after anti-NaI cut were divided into two independent parts: the first with events which passed ϑ_Z cut (Fig.10.11b) and the second with all the rest events (difference between the histograms in Fig.10.11a and Fig.10.11b). These two histograms were fitted simultaneously using the function described above. The coefficients of the polynomials p(W) were free in both cases while the number of resonances was $\epsilon \cdot N_{res}$ for the first histogram and $(1-\epsilon) \cdot N_{res}$ for the second one where ϵ is the efficiency for the ϑ_Z cut.

The results of the fit are shown in Fig. 10.11. There is no significant signal of a narrow resonance for $M_{res} = 1.0 \div 4.3\ GeV/c^2$. The obtained upper limits (at 90% CL, corresponding to fitted N_{res} +1.64 standard deviation) for the value of $(2J+1)\Gamma_{\gamma\gamma}$ are presented in Fig.10.13 and in Table 10.6. In the Table 10.6 the $\gamma\gamma$-mass range $1.0 \div 4.3$ GeV/c^2 was divided into several regions and for each region the maximum value of the upper limit was taken.

For the resonance with $J > 2$ the detection efficiency depends on the helicity of the produced resonance. In the case of pure helicity-2 state the upper limit for the $(2J+1)\Gamma_{\gamma\gamma}$ increases about 2 times.

Table 10.6: Upper limit on $(2J+1)\Gamma_{\gamma\gamma}$ of narrow C-even resonances in the mass region $1.0 \div 4.3$ GeV/c^2.

M_{res} (GeV/c^2)	$(2J+1)\Gamma_{\gamma\gamma}$ (keV), upper limit (90% CL)	M_{res} (GeV/c^2)	$(2J+1)\Gamma_{\gamma\gamma}$ (keV), upper limit (90% CL)
1.0–1.25	92.0	2.75–3.0	13.0
1.25–1.5	9.5	3.0–3.25	24.2
1.5–1.75	12.4	3.25–3.5	34.0
1.75–2.0	39.0	3.5–3.75	329
2.0–2.25	45.2	3.75–4.0	383
2.25–2.5	44.2	4.0-4.3	191
2.5–2.75	46.4		

In summary, using the 23 pb^{-1} sample of e^+e^- collisions in the energy region $2E = 7.2 \div 10.4$ GeV we looked for the reaction $ee \to eeR$ in the double-tag mode, were R is any narrow C-even resonance. No new resonances were observed with a mass within the interval $M_{res} = (1.0 \div 4.3)$ GeV/c^2.

11. Study of $\gamma\gamma$ reactions in no-tag mode

11.1. Process $e^+e^- \to e^+e^- + e^+e^-$

The main contribution to this reaction gives the two photon (Landau–Lifshitz) process described by the diagram shown in Fig.11.1A.

The calculation of the total cross section, taking into account the main diagrams with power

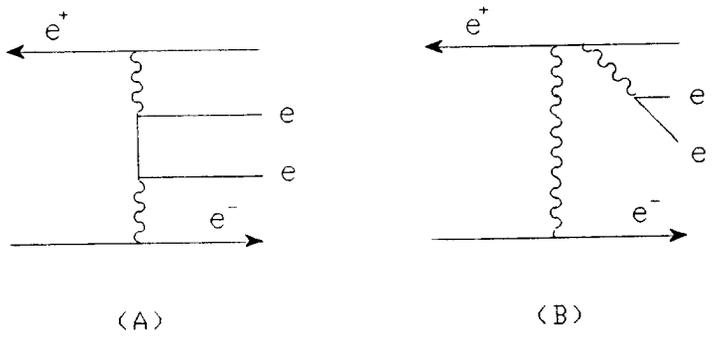

Fig. 11.1: Diagrams for the reaction $e^+e^- \to e^+e^- + e^+e^-$: A - the multiperipheral two photon graph; B - the bremsstrahlung graph.

accuracy on the energy, was done in Refs.[207, 208]

$$\sigma = \frac{\alpha^2 r_0^2}{\pi}(1.03L^3 - 6.6L^2 - 11.7L + 104), \tag{11.1}$$

where α is fine structure constant, r_0 is the classical electron radius, $L = \ln(s/m_e^2)$, $s = (2E)^2$. This cross-section grows with increasing of the beam energy. At the energy E = 1.8 GeV it is equal to $5 \cdot 10^{-27}$ cm^{-2} (see Fig.3.6).

The contribution of the bremsstrahlung diagrams to the total cross section was calculated in Ref.[209]. At the beam energy of 1.8 GeV this contribution is 0.3%. Numerically small (−0.1%) contribution at this energy comes from the account of an identity in the final state [51].

The differential cross section in the invariant mass of produced pair W is given by the following approximate expression [207, 208]:

$$\frac{d\sigma}{dW} = \frac{16\alpha^2 r_0^2}{3\pi} \cdot \frac{m_e^2}{W^3} \cdot \ln^3(\frac{s}{W^2})[2\ln\frac{W}{m_e} - 1]. \tag{11.2}$$

One can see that the main contribution to the cross-section comes from the low invariant mass region. In this experiment [20] the tagging system of MD-1 was not used, and the invariant mass of produced pair (Fig.10.1) was determined in the central part of the detector: $W^2 = (k_1 + k_2)^2$.

Due to magnetic field of MD-1 transverse to the orbit plane, we could measure momenta of particles emerging even at zero angle to the axis of beams and could study $\gamma\gamma$ production of e^+e^- pairs with low invariant masses, nearby the threshold of this reaction. In previous experiments process $\gamma\gamma \to e^+e^-$ was studied at considerably higher invariant masses [54]. For example, minimal invariant mass of pair was 80 MeV in the experiment with the DM-1 detector [210] and 800 MeV in the experiment with the PLUTO detector [211].

As a generator of events under study we used the code [55].

The main background process in this experiment is the production of e^+e^- pair by the synchrotron radiation photons on the electrons of the colliding beam (subsection 3.2). The counting rate of this process grows more rapidly with the increase of the beam energy than for the process under study. At the beam energy of 5 GeV both counting rates are equal. For this experiment the beam energy was chosen equal to 1.8 GeV where the contribution of background process is about 10%.

The e^+e^- pairs in main and background processes are kinematically identical, so the sum of the main and background processes was used for comparison of the calculation with the experimental data.

During the experiment the parameters of the storage ring VEPP–4 were the following: the energy E = 1.8 GeV, currents $I^{\pm}$ = 0.4 mA, the average luminosity $L = 4 \cdot 10^{27} cm^{-2} sec^{-1}$. The luminosity was limited by the collisions effects, which did not permit to have electron and positron currents greater than 0.5 mA. The integrated luminosity of 440 μb^{-1} was collected. 227000 events were recorded on the magnetic tape for head-on collisions ("effect") and 41000 events with separated beams ("background"). The ratio of recording time of "effect" to that of "background" was about 5.5.

Pairs of particles with opposite charges were selected using their spatial characteristics measured in the coordinate system. A picture of the typical event of effect looks like in Fig.3.7.

Along the particle path before the scintillation counters there are 30 mm thick stainless steel walls of the container of coordinate chambers. The probability for the particle detected in the coordinate system to hit a scintillation counter is (12.1±1.3)% for the experiment and (11.8±2.4)% for the simulation. A good agreement between these values gives a good evidence, that the detected particles are the electrons.

The measured and expected distributions in the particle emission angle with respect to the beam direction are shown in Figure 11.2. The experimental distribution is in agreement with the simulated one.

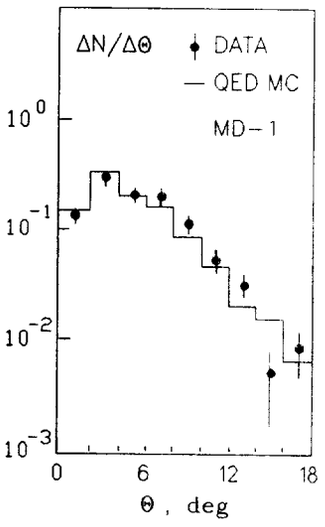

Fig. 11.2: The distribution in particle emission angle in $\gamma\gamma \to e^+e^-$. Background from $\gamma e \to ee^+e^-$ is ≃15%.

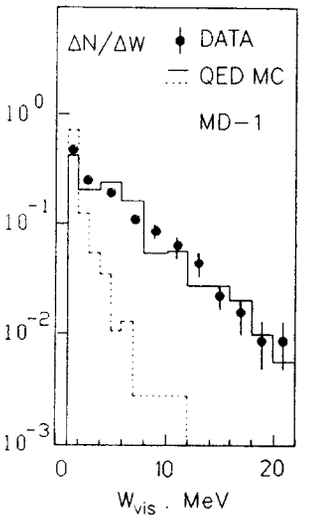

Fig. 11.3: The distribution in the visible invariant mass of e^+e^- pair in $\gamma\gamma \to e^+e^-$. Background from $\gamma e \to ee^+e^-$ is ≃15%. The dashed histogram shows the expected distribution without interaction of the particles with the beam pipe.

The distributions in the visible invariant mass for experimental and simulated events are shown in Fig.11.3. The average reconstructed masses in the experiment and simulation are respectively:

$\overline{W}_{vis}^{exp.} = 5.7 \pm 0.3$ MeV and $\overline{W}_{vis}^{MC} = 5.7 \pm 0.2$ MeV. By the dashed histogram the distribution of the same simulated events without interaction of the particles with the beam pipe is shown. The mean value for this distribution is equal to 2.1 MeV. One can see that the width of the distributions for experiment and Monte Carlo simulation is due to particle interactions with the beam pipe (i.e., multiple scattering, bremsstrahlung).

To compare the experimental and Monte Carlo values of the visible cross sections, we used the correction factor due to the chambers inefficiency. It was obtained experimentally and equals 1.19± 0.02. As a result, the experimental visible cross section equal to $\sigma_{exp} = 1.61 \pm 0.12$ μb was obtained. The error comes from: luminosity measurement (5%), statistics (4%), and correction for the chamber inefficiencies (2%).

The calculated visible cross-section for the process $e^+e^- \to e^+e^- + e^+e^-$ is equal to 1.58±0.15 μb. According to Ref.[51] the radiative corrections for this process are less than 0.5%. The contribution from the background process of e^+e^- pair production by the synchrotron radiation on colliding beam equals 0.24±0.06 μb. Thus, the calculated visible cross section for e^+e^--pair production is $\sigma_{MC} = 1.82 \pm 0.16$ μb in good agreement with the measured one.

Based upon the results of this experiment we obtained an upper limit for the two photon width of particle with mass of 1.8 MeV [212]. Some hints on a structure with mass of about 2 MeV decaying to e^+e^- pair were obtained in collisions of heavy ions [213] some time ago. From our experiment the upper limit for such particle is the following:

$$\Gamma_{\gamma\gamma} B_{ee} < 2\, eV \ (90\%\ \mathrm{CL}).$$

11.2. Measurement of $\gamma\gamma \to \pi^+\pi^-$ *and* $\Gamma_{\gamma\gamma}(f_2(1270))$

The process of two-photon $\pi^+\pi^-$-pair production was studied already in many experiments [211], [215]–[222] in the reaction

$$e^+e^- \to e^+e^- + \pi^+\pi^- \tag{11.3}$$

It was found that the dominant contribution to the cross section is given by $f_2(1270)$-meson, interfering with a non-resonant background. Usually to obtain the two-photon width of the f_2 meson it is assumed that f_2 meson is produced in a helicity-2 state and its amplitude interferes with Born term.

The important experimental problem in the analysis of the $\pi^+\pi^-$ final state is a large background from the two-photon reactions:

$$e^+e^- \to e^+e^- + e^+e^-, \tag{11.4}$$

$$e^+e^- \to e^+e^- + \mu^+\mu^-, \tag{11.5}$$

especially in the low mass region. Almost in all experiments the contributions of these reactions were calculated and subtracted (at least $\mu^+\mu^-$).

In this experiment [214] the processes (11.3), (11.4), (11.5) were separated in the whole region above detection threshold ($M_{\pi\pi} > 0.45$ GeV/c^2).

The luminosity integral used is 20 pb^{-1} at c.m. energy range 2E=7.2-10 GeV. Scattered electrons are not used in the analysis.

To reject the background from bremsstrahlung and other processes with small transverse momenta a strip in shower-range chamber (SRC) of ± 11 cm width, lying in the orbit plane, was excluded from the trigger. Cosmic background was suppressed using time coincidence of scintillation counters with the beam phase.

To study the reactions (11.3) – (11.5) events with two unlike-charged particles with momenta 270 – 2500 MeV/c were selected. To reject high rate processes (mainly single bremsstrahlung), transverse momentum $P_t > 30$ MeV/c was required for each selected particle. Cuts on the geometry of event (small difference of P_t of particles, small acoplanarity and some others [214]) were imposed to reduce the background from cosmic rays, $e^+e^- \to e^+e^-(\mu^+\mu^-)$, and multihadronic events. After these cuts predominantly e^+e^-, $\mu^+\mu^-$, $\pi^+\pi^-$ -pairs of two photon nature remain in the proportion 1:2:0.4, as it follows from simulation.

For the particle identification, the trajectory of the particle is traced through the detector taking into account ionization losses for each possible type of the particle (μ, π, K, p). When the particle crosses any system of detector, the expected average parameters are calculated, i.e. ionization losses in the scintillation counter (SC), average number of photoelectrons in the Cherenkov counter ($\hat{C}C$), coordinates and range (due to ionization losses only) in the SRC. The result obtained with MC simulated events of the processes (11.3)-(11.5) are presented below.

The scintillation counters provide good identification of electrons due to $1.7X_0Fe$ in front of the counters. Requiring the ratio $R = A_{sc}/\overline{A_{sc}}$ (where A is a pulse height measured in a counter and $\overline{A_{sc}}$ is the calculated average pulse height for π-meson hypothesis) to be in the range 0.2-2.2 for each crossed counter, the number of events of the process (11.4) decreases by a factor of 10 at $\epsilon_{\pi\pi} = 90\%$ for the process (11.3). To select e^+e^- pairs it is sufficient to require $R > 3$ for each counter and the remaining $\pi\pi$, $\mu\mu$ background will not exceed 1%.

The Cherenkov counters are used in the following way. The probability p is calculated for the π-meson to give the same or larger number of photomultiplies as the measured number. The event is assigned to π-μ class, if p < 0.01 for at least one particle. On average the Cherenkov counters suppress electron pairs by a factor of 10 at $\epsilon_{\pi\pi} \simeq 93\%$.

For electron rejection one additional "soft cut", based on SRC, is also used: hits in the first two chambers are required (if the particle passed farther). This gives an additional suppression of e^+e^- pairs by a factor of 2.

The described cuts suppress the process (11.4) by a factor $\sim$250 at 75% efficiency for $\pi^+\pi^-$ pairs.

For the μ/π separation the ranges of particles in the SRC were used. For analysis we take particles which stop inside SRC. At equal momenta π-mesons have, as a rule, smaller ranges than muons due to both ionization losses and nuclear interactions. Pions are stopped in the SRC due to ionization losses up to momentum of 350-420 MeV/c, so that in f_2-meson region pions are stopped in SRC only due to nuclear interactions. Comparing the measured and calculated range for a particle assumed to be muon and applying some reasonable cuts [214], we reduced the number of $\mu\mu$-pairs by a factor of 60 at $\epsilon_{\pi\pi} \sim 50\%$. As a result of μ/π separation we have obtained $N_{\pi\pi}/N_{\mu\mu} \simeq 6{:}1$.

Before comparison of the experimental data with MC simulation the corrections have been done of all detector efficiencies [214]. The estimated overall systematic error of detection efficiency after corrections is $\pm 2\%$

Two-photon processes were simulated in the equivalent photon approximation [50]:

$$d\sigma = \sigma_{\gamma\gamma}(M) dn_1 dn_2, \tag{11.6}$$

where

$$dn_i = \frac{2\alpha E E_i}{\pi q_i^2 \omega_i}\left[1 - \frac{\omega_i}{E} + \frac{\omega_i^2}{2E^2} + \frac{m_e^2}{q_i^2}\frac{\omega_i^2}{E^2} d(-\cos(\vartheta_i))\right] d\omega_i \tag{11.7}$$

$$q_i^2 = \frac{m^2\omega^2}{EE_i} + 2EE_i(1 - \cos(\vartheta_i)), \tag{11.8}$$

$$\omega_i = E - E_i,\ M^2 \approx 4\omega_1\omega_2. \tag{11.9}$$

The variables are shown in Fig.10.1. With our restrictions on q_i^2 this approximation provides percent level accuracy. Radiative corrections were not taken into account, because they do not exceed 1-2% [199]. The cross sections of two-photon QED processes are well known and can be found elsewhere [228]-[229].

The cross section of $\gamma\gamma \to \pi^+\pi^-$ was described by Born term (see, e.g., [229]) interfering with Breit-Wigner (B-W) amplitude of $f_2(1270)$-meson. It was assumed, that f_2-meson is produced in the helicity-2 state and, therefore, interferes only with Born term of the same helicity. The cross section is defined as

$$\frac{d\sigma}{d\Omega}(\gamma\gamma \to \pi^+\pi^-) = \mid F_B^{\lambda=0} \mid^2 + \mid F_B^{\lambda=2} + F_R \mid^2, \tag{11.10}$$

where the sign of B-W amplitude was chosen such that below the $f_2(1270)$ mass (M_f) the interference is constructive (as it follows from previous experiments).

The B-W amplitude of f_2 meson is given by

$$F_R = \frac{5}{\sqrt{2s}} \frac{g(s)\sin^2(\vartheta)}{M_f^2 - s - iM_f\Gamma}. \tag{11.11}$$

Here $s = M_{\pi\pi}^2$, $g(s) = M_f \cdot [\Gamma_{\gamma\gamma}^0(s)\Gamma_{\pi\pi}(s)]^{1/2} + i\mathrm{Im(g)}$, $\Gamma_{\pi\pi} = 0.86 \cdot \Gamma(s)$, $\Gamma(s)$ is the full width of f_2 meson, and $\Gamma_{\gamma\gamma}^0$ is the two-photon width of a direct $f_2 \to \gamma\gamma$ transition, ϑ is polar angle of the particles, defined with respect to the beam direction in the $\gamma\gamma$ center of mass.

The imaginary part of g(s) arises as a result of unitarization of D-wave amplitude [230, 231]. Unitarization is necessary because a sum of Born and B-W amplitudes does not satisfy unitarity. Numerically [231],

$$\mathrm{Im(g)} = 0.0002 \pm 0.00007\ \mathrm{GeV}^2.$$

The two-photon width $\Gamma_{\gamma\gamma}$ is defined by the expression

$$\mid g \mid^2 = M_f^2 \Gamma_{\gamma\gamma}\Gamma_{\pi\pi}(M_f).$$

Then

$$\Gamma_{\gamma\gamma} = \Gamma_{\gamma\gamma}^0 + 0.257(\mathrm{keV}).$$

This corresponds to definition by Lyth [230], however it is not generally accepted. The s dependence of the total width $\Gamma(s)$ was parameterized according to [230, 231]:

$$\Gamma(s) = \Gamma_f \left(\frac{p}{p_0}\right)^5 \left(\frac{s_0}{s}\right)^2 \left(\frac{s_0 + a}{s + a}\right)^2, \tag{11.12}$$

where $\Gamma_f = 0.18 \pm 0.02$ GeV, $p = 0.5\sqrt{s - 4m_\pi^2}$, $p_0 = 0.5\sqrt{s_0 - 4m_\pi^2}$, $s_0 = M_f^2$, $s = M_{\pi\pi}^2$, a=0.5 GeV^2.

The $\Gamma_{\gamma\gamma}(s)$ was parameterized using the same equation with m_π replaced by $m_\gamma = 0$ [231]. The cross section with such parameterization (but without unitarization) is close to that used in other works [231, 217, 218, 221]. It should be noted that in publications on $\gamma\gamma \to \pi^+\pi^-$, K^+K^- there is no agreement on a power of s in the B-W formula. Moreover, there is no generally accepted $\Gamma_{\gamma\gamma}(s)$ dependence. Due to variety of opinions we included in our result the systematic error, corresponding to change of power by ± 1.

To select $\gamma\gamma \to e^+e^-$ only one cut was imposed besides the common requirements: the pulse height in each scintillation counter must exceed the calculated one for π-meson by at least a factor 3.5. The invariant mass distribution for selected events is shown in Fig.11.4 together with the expected spectrum for $\gamma\gamma \to e^+e^-$ (π-meson mass is assigned to all particles). The distributions are in a good agreement ($(P(\chi^2) = 10\%$). The calculated fraction of $\mu^+\mu^-$ and $\pi^+\pi^-$ is less than 1%.

To suppress electrons we used cuts based on SC, $\hat{C}C$ and SRC explained before. As a result the number of electrons was reduced by a factor of $\sim$ 250 at 70-75% efficiency for $\pi^+\pi^-$ and $\mu^+\mu^-$. The resulting pair mass distribution is shown in Fig.11.5.

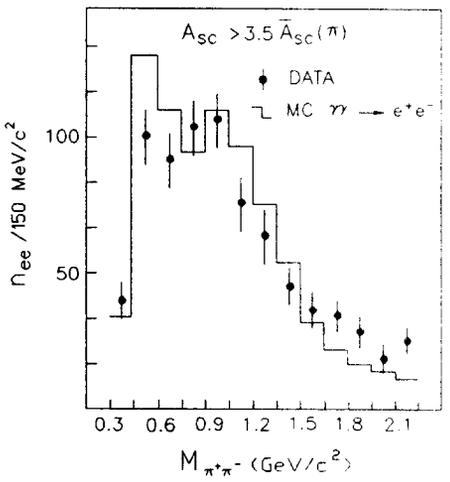

Fig. 11.4: The invariant mass spectrum of pairs when pulse heights in both scintillation counters $A_i > 3A_\pi$(calc.) are required. Errors of simulation $\sim$ 1.5 times larger than ones of data.

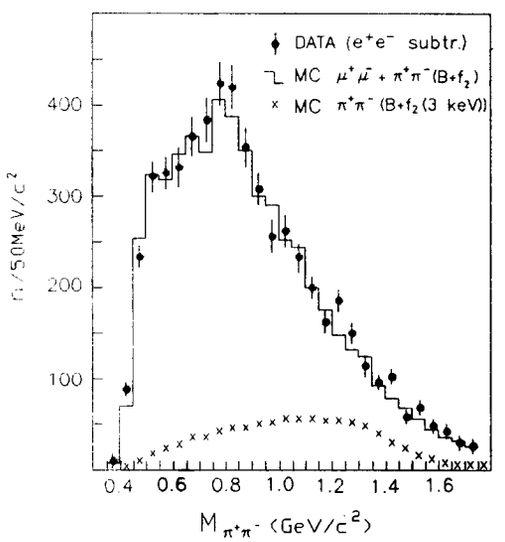

Fig. 11.5: The invariant mass spectrum of pairs after rejection of electrons.

From these sample a small contribution ($\sim$ 2%) of processes other than $\gamma\gamma \to \pi^+\pi^-, \mu^+\mu^-$ was subtracted. The multihadronic background ($\sim$ 1.5%) was determined by comparison of acoplanarity angle ($\Delta\varphi$) distributions in the experiment and simulation [214]. Backgrounds of

the processes with narrow $\Delta\varphi$ distributions were found by modelling and equal: $\gamma\gamma \to K^+K^-$ -0.3%, $\gamma\gamma \to e^+e^-$ -0.15%, $ee \to \mu^+\mu^-$ -0.15%, $ee \to \tau^+\tau^-$ <0.15%. Cosmic rays background was determined from the time difference distribution between scintillation counters and beam phase and accounts for less than 0.5%. Contribution of the Bhabha scattering, as follows from pulse height distribution in the shower-range chambers, is negligible. Polar angle and collinearity angle distributions show good agreement between experiment and simulation as well.

The ratio $N_{\rm exp}/N_{MC}(\mu\mu + \pi\pi)$ for the obtained data equals 1.015±0.016 ± 0.03. The systematic error is connected with uncertainty in the expected number of $\pi^+\pi^-$ (in the simulation $\Gamma_{\gamma\gamma}(f_2(1270)) = 3$ keV was assumed). In fact, these results confirm our understanding of the detector, precision of corrections, luminosity measurements, and MC simulation.

As shown before, after electron suppression only $\mu^+\mu^-$ and $\pi^+\pi^-$ pairs remain in a ratio ~ 5:1 on average and about (15-20):1 in the 500-600 MeV/c^2 mass region (see Fig.11.5). Muon/pion separation was done by using their ranges in the shower-range chambers as was described before.

Multihadronic background was found, as before, by comparison of acoplanarity angle distributions in the experiment and MC simulation for each mass bin. The contributions of the processes $\gamma\gamma \to e^+e^-$, $\mu^+\mu^-$ and K^+K^- were obtained by MC simulation. The $\gamma\gamma \to K^+K^-$ cross section was taken from [232].

The mass spectrum of π-pairs after background subtraction is plotted in Fig.11.6.

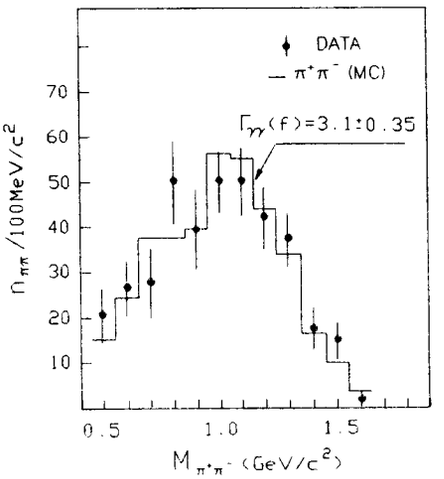

Fig. 11.6: The invariant mass spectrum of $\pi^+\pi^-$-pairs together with the optimum fit.

The data were fitted according to unitarized model of Lyth, considering Born amplitude interfering with $f_2(1270)$-meson. Histogram is the optimum fit with the only free parameter $\Gamma_{\gamma\gamma}(f_2)$. The f_2-meson peak is strongly widened due to detector resolution. Histograms for different $\Gamma_{\gamma\gamma}$ were obtained from one set of simulated events (at $\Gamma_{\gamma\gamma} = 3$ keV) by changing the weight of each event according to dependence of the differential cross sections on $\Gamma_{\gamma\gamma}$. The optimum two-photon width is

$$\Gamma_{\gamma\gamma}(f_2) = 3.1 \pm 0.35 \pm 0.35 \text{ keV}.$$

All histogram channels were included in the fit. The result changes negligibly when only f_2-meson region is taken. The systematic error is determined mainly by the following factors (in

% to $\Gamma_{\gamma\gamma}$): the luminosity - 3.5%, $\epsilon_{\pi\pi}$ - 3.5%, multihadronic background - 6%, uncertainty in parameterization of $\Gamma(s)$ (± 1 power of $M_{\pi\pi}$) - 6%; $\mu^+\mu^-$ background - 3.5%, unitary corrections -6%.

The fit without unitarization gives $\Gamma_{\gamma\gamma}(f_2)$=2.6±0.35±0.3 keV. Unitarization increases direct coupling width $\Gamma^0_{\gamma\gamma}$ by 0.25 keV. Our final result contains also an additional supplement of 0.257 keV arising in the model of Lyth.

The overall average value is $\Gamma_{\gamma\gamma}(f_2) = 2.76 \pm 0.14$ keV [232]. The averaged experiments used various parameterizations, mostly without unitarization and none of them used Lyth's model. The latest Mark-II analysis[222, 226] gives $\Gamma_{\gamma\gamma}(f_2) = 3.15 \pm 0.04 \pm 0.28$ with parameterization of Lyth. With the given comments our two-photon width of $f_2(1270)$ is in agreement with other results [87].

12. Conclusions

The main physical results obtained by the MD-1 detector at the VEPP-4 collider are listed below:

1. The following QED processes were studied:

   $e^+e^- \to e^+e^-\gamma$. Effect of impact parameter cut-off was discovered [25].

   $\gamma e \to ee^+e^-$. Process was observed on free electron [21].

   $e^+e^- \to e^+e^- + \mu^+\mu^-$. Measurements in no [8, 214]-, single [8]- and double [8]-tag modes.

   $e^+e^- \to e^+e^- + e^+e^-$ [14, 214]. In [14] the process was measured nearby a threshold.

2. Precise measurements of $\Upsilon(1S)$, $\Upsilon(2S)$, $\Upsilon(3S)$ meson masses were performed:

   $M(\Upsilon(1S)) = 9460.59 \pm 0.09 \pm 0.05$ MeV [56, 63, 73, 74].

   $M(\Upsilon(2S)) = 10023.6 \pm 0.5$ MeV [63, 64].

   $M(\Upsilon(3S)) = 10355.3 \pm 0.5$ MeV [63, 64].

3. The electron widths of $\Upsilon(1S)$ and $\Upsilon(2S)$ mesons and muon branching ratio of $\Upsilon(1S)$ meson were measured:

   $\Gamma_{ee}(\Upsilon(1S)) \cdot B_{had} = 1.187 \pm 0.023 \pm 0.031$ keV [74],

   $\Gamma_{ee}(\Upsilon(2S)) \cdot B_{had} = 0.552 \pm 0.031 \pm 0.017$ keV [92],

   $B_{\mu\mu}(\Upsilon(1S)) = 2.12 \pm 0.20 \pm 0.10\%$ [22].

4. The following upper limits at 90% CL were established for rare decays of $\Upsilon(1S)$:

   $B(\Upsilon(1S) \to \gamma\xi(2.2)) \times B(\xi \to K^+K^-) < 2 \cdot 10^{-4}$ [118].

   $B(\Upsilon(1S) \to \gamma X(2.2)) \times B(X \to \phi\phi) < 3 \cdot 10^{-4}$ [118].

$B(\Upsilon(1S) \to \rho^0\pi^0) < 3.3 \cdot 10^{-4}$ [130].

$B(\Upsilon(1S) \to \pi^+\pi^-) < 5 \cdot 10^{-4}$ [22].

$B(\Upsilon(1S) \to K^+K^-) < 5 \cdot 10^{-4}$ [22].

$B(\Upsilon(1S) \to p\bar{p}) < 4 \cdot 10^{-4}$ [105].

5. The following inclusive rates for $\Upsilon(1S)$ decays and continuum were measured:
a) Λ production [136]:

$< n_\Lambda(\Upsilon(1S)_{\rm dir}) >= 0.194 \pm 0.018 \pm 0.017,$

$< n_\Lambda >= 0.070 \pm 0.027 \pm 0.020$ at $2E = 7.2 \div 9.4$ GeV ,

$< n_\Lambda >= 0.098 \pm 0.027 \pm 0.014$ at $2E = 9.4 \div 10.0$ GeV .

b) Ξ production [136]:

$< n_\Xi(\Upsilon(1S)_{\rm dir}) >= 0.038 \pm 0.015 \pm 0.009.$

6. The following parameters of Bose-Einstein correlations were obtained [156]:

At the direct $\Upsilon(1S)$ decays: $\lambda = 0.73 \pm 0.16$, $r_0 = 0.69 \pm 0.19\ fm$.

In the continuum at $2E = 7.2 \div 10.3$ GeV: $\lambda = 0.52 \pm 0.19$, $r_0 = 0.80 \pm 0.22\ fm$.

7. In the study of reaction $e^+e^- \to hadrons$ the following results were obtained:
a) In search for narrow resonances the upper limits on Γ_{ee} at 90% CL are [165]:

$2E = 7.23 \div 7.99$ GeV $\Gamma_{ee} < 98$ eV,

$2E = 7.99 \div 8.67$ GeV $\Gamma_{ee} < 123$ eV,

$2E = 8.67 \div 8.88$ GeV $\Gamma_{ee} < 27$ eV,

$2E = 8.88 \div 9.23$ GeV $\Gamma_{ee} < 54$ eV,

$2E = 9.23 \div 9.42$ GeV $\Gamma_{ee} < 58$ eV,

$2E = 9.42 \div 9.445$ GeV $\Gamma_{ee} < 15$ eV,

$2E = 9.50 \div 10.00$ GeV $\Gamma_{ee} < 51$ eV,

$2E = 10.00 \div 10.34$ GeV $\Gamma_{ee} < 100$ eV.

b) The value of R is [91]:

$2E = 7.25 \div 10.34$ GeV $\overline{R} = 3.578 \pm 0.021 \pm 0.140.$

8. In study of $\gamma\gamma$ reactions the following results were obtained:
a) Total hadronic cross section $\gamma\gamma \to hadrons$ was measured in double-tag mode [191]:

$W_{\gamma\gamma} = 1.5 \div 2.0$ GeV $\quad \sigma_{tot} = 448 \pm 56$ nb,

$W_{\gamma\gamma} = 2.0 \div 3.0$ GeV $\quad \sigma_{tot} = 334 \pm 29$ nb,

$W_{\gamma\gamma} = 3.0 \div 4.0$ GeV $\quad \sigma_{tot} = 257 \pm 34$ nb.

b) Cross section $\gamma\gamma \to \pi^+\pi^-$ was measured at $M_{\pi\pi} = 0.5 \div 1.5$ GeV/c^2 in no-tag mode [214].
c) The $\gamma\gamma$-widths of resonances measured by MD-1 are the following:

$\Gamma_{\gamma\gamma}(a_2) = 1.26 \pm 0.26 \pm 0.18$ keV [198].

$\Gamma_{\gamma\gamma}(\eta') = 4.6 \pm 1.1 \pm 0.6$ keV [198].

$\Gamma_{\gamma\gamma}(\eta) = 0.51 \pm 0.12 \pm 0.05$ keV [198].

$\Gamma_{\gamma\gamma}(f_2) = 3.1 \pm 0.35 \pm 0.35$ keV [214].

d) The following upper limit at 90% CL was established for decays of particle X of mass 1.8 MeV:

$\Gamma_{\gamma\gamma}(X) \times B(X \to e^+e^-) < 2$ eV [212].

e) In search for narrow C-even resonances the upper limits on $(2J+1)\Gamma_{\gamma\gamma}$ at 90% CL are [205]:

$M_{res} = 1.0 \div 1.25$ GeV/c^2 $\quad (2J+1)\Gamma_{\gamma\gamma} < 92.0$ keV,

$M_{res} = 1.25 \div 1.5$ GeV/c^2 $\quad (2J+1)\Gamma_{\gamma\gamma} < 9.5$ keV,

$M_{res} = 1.5 \div 1.75$ GeV/c^2 $\quad (2J+1)\Gamma_{\gamma\gamma} < 12.4$ keV,

$M_{res} = 1.75 \div 2.0$ GeV/c^2 $\quad (2J+1)\Gamma_{\gamma\gamma} < 39.0$ keV,

$M_{res} = 2.0 \div 2.25$ GeV/c^2 $\quad (2J+1)\Gamma_{\gamma\gamma} < 45.2$ keV,

$M_{res} = 2.25 \div 2.5$ GeV/c^2 $\quad (2J+1)\Gamma_{\gamma\gamma} < 44.2$ keV,

$M_{res} = 2.5 \div 2.75$ GeV/c^2 $\quad (2J+1)\Gamma_{\gamma\gamma} < 46.4$ keV,

$M_{res} = 2.75 \div 3.0$ GeV/c^2 $\quad (2J+1)\Gamma_{\gamma\gamma} < 13.0$ keV,

$M_{res} = 3.0 \div 3.25$ GeV/c^2 $\quad (2J+1)\Gamma_{\gamma\gamma} < 24.2$ keV,

$M_{res} = 3.25 \div 3.5$ GeV/c^2 $\quad (2J+1)\Gamma_{\gamma\gamma} < 34.0$ keV,

$M_{res} = 3.5 \div 3.75$ GeV/c^2 $\quad (2J+1)\Gamma_{\gamma\gamma} < 329$ keV,

$M_{res} = 3.75 \div 4.0$ GeV/c^2 $\quad (2J+1)\Gamma_{\gamma\gamma} < 383$ keV,

$M_{res} = 4.0 \div 4.3$ GeV/c^2 $\quad (2J+1)\Gamma_{\gamma\gamma} < 191$ keV.

Using experience of the MD-1 detector performance, the KEDR detector [233] was designed. Construction of the KEDR is being completed in Novosibirsk now. The experimental program will be focused on the study of b physics and $\gamma\gamma$ reactions also. The luminosity of the upgraded VEPP-4 will be more than 10 times larger than the luminosity during the experiments with the MD-1.

Study of the b physics gives opportunity to find answers on the important questions in the particle physics. Progress in this field, especially due to the experiments of ARGUS and CLEO, is the basis of the B factory projects. The SLAC and KEK asymmetric B factories will come into operation after 1998. These machines will give the best opportunity to study CP violation in neutral B decays.

References

[1] S.W.Herb et al, Phys. Rev. Lett. 39(1977)252.
W.R.Innes et al., Phys. Rev. Lett. 39(1977)1240.

[2] P.Franzini and J.Lee-Franzini, Phys. Rep. 81(1982)241.
M.B.Voloshin, Yu.M.Zaitsev, Usp. Fiz. Nauk 152(1987)361.
D.Besson, T.Skwarnicki, Ann. Rev. Nucl. Sci. 43(1993)333.

[3] M.Danilov, Proc. Int. Europh. Conf. on High En. Phys., p.851. Marseille 1993.
B decays, revised 2nd edition. Edited by Sheldon Stone. World Scientific Publishing Co.Pte.Ltd. 1994.

[4] Proc. of the X Int. Conf. on High Energy Accelerators, Protvino, July 1977 vol.1, p.421.

[5] A.A.Zholentz et al., Phys. Lett. 96B(1980)214.

[6] S.E.Baru et al. (MD-1 collaboration), Preprint INP 83-39. Novosibirsk 1983.

[7] A.E.Bondar et al., Nucl. Instr. and Meth. 207(1983)379.

[8] V.M.Aulchenko et al. (MD-1 collaboration), Preprint BudkerINP 94-12. Novosibirsk 1994.

[9] S.E.Baru et al., 3-d International Meeting on Proportional and Drift Chambers. Dubna 1978. p.272.

[10] A.P.Onuchin, Yu.A.Tikhonov, Preprint INP 77-77, Novosibirsk 1977.

[11] A.D.Bukin et al., Preprint INP 84-33. Novosibirsk 1984.

[12] A.D.Bukin et al., Preprints INP 90-93, 90-95, 90-96, 92-93, 94-20. Novosibirsk 1990-1994.

[13] R.Brun, F.Bruyant, M.Maire et al., GEANT3. CERN preprint DD/EE/84-1, Geneve, 1987.

[14] A.D.Bukin et al., Proceedings of Workshop on Detector and Event Simulation in Hight Energy Physics, 8 – 12 April 1991, NIKHEF, Amsterdam, The Netherlands, p. 79.

[15] S.I.Dolinsky et al., Phys. Rep. 202(1991)99.

[16] K.Hänßgen et al., Preprint KMU-HEP 80-07, Leipzig, 1980.
K.Hänßgen, J.Ranft., Preprint KMU-HEP 82-11, Leipzig, 1982.
K.Hänßgen, J.Ranft., Comp. Phys. Comm. 39(1986)37; ibid 39(1986)53.

[17] A.D.Bukin et al., Preprint INP 82-13. Novosibirsk 1982.

[18] A.D.Bukin and G.N.Skovorodnikova., Preprint INP 84-158. Novosibirsk 1984.

[19] A.E.Blinov et al., Nucl. Instr. and Meth. A273(1988)31.

[20] A.E.Blinov et al. (MD-1 collaboration), Yad. Fiz. 44(1986)626.

[21] A.E.Blinov et al. (MD-1 collaboration), Yad. Fiz. 45(1986)1008.

[22] S.E.Baru et al. (MD-1 collaboration), Z. Phys. C54(1992)229.

[23] C.Bernandini et al, Nuovo Cimento 34(1964)1473.

[24] P.I.Golubnichy et al., Yad. Fiz. 76(1968)24.

[25] A.E.Blinov et al. (MD-1 collaboration), Phys. Lett. 113B(1982)423.

[26] G.A.Altarelly and F.Buchella, Nuovo Cimento 34(1964)1337.

[27] V.N.Baier, V.S.Fadin and V.A.Khoze, Zh. Eksp. Teor. Fiz. 51(1966)1135.

[28] L.D.Landau and I.Ya.Pomeranchuk, Dokl. Akad. Nauk SSSR 92(1953)535; ibid 735.

[29] A.A.Varfolomeev et al., Zh. Eksp. Teor. Fiz. 69(1975)429.

[30] V.Ch.Zhukovsky, Zh. Eksp. Teor. Fiz. 66(1974)9.

[31] A.I.Nikishov, Preprint LPI 118 (Moscow, 1971).

[32] V.N.Baier and V.M.Katkov, Dokl. Akad. Nauk SSSR 207(1972)68.

[33] V.N.Baier, V.M.Katkov and V.M.Strakhovenko, Dokl. Akad. Nauk SSSR 260(1981)861.

[34] V.N.Baier, V.M.Katkov and V.M.Strakhovenko, Preprint INP 81-59. Novosibirsk 1981.

[35] A.V.Burov and Ya.S.Derbenev, Preprint INP 81-64. Novosibirsk 1981.

[36] V.M.Katkov and V.M.Strakhovenko. Dokl. Akad. Nauk SSSR 231(1976)582.

[37] V.M.Katkov and V.M.Strakhovenko, Yad. Fiz. 25(1977)1245.

[38] V.M.Katkov and V.M.Strakhovenko, Yad. Fiz. 32(1980)1067.

[39] V.N.Baier and Galitsky, Phys. Lett. 13(1964)335.
V.N.Baier and Galitsky, Pis'ma Zh. Eksp. Teor. Fiz. 2(1965)259.
V.N.Baier, V.S.Fadin and V.A.Khoze, Zh. Eksp. Teor. Fiz. 50(1968)1611.
V.N.Baier et. al., Yad. Fiz. 8(1968)1174.
V.N.Baier and V.V.Geidt, Yad. Fiz. 13(1971)350.

[40] G.L.Kotkin, V.G.Serbo, A.Shiller, Int. Jour. of Mod. Phys. A7(1992)4707.

[41] K.Piotrzkowski, Internal report DESY F35D-93-06. October 1993.

[42] J.W.Motz et al., Rev. Mod. Phys. 41(1969)581.
Y.-S.Tsai, Rev. Mod. Phys. 46(1974)815.

[43] H.A.Bethe, W.Heitler, Proc. Roy. Soc.(London), A146(1934)83.

[44] K.J.Mork, Phys. Rev. 160(1967)1065.

[45] D.Benaksas, R.Morrison, Phys. Rev. 160(1967)1245.

[46] A.E.Blinov et al., Nucl. Instr. and Meth. A241(1985)80.

[47] I.M.Ternov, V.V.Michailin, V.R.Chalilov, Synchrotron radiation and its application. Moskow University. 1980. (In Russian).

[48] L.D.Landau, E.M.Lifshitz, Phys. Zs. Sowjet, 6(1934)244.

[49] V.E.Balakin et al., Phys. Lett. 34B(1971)663.
V.E.Balakin et.al., Yad. Fiz. 16(1972)729.

[50] V.M.Budnev, I.F.Ginsburg, G.V.Meledin, V.G.Serbo, Phys. Rep. 15C(1975)181.

[51] V.N.Baier et al., Phys. Rep. 78(1981)293.

[52] F.A.Berends et al., Nucl. Phys. B253(1985)441.

[53] M.Pohl, Preprint DESY 83-047. June 1983.

[54] H.Kolanosky, Two Photon Physics at e^+e^- Storage Rings. Springer Tracts in Modern Physics. V.105. 1984.

[55] R.Bhattacharya et al., Phys. Rev. D15(1977)3267.

[56] A.S.Artamonov et al. (MD-1 collaboration), Phys. Lett. 118B(1982)225.

[57] V.E.Balakin, G.I.Budker, A.N.Skrinsky, Preprint INP 78-101. Novosibirsk 1978.

[58] S.I.Serednyakov et al., Zh. Eksp. Teor. Fiz. 71(1976)2026.

[59] Ya.S. Derbenev et al., Part. Acc. 10(1980)177.

[60] A.D.Bukin et al., Yad. Fiz. 27(1978)976.

[61] L.M.Barkov et al., Nucl. Phys. B148(1979)53.

[62] L.M.Barkov et al., Preprint INP 83-85. Novosibirsk 1983.

[63] A.S.Artamonov et al. (MD-1 collaboration), Phys. Lett. 137B(1984)272.

[64] S.E.Baru et al. (MD-1 collaboration), Z. Phys.C 32(1986)622

[65] W.W.MacKay et al. (CUSB collaboration), Phys. Rev. D29(1984)2483.

[66] D.P.Barber et al., Phys. Lett. 135B(1984)498;

[67] V.Bargmann et al., Phys. Rev. Lett. 2(1959)435.

[68] I.M.Ternov et al., Zh. Eksp. Teor. Fiz. 41(1961)1294.

[69] A.A.Sokolov and I.M.Ternov, Dokl. Akad. Nauk SSSR 153(1963)1052.

[70] Ya.S.Derbenev and A.M.Kondratenko, Dokl. Akad. Nauk SSSR 217(1974)311.

[71] Ya.S.Derbenev, A.M.Kondratenko and A.N.Skrinsky, Part. Accel. 9(1979)247; Preprint INP 77-60. Novosibirsk, 1977.

[72] V.N.Baier and V.A.Khoze, Yad. Fiz. 9(1969)409.

[73] S.E.Baru et al. (MD-1 collaboration), Z. Phys. C30(1986)551.

[74] S.E.Baru et al. (MD-1 collaboration), Z. Phys. C56(1992)547.

[75] Particle Data Group, Phys.Lett.118B(1982).

[76] C.Berger et al. (PLUTO collaboration), Z. Phys. C1(1970)343.

[77] P.Bock et al. (DESY-Heidelberg collaboration), Z. Phys. C6(1980)125.

[78] H.Albrecht et al. (DASP collaboration), Phys. Lett. B116(1982)383.

[79] B.Niczyporuk et al. (LENA collaboration), Z. Phys. C15(1982)299.

[80] P.M.Tuts (CUSB collaboration), Int. Symp. on Lepton and Photon Interaction at High Energy, Ithacka, N.Y. (1983)284.

[81] R.Giles et al., Phys. Rev D29(1984)1285.

[82] Z.Jakubovsky et al. (Crystal Ball collaboration), Z. Phys. C40(1988)49.

[83] H.Albrecht et al. (ARGUS collaboration), Preprint DESY 94-121, July 1994.

[84] A.S.Artamonov et al., Preprint INP 84-97. Novosibirsk 1984.

[85] E.A.Kuraev, V.S.Fadin, Yad. Fiz. 41(1985)733.

[86] S.E.Baru et al. (MD-1 collaboration), Z. Phys. C32(1986)662.

[87] Particle Data Group, Phys. Let 239B(1990) VII.157.

[88] W.Buchmueller, S.Cooper, 'High Energy Electron-Positron Physics' Editors: A.Ali, P.Söding (World scientific 1988),p.412.

[89] J.P.Alexander et al., Nucl. Phys. B320(1989)45.

[90] T.Sjostrand, M.Bengtsson, Preprint LU TP 86-22

[91] A.E.Blinov et **al.,** (MD-1 collaboration). Preprint BudkerINP 93-54. Novosibirsk 1993.

[92] S.E. Baru et al. (MD-1 collaboration), to be published.

[93] B.Niczyporuk et al., Phys. Lett. B99(1981)169.

[94] D.Andrews et al. (CUSB collaboration), Phys. Rev. Lett. 50(1983)807.

[95] D.Besson et al. (CLEO collaboration), Phys. Rev. D30(1984)1433.

[96] H.Albrecht et al. (ARGUS collaboration), Z. Phys. 35(1987)283.

[97] W.-Y.Chen et al. (CUSB collaboration), Phys. Rev. D39(1989)3528.

[98] T.M.Kaarsberg et al. (CLEO collaboration), Phys. Rev. Lett. 62(1989)2077.

[99] F.A.Berends, R.Kleiss., Nucl. Phys. B177(1981)237.
F.A.Berends, et al., Nucl. Phys. B202(1982)63.

[100] F.A.Berends, R.Kleiss., Comp. Phys. Comm. 29(1983)185.

[101] F.A.Berends, R.Kleiss., Nucl. Phys. B115(1976)114.

[102] Y.S.Tsai., SLAC-PUB-1515, Dec.7, 1974.

[103] J.D.Jackson, D.L.Scharre, Nucl. Inst. and Meth., 128(1975)13.

[104] V.L.Chernyak, A.R.Zhitnitsky., Phys. Rep. 112(1984)175.

[105] S.E.Baru et al. (MD-1 collaboration), to be published.

[106] M.Claudson et.al., Phys. Rev. D25(1982)1345.

[107] D.Hitlin (MARK III collaboration), In: Proc.1983 Intern. Symp. on Lepton and Photon Interactions at High Energies, D.G.Cassel, D.L.Kreinick (eds.) (Laboratory of Nuclear Studies, Cornell University, Ithaca, NY, 1983), p.746.

[108] R.M.Baltrusaitis et al. (MARK III collaboration), Phys. Rev. Lett. 56(1986)107.

[109] L. Köpke (MARK III collaboration), in: Proc of the XXIII Intern. Conf. on High Energy Physics, Berkeley, CA, 1986, v.1, p.692.
Usha Mallik (MARK III collaboration), Preprint SLAC-PUB-4238,1987.

[110] J.E.Augustin et al. (DM2 collaboration), Phys. Rev. Lett. 60(1988)2238.

[111] B.V.Bolonkin et al. (MIS ITEP collaboration), Preprint 52, ITEP, 1987.

[112] D.Aston et al. (LASS collaboration), Preprint SLAC-PUB-4202, 1987.
D.Aston et al. (LASS collaboration), Nucl. Phys. B301(1988)525.

[113] D.Alde et al. (GAMS-2000 and GAMS-4000 collaboration), Phys. Lett. B177(1986)120.

[114] H.E.Haber, G.L.Kane, Phys. Lett. B135(1984)196.
R.S.Willey, Phys. Rev. Lett. 52(1984)585.
R.M.Barnett, G.Senjanović, D.Wyler, Phys. Rev. D30(1984)1529.

[115] M.S.Chanowitz, S.R.Sarpe, Phys. Lett. B132(1983)413.
B.F.L.Ward, Phys. Rev. D31(1985)2849.

[116] S.Godfrey, R.Kokoski, N.Isgur, Phys. Lett. 141B(1984)439.

[117] M.P.Shatz, Phys. Lett. B138(1984)209.
S.Pakvasa, M.Suzuki, S.F.Tuan, Phys. Lett. B145(1984)135.
S.Pakvasa, M.Suzuki, S.F.Tuan, Phys. Rev. D31(1985)2378.
S.Ono, Phys. Rev. D35(1987)944.

[118] S.E.Baru et al. (MD-1 collaboration), Z. Phys. C42(1989)505.

[119] S.Behrends et al., Phys. Lett. B137(1984)277.

[120] R.Fulton et al., Preprint CLNS 89/913, 1989.

[121] S.Youssef et al., Phys. Lett. 139B(1984)332.

[122] P.Franzini et al., Phys. Rev. D35(1987)2883.

[123] S.T.Lowe, Ph.D. dissertation, SLAC-307,1986.

[124] H.Albrecht et al. (ARGUS collaboration), Z. Phys. C42(1989)349.

[125] D.Bisello et al. (DM2 collaboration), Phys. Lett. 179B(1986)294.

[126] J.Lee-Franzini (MARK III collaboration), Proc. 1987 Intern. Symp. on Lepton and Photon Interactions at High Energies. W.Bartel, R.Rückl (eds.) Hamburg, 1987, p.139.

[127] S.J.Brodsky and G.P.Lepage, Proc. Conf. on High energy physics with polarized beam and polarized targets, eds. C.Joseph and J.Soffer (Lausanna, Switzerland, 1980) p.169;

[128] Particle Data Group, Phys. Lett. B204(1988)1.

[129] B.Niczyporuk et al. (LENA collaboration), Z. Phys. C17(1983)197.

[130] A.E.Blinov et al. (MD-1 collaboration), Phys. Lett. B254(1990)311.

[131] G.J.Gounaris and J.J.Sakurai, Phys. Rev. Lett. 21(1968)244.

[132] F.A.Berends and R.Kleiss, Nucl. Phys. B178(1981)141.

[133] A.D.Bukin, Preprint INP 85-124, Novosibirsk, 1985.

[134] P.A.M.Dirac, Proc. Cambr. Phil. Soc. 26(1930)361.

[135] F.A.Berends, W.L. van Neerven, and G.J.H.Burgers, Nucl. Phys. B297(1988)429.

[136] A.E.Blinov et al. (MD-1 collaboration), Z. Phys. C62(1994)367.

[137] In [136] this cut was erroneously formulated for distance between tracks instead of half-distance.

[138] T.Sjöstrand, Comp. Phys. Comm. 27(1982)243; ibid 28(1983)227.

[139] S.Behrends et al. (CLEO collaboration), Phys. Rev. D31(1985)2161.

[140] H.Albrecht et al. (ARGUS collaboration), Z. Phys. C39(1988)177.

[141] G.Goldhaber et al., Phys. Rev. 120(1960)300.

[142] E.V.Shuryak, Phys. Lett. B44(1973)387

[143] G.Kopylov and M.Podgoretzki, Yad. Fiz. 18(1973)656 [Sov. J. Nucl. Phys. 18(1974)336].

[144] G.Cocconi, Phys. Lett. B49(1974)459.

[145] B.Lörstad, Int. Jour. of Mod. Phys. A4(1989)2861.

[146] M.Gyulassy, S.K.Kauffman and L.W.Wilson, Phys. Rev. C20(1979)2267.

[147] M.Podgoretzki, Fiz. Elem. Chast. i Atom. Yad. 20(1989)629 [Sov. J. Part. Nucl. 20(1989)266].

[148] H.Aihara et al. (TPC Collaboration), Phys. Rev. D31(1985)996.

[149] P.Avery et al. (CLEO Collabollaboration), Phys. Rev. D32(1985)2294.

[150] M.Althoff et al. (TASSO Collababoration), Z. Phys. C30(1986)355.

[151] I.Juricic et al. (MARK II Collababoration), Phys. Rev. D39(1989)1.

[152] R.C.Walker et al. (AMY Collaboration), preprint UR-1176(1990).

[153] P.D.Acton et al. (OPAL Collaboration), Phys. Lett. B267(1991)143.

[154] D.Decamp et al. (ALEPH Collaboration), Z. Phys. C54(1992)75.

[155] P.Abreu et al. (DELPHI Collaboration), Phys. Lett. B286(1992)201.

[156] A.E.Blinov et al. (MD-1 collaboration), Preprint BudkerINP 95-8. Novosibirsk 1995. To be published.

[157] T.Sjostrand, M.Bengtsson, Comp. Phys. Comm. 43(1987)367.

[158] H.Albreht et al. (ARGUS Collaboration), Z. Phys. C46(1990)15.

[159] H.Albreht et al. (ARGUS Collaboration), Z. Phys. C58(1993)199.

[160] H.Albreht et al. (ARGUS Collaboration), Z. Phys. C61(1994)1.

[161] P.Grassberger, Nucl. Phys. B120(1977)231.

[162] B.Andersson and W.Hofmann, Phys. Lett. B169(1986)364.

[163] X.Artru and M.G.Bowler, Z. Phys. C37(1988)293.

[164] M.G.Bowler, Part. World 2(1991)1.

[165] A.E.Blinov et al. (MD-1 collaboration), Z. Phys. C49(1991)239.

[166] J.Siegrist et al. (MARK-1 collaboration), Phys. Rev. D26(1982)969.

[167] C.Peck et al.(Crystal Ball collaboration), SLAC-PUP 3380(1984);
Proc.of the XXII International Conference High Energy Physics. Leipzig, 1984.

[168] H.Albrecht et al. (ARGUS collaboration), Z. Phys. C29(1985)167.

[169] H.Tye, C. Rosenfeld, Phys. Rev. Lett. 53(1984)1215.

[170] A.Ignatiev et al., Pis'ma ZhETF 40(1984)211.

[171] L.R.Surguladze, M.A.Samuel, Phys. Rev. Lett. 66(1991)560.
S.G.Goishny, A.L.Kataev, S.A.Larin, Phys. Lett. B259(1991)144.

[172] R. Marshall, Z. Phys. C43(1989) 595.

[173] B.Bartoli et al., Nuovo Cimento 70A(1970)615.

[174] C.Bacci et al., Phys. Lett. B38(1972)551.

[175] L.M.Kurdadze et al., Phys. Lett. 40B(1972)685.

[176] Particle Data Group, Phys. Rev. D45(1992) III.54.

[177] F.A.Berends, R.Kleis, S.Jadach, Nucl. Phys. B202(1982)201;
F.A.Berends et al., Comput. Phys. Comm. 29(1983)98.

[178] C.Berger et al. (PLUTO collaboration), Phys. Lett. B81(1979)410.

[179] L.Gregee, G.Knies, Phys. Rep. C83(1982)151.

[180] E.Rice et al. (CUSB collaboration), Phys. Rev. Lett. 48(1982)906.

[181] H.Albrecht et al. (ARGUS collaboration), Z. Phys. C54(1982)13.

[182] E. Fernandez et al. (MAC Collaboration), Phys. Rev. D28(1983)2721.
D.Bintinger et al. (PEP-9 Collaboration), Phys. Lett. B147(1984)232.
A.Courau et al. (DM1 Collaboration), Nucl. Phys. B271(1986)1.
H.-J.Behrend et al. (CELLO Collaboration), Z. Phys. C43(1989)1.
A.Roussarie et al. (Mark-II Collaboration), Phys. Rev. D42(1990)2171.
Y.H. Ho et al. (AMY Collaboration), Phys. Lett. B244(1990)573.
H. Hayashii et al. (TOPAZ Collaboration), Phys. Lett. B279(1992)422.
R.Akers et al. (OPAL Collaboration), Z. Phys. C60(1993)593.
L3 Collaboration, contributed paper for ICHEP94.

[183] Ch.Berger et al (PLUTO collaboration), Phys. Lett. 89B(1981)287.

[184] E.Higler: Proceedings of the Int. Workshop on $\gamma\gamma$-Collisions, Amiens, ed. G.Cohard and P.Kessler (eds) (Lecture Notes in Physics Vol.134) Berlin, Heidelberg, New York: Springer 1980.

[185] I.F.Ginzburg, V.G.Serbo, Phys. Lett. 109B(1982)231.

[186] Ch.Berger et al. (PLUTO collaboration), Phys. Lett. 149B(1984)421.

[187] D.Bintinger et al. (TPC/2γ collaboration), Phys. Rev. Lett. 54(1985)763.
J.C.Armitage et al. (TPC/2γ collaboration), Contrib. to the XXII Int. Conf. on High Energy Physics, Leipzig, 1984, Ref.Code B20.

[188] M.Feindt, Talk at the II Int.Workshop on Photon-Photon Collisions, Paris, 1986.

[189] H.Aihara et al. (TPC/2γ collaboration), Phys. Rev. D41(1990)2667.

[190] A.E.Blinov et al. (MD-1 collaboration), Preprint INP 85-95, Novosibirsk 1985, presented at the Int. Symposium on Lepton and Photon Interactions at High Energy, Kyoto, 1985.
S.E.Baru et al. (MD-1 collaboration), Preprint INP 86-108, submitted to XXIII Intern. Conf. on High Energy Physics, Berkley, 1986.
S.E.Baru et al. (MD-1 collaboration). Talk at the XXV Intern. Conf. on High Energy Physics, Singapore, 1990.

[191] S.E.Baru et al. (MD-1 collaboration), Z. Phys.C53(1992)219.

[192] J.L.Rosner, BNL Report 17522(1972)316.

[193] G.Alexander et al., Phys. Lett. 131B(1983)224.

[194] E.Gostman, U.Maor, Phys. Rev. D28(1983)2149.

[195] A.Levy, Phys. Lett. 181B(1986)2149.

[196] Z.Koba, H.B.Nielsen, P.Olesen, Nucl. Phys. B40(1972)317.
A.Copella et al., Phys. Rev. D37(1988)1763.

[197] L.Criege, G.Knies, Phys. Rep. 83(1982)44.

[198] S.E.Baru et al. (MD-1 collaboration), Z. Phys. C48(1990)581.

[199] M.Landro et al., Phys. Rev. D36(1987)44.

[200] D.Antreasyan et al., Z. Phys. C48(1990)561.

[201] Particle Data Group, Phys. Rev. D50(1994)1173.

[202] D.Antreasyan et al., Phys. Rev. D33(1987)1847.

[203] Proceedings of 7th(1984), 8th(1988) and 9th(1992) International Workshops on Photon-Photon Collisions.

[204] Proc. of the 23d ICHEP, Standfort, 1986, p.1121

[205] A.E.Blinov et al. (MD-1 collaboration), to be published.

[206] I.F.Ginzburg, S.I.Polityko, Preprint TP-19(53). Novosibirsk 1987.
I.F.Ginzburg, Yad. Fiz. 46(1987)840.

[207] V.N.Baier and V.S.Fadin, Zh. Eksp. Teor. Fiz. 6(1971)476.

[208] E.A.Kuraev and L.N.Lipatov, Yad. Fiz. 16(1972)1060.

[209] E.A.Kuraev and L.N.Lipatov, Yad. Fiz. 20(1974)112.

[210] A.Courau et al. (DM-1 collaboration), Phys. Lett. 84B(1979)145: ibid 96B(1980)402.

[211] Ch.Berger et al. (PLUTO collaboration), Phys. Lett. 94B(1980)254.

[212] A.E.Blinov et al. (MD-1 collaboration), Yad. Fiz. 47(1988)889.

[213] M.Clement et al., Phys. Lett. 137B(1984)2261.
T.Cowan et al., Phys. Rev. Lett. 54(1985)1761.
T.Cowan et al., Phys. Rev. Lett. 56(1986)444.

[214] A.E.Blinov et al. (MD-1 collaboration), Z. Phys. C53(1992)33.

[215] A.Roussarie et al. (Mark 2 collaboration, SPEAR), Phys. Lett. 105B(1981)304.

[216] R.Brandelik et al. (TASSO collaboration), Z. Phys. C10(1981)117.

[217] J.R.Smith et al. (Mark 2 collaboration, PEP), Phys. Rev. D30(1984)851.

[218] A.Courau et al. (DELCO collaboration), Phys. Lett. 147B(1984)227.

[219] Ch.Berger et al. (PLUTO collaboration), Z. Phys. C26(1984)199.

[220] H.J.Behrend et al. (CELLO collaboration), Z. Phys. C23(1984)223.

[221] H.Aihara et al. (PEP4/9,TPC collaboration), Phys. Rev. Lett. 57(1987)404.

[222] J.Boyer et al. (Mark-2 collaboration), SLAC-PUB-4595(1987).

[223] Z.Ajaltonni et al. (DM1,DM2 collaboration), Phys. Lett. 194B(1987)573.

[224] H.Marsiske et al. (Crystal Ball), Phys. Lett. D41(1990)3324.

[225] T.Oest et al. (JADE collaboration), Z. Phys. C47(1990)343.

[226] D.Morgan, M.R.Pennington, Z. Phys. C48(1990)623.

[227] M.Feindt, J.Harjes, DESY 90-146(1990).

[228] H.Terazawa, Rev. Mod. Phys.45(1973)615.

[229] M.Poppe, Int. Jour. of Mod. Phys., A1(1986)545.

[230] D.H.Lyth, J. Phys. G10(1984)39; G11(1985)459.

[231] R.Jonson, SLAC-Report-294, 1986. Ph.Dissertation.

[232] H.Albrecht et al. (ARGUS collaboration), Z. Phys. C48(1990)183.

[233] V.V.Anashin et al., Proceedings of the International Symposium on Position Detectors in High Energy Physics, p.58. Dubna 1988.

S.E. Baru, A.E. Blinov, V.E. Blinov, A.E. Bondar,
A.D. Bukin, V.R. Groshev, Yu.I. Eidelman, V.A. Kiselev,
S.G. Klimenko, G.M. Kolachev, S.I. Mishnev, A.P. Onuchin,
V.S. Panin, V.V. Petrov, I.Ya. Protopopov, A.G. Shamov,
V.A. Sidorov, Yu.I. Skovpen, A.N. Skrinsky, V.A. Tayursky,
V.I. Telnov, Yu.A. Tikhonov, G.M. Tumaikin, A.E. Undrus,
A.I. Vorobiov, V.N. Zhilich

Experiments with the MD-1 Detector at the e^+e^- Collider VEPP-4 in the Energy Region of Υ-Mesons

Budker INP 95-36

С.Е. Бару, А.Е. Блинов, В.Е. Блинов, А.Е. Бондарь,
А.Д. Букин, В.Р. Грошев, Ю.И. Эйдельман, В.А. Киселев,
С.Г. Клименко, Г.М. Колачев, С.И. Мишнев, А.П. Онучин,
В.С. Панин, В.В. Петров, И.Я. Протопопов, А.Г. Шамов,
В.А. Сидоров, Ю.И. Сковпень, А.Н. Скринский, В.А. Таюрский,
В.И. Тельнов, Ю.А. Тихонов, Г.М. Тумайкин, А.Е. Удрус,
А.И. Воробьев, В.Н. Жилич

Эксперименты с детектором МД-1 на e^+e^- коллайдере ВЭПП-4 в области энергий Υ-мезонов

Ответственный за выпуск С.Г. Попов
Работа поступила 12.04.1995 г.

Сдано в набор 12.04.1995 г.
Подписано в печать 18.04.1995 г.
Формат бумаги 60×90 1/16 Объем 5.8 печ.л., 4.6 уч.-изд.л.
Тираж 170 экз. Бесплатно. Заказ N° 36

Обработано на IBM PC и отпечатано на
ротапринте ГНЦ РФ "ИЯФ им. Г.И. Будкера СО РАН",
Новосибирск, 630090, пр. академика Лаврентьева, 11.